Chapter 9

NON-LINEAR BEHAVIOR

9.1 Introduction

A physical description of nonlinear wave excitation forces as well as the response of floating structures has been given in chapter 6, where the so-called **second order wave drift forces** are described. They consist of **mean wave drift forces** and **low-frequency wave drift forces**. Both are the result of a non-linear behavior of the structure in the waves.
The present chapter - in which the theory is part based for a major part on the doctor's thesis of [Pinkster, 1980] on low-frequency second order wave exciting forces on floating structures - starts by describing situations in which higher order wave forces are important. These motivate the more detailed treatment of the associated computations later in this chapter.

9.2 Some Typical Phenomena

Investigations into the fundamental aspects of the behavior of offshore structures have often been guided by the behavior as observed at sea and as determined from model testing of such structures in realistically simulated wind, wave and current environments.
This section describes examples of the behavior of these structures which have been shown to be of significant influence on the design of the structures or on operational aspects of offshore work. All of these examples have motivated extensive fundamental research to explain the observed behavior.

9.2.1 Bow-Hawser Moored Vessel in Wind and Current

Shuttle tankers, either loading or discharging crude oil offshore, are often moored to a single point mooring (SPM) with a bow hawser.
It has been observed that such vessels can have **large amplitude horizontal motions** (surge, sway and yaw) **in steady winds and currents**. These motions lead in turn to large peak loads in the bow hawser. An example, showing the time record of the bow

[0] J.M.J. Journée and W.W. Massie, *"OFFSHORE HYDROMECHANICS"*, First Edition, January 2001, Delft University of Technology. For updates see web site: http://www.shipmotions.nl.

hawser force of a 200 thousand ton deadweight (kTDW) tanker, is given in figure 9.1. The lower part of the figure shows the bow hawser tension force as a function of time.

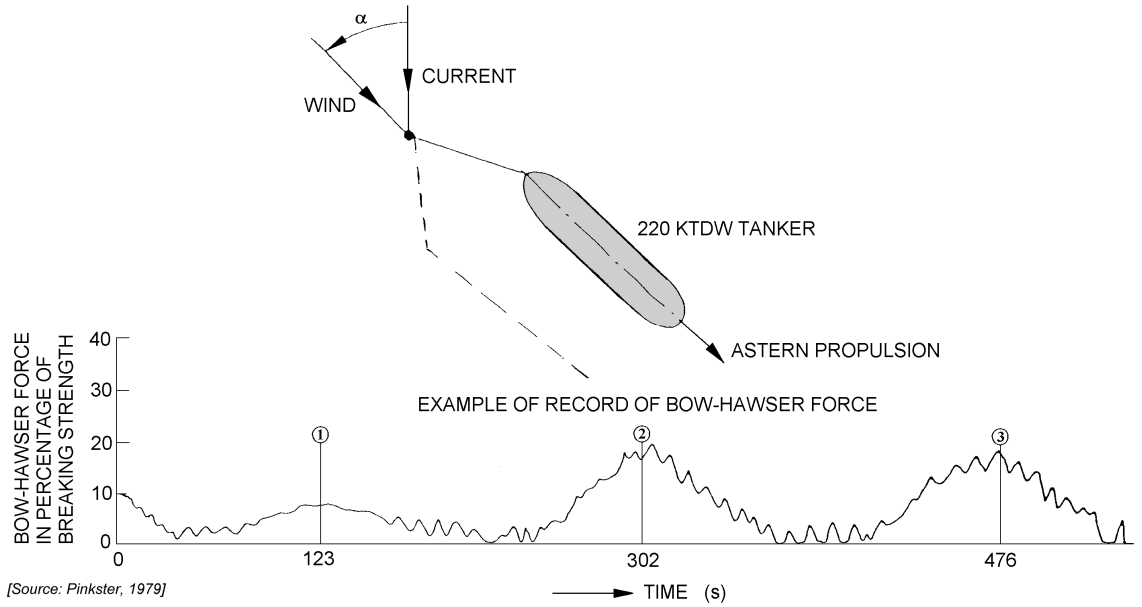

Figure 9.1: Unstable Horizontal Motions of a Bow Hawser Moored Tanker

This example shows that significant dynamic effects can occur, even in the absence of time variations in the environmental forces. In this particular case, these effects are due to inherent instabilities in the horizontal motions of the tanker, which are related to the length of the bow-hawser.
Figure 9.2 shows the regions of unstable horizontal motions as a function of the angle between the wind and current on the one hand and the length of the bow-hawser on the other hand. See [Wichers, 1979] for further details.

9.2.2 Large Concrete Structure under Tow

After completion of a large concrete Gravity Base Structure in sheltered deep water, it is towed out to the field by 6 to 8 large ocean going tugs. Narrow and shallow fjord passages have to be negotiated on the way out to the open sea. These passages put restrictions on the swept path and the draft of the platform.
Figure 9.3 shows that while under tow, this type of platform performs oscillatory motions in all six degrees of freedom in addition to its constant forward motion. These oscillatory motions are related - to a considerable extent - to the oscillatory components in the flow about the platform, as well as the inherent "towing stability" of the platform.
Important aspects of the flow about the platform are the vortex-shedding phenomenon about the large diameter vertical columns and flow separation about the large base structure. The towing force needed for the transportation of the platform is important; this determines the number and size of the tugs. The force necessary to hold the platform on location prior to being ballasted down to rest on the sea bed is determined by, among other factors, the current force that may be exerted by a tidal current. Figure figure 9.4 shows an example of the quadratic increase of the current force with the current velocity.

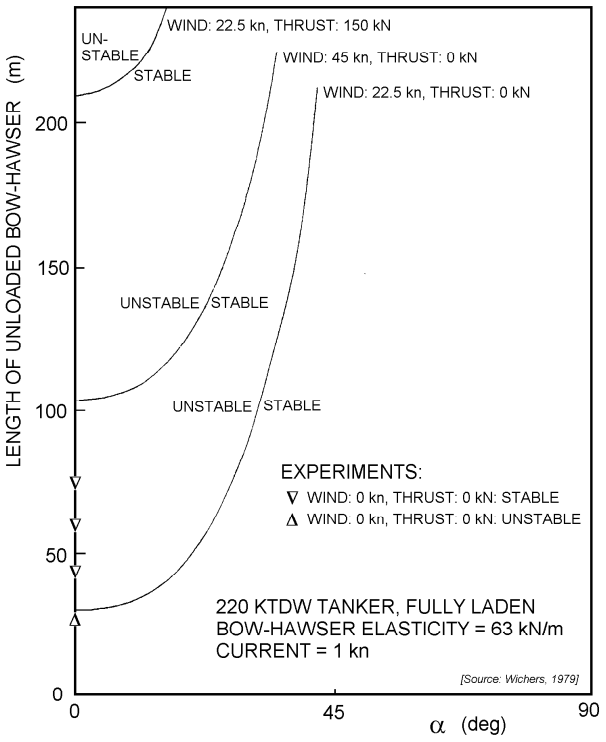

Figure 9.2: Stability Criterion for a Tanker as a Function of Bow Hawser Length

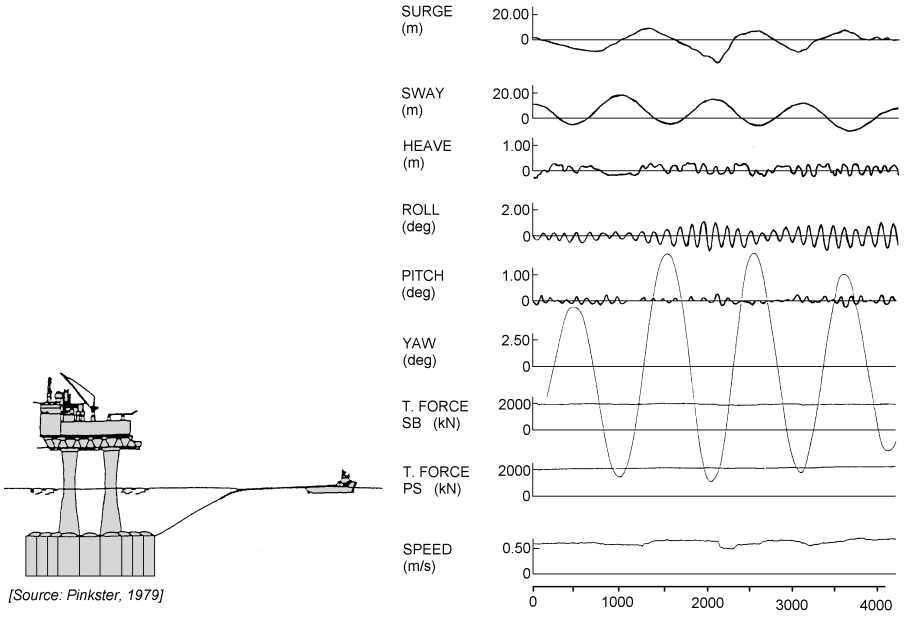

Figure 9.3: Motions of a Large Concrete Platform

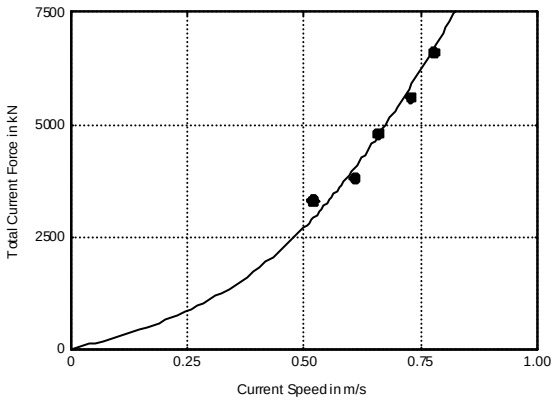

Figure 9.4: Current Force on Gravity Base Structure

Currents are usually assumed to be constant in time, but in some cases, such as during the positioning of this type of platforms, current speed variations may also give rise to undesirable horizontal platform motions. Figure 9.5 shows an example of current velocity variations - expressed in terms of the measured mean, maximum and minimum current velocities - and the spectral density of the current velocity.

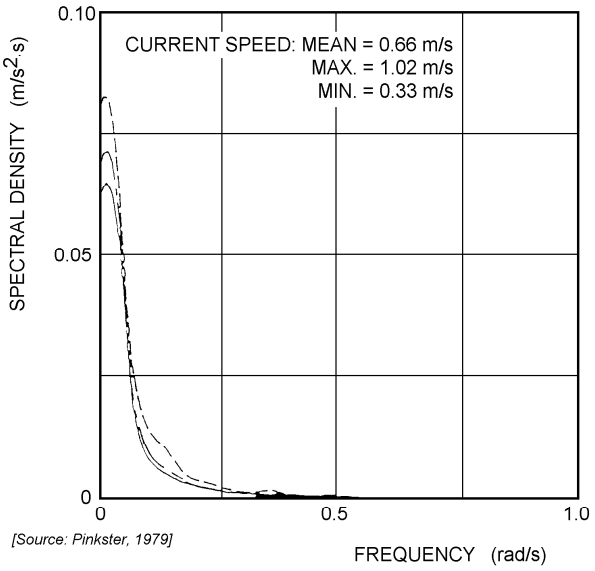

Figure 9.5: Current Speed Fluctuations

As is seen in figure 9.5, velocity variations are of low-frequency nature. Often the natural frequency of the horizontal motions of a moored structure (or a structure being positioned) is low due to the large mass on the one hand and the relatively soft restraining system on the other hand. There is little damping at such low frequencies as well; relatively large dynamic motions can result.

9.2.3 Horizontal Motions of Moored Tankers in Waves

Figure 9.6 shows the wave elevation record and the motions of a permanently moored tanker in high head sea conditions. It is seen that the heave and pitch motions contain the same frequencies; their amplitudes are in the order of the wave amplitudes and wave slopes respectively. This behavior is predicted using methods as given in chapters 6 and 8.

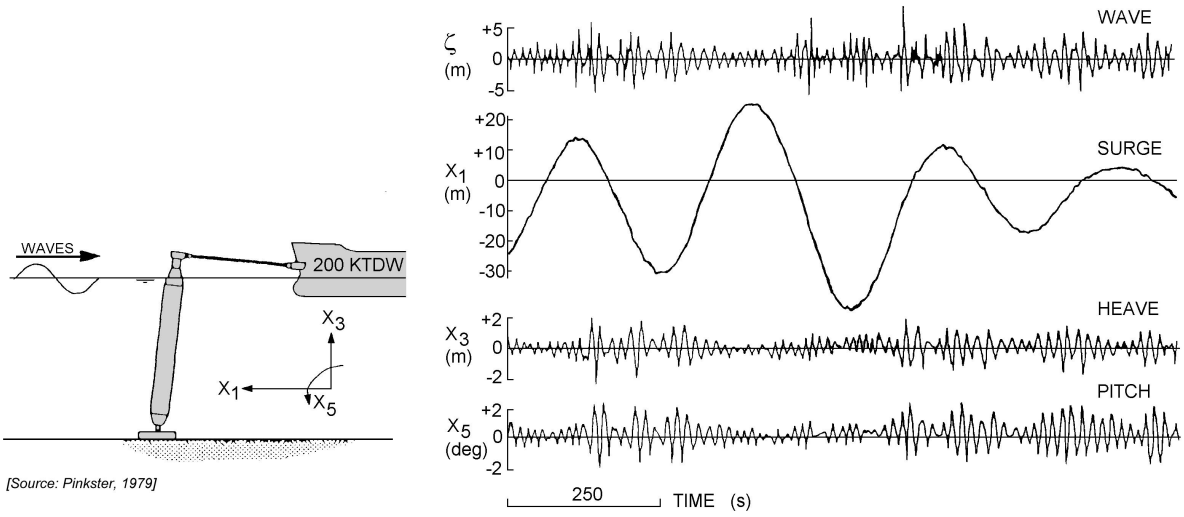

Figure 9.6: Record of the Motions of a Moored Tanker Model in Head Waves

The surge motion, besides containing a (small) wave frequency motion component, is dominated by a low frequency component with a significant larger amplitude.
Upon closer examination it appears that the large amplitude surge motion contains frequencies near the natural surge period of the moored vessel as dictated by the combination of the vessel mass and the mooring stiffness. The vessel is in fact carrying out resonant low frequency surge motions in response to small wave forces containing frequencies corresponding to the low natural surge frequency of the moored vessel. The response is further aggravated by the fact that surge motion damping is especially small at this low frequency. It will be clear that the mooring system forces will be dominated by this effect; its design must account for this. This requires a careful analysis of the phenomena involved. A brief introduction is given here.

Wave loads on structures as well as their responses to those loads can be split into several components. A table of these is given in chapter 6. These are summarized here too.
Firstly there are wave loads which have the same frequencies as the waves and are linearly proportional in amplitude to the wave amplitudes. These are known as **first order wave forces**. Secondly, there are wave load components which have frequencies both higher and lower than the frequencies of the waves. These forces are proportional to the square of the wave amplitudes and known as **second order wave forces**.
Low frequency second order wave forces have frequencies which correspond to the frequencies of wave groups present in irregular waves. These forces, which, beside containing time-varying components, also contain a non-zero mean component, are known as **wave drift forces**. This name is a consequence of the fact that a vessel, floating freely in waves,

will tend to drift in the direction of propagation of the waves under influence of the mean second order forces.
High frequency second order forces contain frequencies corresponding to double the frequency of the waves (also known as **sum frequencies**). The horizontal motions response of moored structures to these forces is generally small.
The fact that low frequency drift forces can cause large amplitude horizontal motion responses in moored vessels and that these motions are related to the wave group phenomenon was demonstrated by [Remery and Hermans, 1971] in chapter 6. One of the results of their investigations is shown in figure 9.7. In this figure the low frequency surge motion amplitude of a barge moored in head seas consisting of regular wave groups (superposition of two regular waves with small frequency difference corresponding to the wave group frequency) is shown. It is seen that when the period of the wave groups equals the natural surge period of the moored vessel, large motion amplitudes are the result.

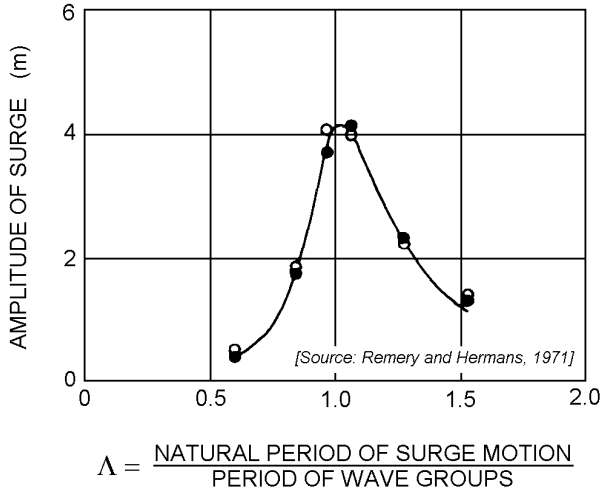

Figure 9.7: Surge Motions of a Moored Barge in Regular Head Wave Groups

Figure 9.8, taken from reference [Pinkster, 1976], shows that the low frequency surge motions of a barge moored in head seas increase more or less as a linear function of the square of the significant wave height. This implies that the wave force is a **quadratic function** of the wave amplitude.

9.2.4 Motions and Mooring Forces of Semi-Submersibles

Figure 9.9 shows that not only tankers and other mono-hull vessels are subject to the effects of first and second order wave forces. This figure shows the surge motion of a large semi-submersible crane vessel (SSCV) and the forces in the mooring lines. A large low frequency component is superimposed on wave frequency components.
Figure 9.10 shows a time record of the low frequency second order wave drift force on a semi-submersible. The relationship between the occurrence of groups of waves in the incident wave train and peaks in the wave drift force are very clear.
A tension leg platform (TLP) is a semi-submersible structure with vertical mooring tethers which restrain the vertical motions of the platform. It is also subject to these wave loads.

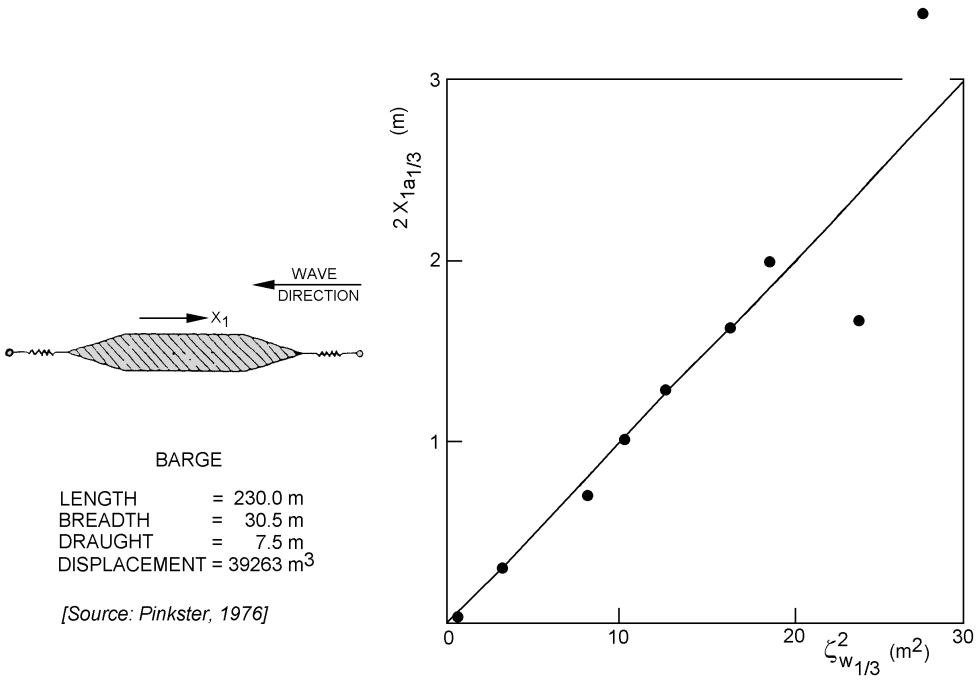

Figure 9.8: Low Frequency Surge Motions of a Barge in Irregular Head Waves

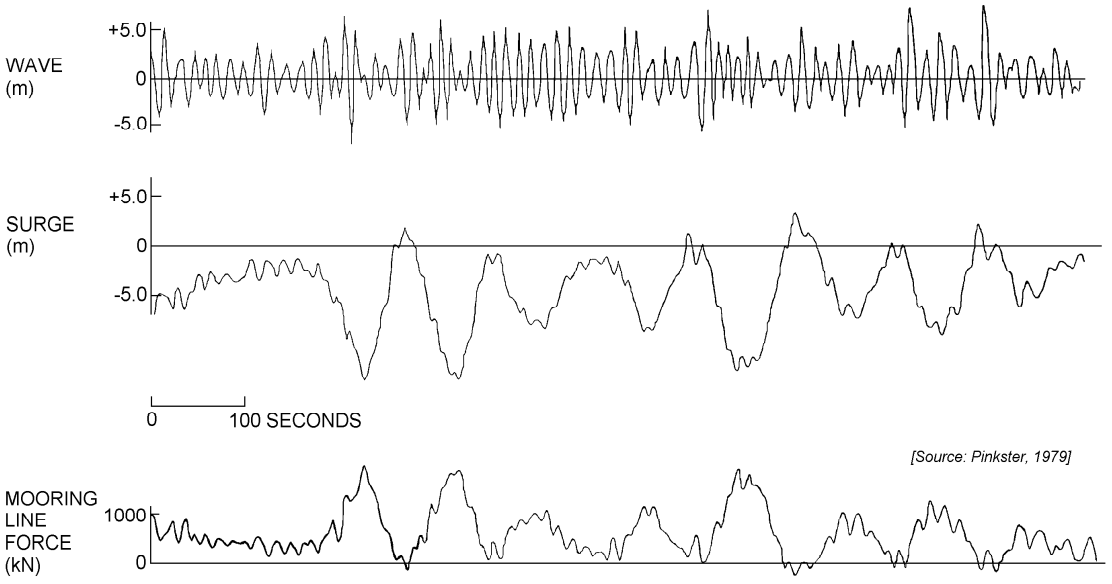

Figure 9.9: Surge Motions and Mooring Line Forces of a SSCV

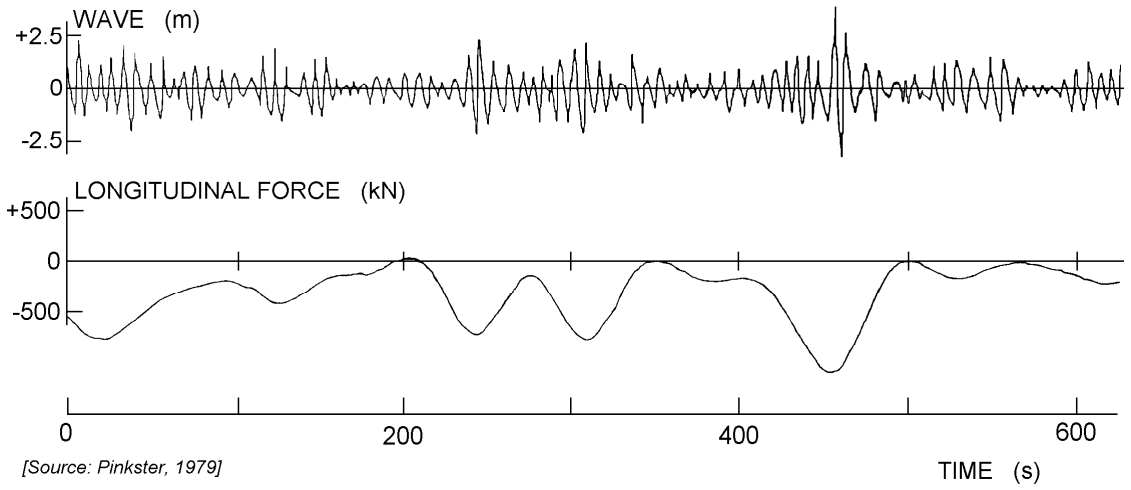

Figure 9.10: Second Order Wave Forces of a Semi-Submersible

Figure 9.11 shows the surge sway and yaw motions of a TLP in irregular waves coming at an angle to the longitudinal axis of the platform. The low frequency components in all three motion components is clear. The corresponding forces in the mooring tethers of the TLP - given in figure 9.12 - are dominated by wave frequency components, however. Although not apparent from this figure, tether forces sometimes contain contributions from sum-frequency second order wave forces which can have frequencies coinciding with the natural frequency of the vertical motion of a TLP. These frequencies can be high due to the high axial stiffness of the tethers.

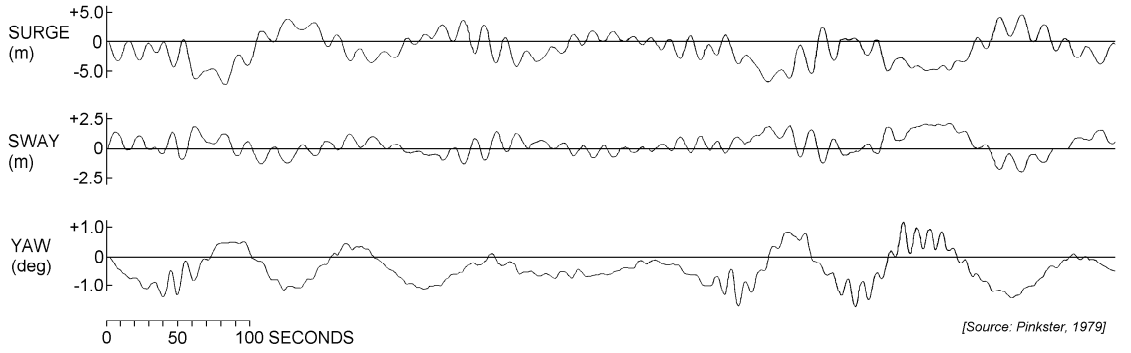

Figure 9.11: Horizontal TLP Motions in Irregular Seas

9.2.5 Vertical Motions of Ships in Long Waves

A different non-linear effect in irregular waves is the occurrence of wave set-down. This is the phenomenon whereby the "mean" water level is lower under groups of higher waves and higher under groups of smaller waves. The phenomenon has been extensively analyzed using potential theory. Set-down appears as low-frequency second order term in the power series expansion of the potential and the corresponding wave elevation.

Figure 9.12: TLP Tether Forces in Irregular Seas

An example of the set-down measured in an irregular wave train is shown in figure 9.13. In this case the set-down record has been obtained by low-pass filtering of the measured wave elevation record. Bearing in mind the time scale shown in the figure, it is clear that the set-down wave components can be considered to be equivalent to long waves.

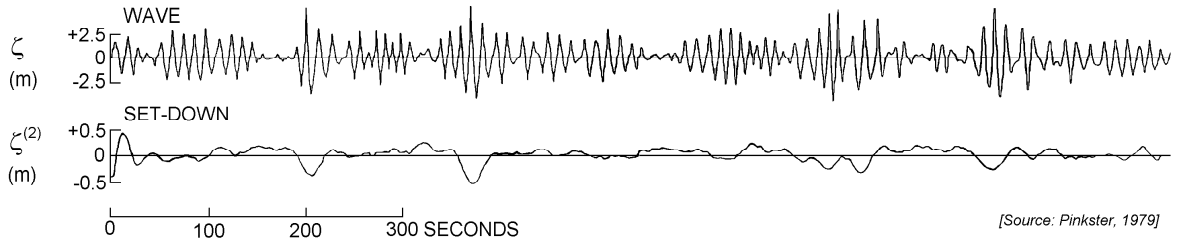

Figure 9.13: Wave and Set-Down Records

When the horizontal dimensions of a floating object are small compared to this wave length the vertical motions of the object follows the wave elevation and slope closely. A sea gull swimming in waves is an extreme example of this. One can conclude from figure 9.14 that this must be true for even relatively large vessels such as a 125,000 m^3 LNG carrier. If the water depth is about 15 meters, then with an "average" long wave period of about 80 seconds, the wave length will be in the order of a kilometer; this is long enough to let the LNG tanker behave like a sea gull.

Figure 9.15 finally, shows the three components contributing to the total vertical motions of the LNG carrier sailing in shallow water. The total vertical displacement consist of a sinkage contribution (a static contribution related to square of the forward speed), a wave

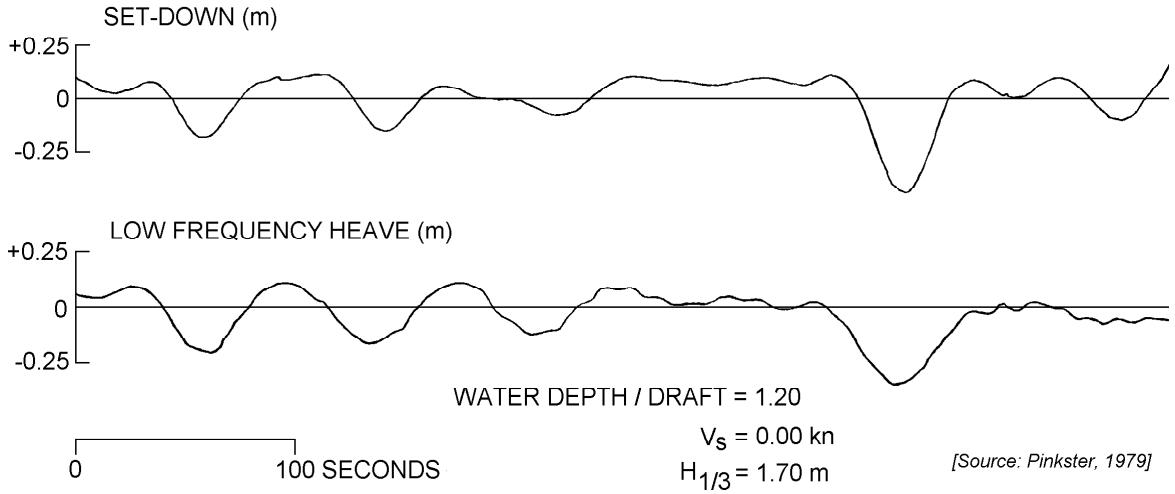

Figure 9.14: Second Order Vertical Motions of an LNG Carrier in Head Seas

frequency contribution (linearly related to the wave elevation) and a **group frequency** contribution (due to the second order wave set-down effect in the incident waves).

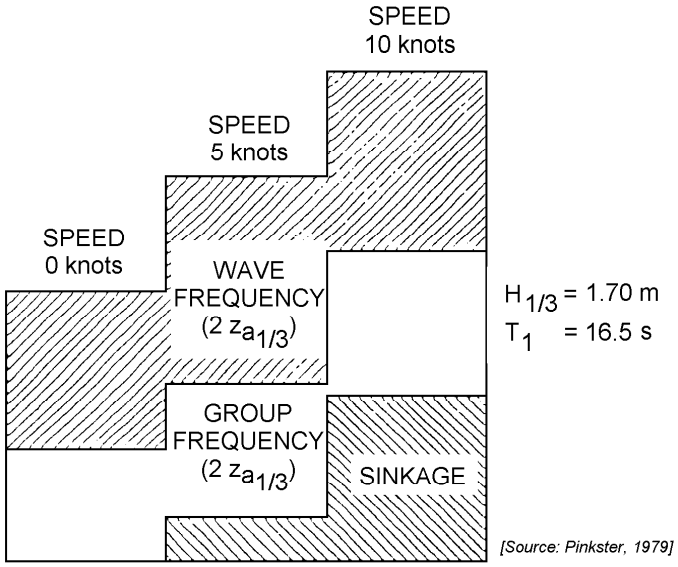

Figure 9.15: Heave Motion Components of an LNG Carrier in Head Waves

9.2.6 Behavior of a Jetty-Moored Tanker

In most harbors, tankers are moored to jetties by means of mooring lines and fenders. A number of these jetties are situated at open locations so that the vessels moored to them are subject to the effects of wind, waves and current. Vessel motions and mooring system forces are the result. Sometimes passing ships induce significant transient mooring loads as well.

Figures 9.16 through 9.20 - with data taken from [Oortmerssen et al., 1984] - give some results of model tests and simulations with a 200 kTDW tanker moored to a jetty in wind and waves.
Figure 9.16 shows the spectral density of the three irregular waves in which the model tests were carried out.
Figure 9.17 shows a record of the horizontal motions and the mooring line and fender forces in beam waves with a relatively short period (spectrum 3) and a steady beam wind of 20 m/s.
Figure 9.18 shows the spectra of the sway motion in beam waves with a long period (spectrum 1) and a steady beam wind of 20 m/s.
Figure 9.19 shows a record of the horizontal motions and the mooring line and fender forces in bow-quartering waves and a steady beam wind of 20 m/s.
Figure 9.20 shows the spectra of the sway motion and the fender forces in beam waves with a relatively short period (spectrum 3) without wind effects.
These results clearly show that the motions and mooring forces show two distinct frequency ranges: components with wave frequencies and components with very low frequencies.

From foregoing discussions it will be clear that low frequency components in the motions and forces are related to the drift force phenomenon. However, in the case of jetty moorings, which have highly nonlinear restoring characteristics (fenders are much stiffer than mooring lines), even monochromatic wave frequency excitation of the vessel can induce motions and mooring forces which contain significant sub- and super-harmonics of the wave frequency. An example is shown in figure 9.21, which has been taken from [Oortmerssen, 1976b]. Note that in this case the excitation side of the equations of motion will be reasonably linear while it is now the left hand side which has a distinctly nonlinear spring term. This is an example of a sub-harmonic excitation. The period of the excitation is now an integer multiple of the excitation frequency as was pointed out in chapter 6.

9.3 Wave Drift Forces and Moments

It is generally acknowledged that the existence of wave drift forces was first reported by [Suyehiro, 1924]. While experimenting with a model rolling in beam seas, he found that the waves exerted a steady horizontal force which he attributed to the reflection of the incoming waves by the model. The importance of the mean and low frequency wave drift forces from the point of view of motion behavior and mooring loads is generally recognized nowadays. It has been mentioned in chapter 6 that work by [Hsu and Blenkarn, 1970] and [Remery and Hermans, 1972] indicated that large amplitude low frequency horizontal motions of moored vessels could be induced by slowly varying wave drift forces in irregular waves. These authors also stressed the importance of knowledge of the mean second order forces in regular waves in this problem. A considerable number of papers have been published since, reflecting increased insight in the phenomena involved.
Initially, the solution to the problem of predicting motions and mooring forces was sought in better quantitative data on the low frequency wave drift forces. Accurate knowledge of these forces, it was felt, would allow accurate estimates to be made of low frequency horizontal motions and mooring forces. Due to the resonant motion response of the moored vessels to the wave drift forces, it is nowadays known that for accurate prediction of low frequency motions in irregular seas attention must also be paid to the hydrodynamic reac-

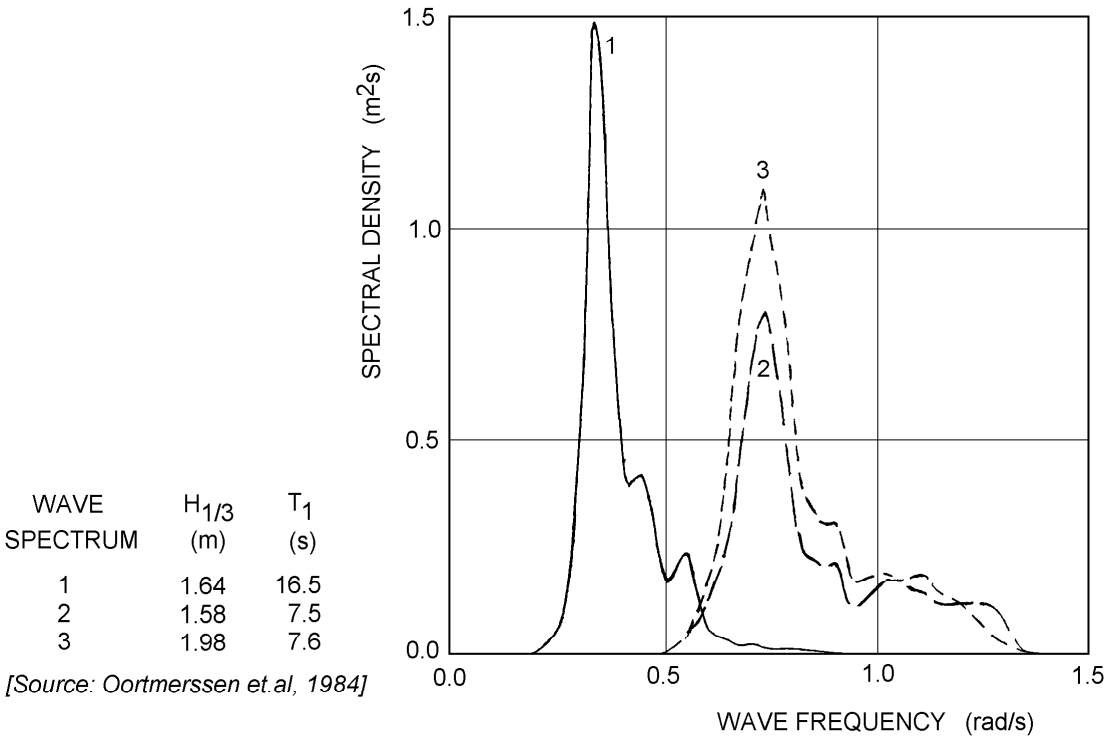

WAVE SPECTRUM	$H_{1/3}$ (m)	T_1 (s)
1	1.64	16.5
2	1.58	7.5
3	1.98	7.6

[Source: Oortmerssen et.al, 1984]

Figure 9.16: Wave Spectra Used for a Jetty Moored Tanker

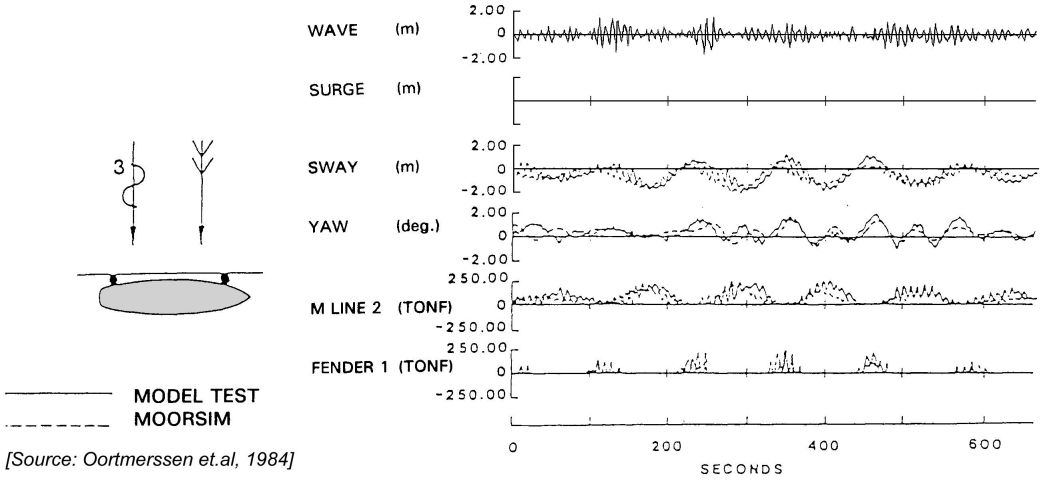

[Source: Oortmerssen et.al, 1984]

Figure 9.17: Behavior in Beam Waves and Beam Wind

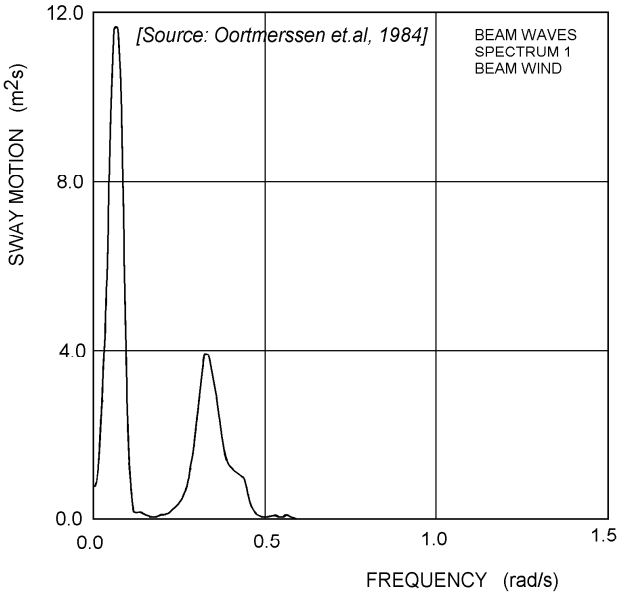

Figure 9.18: Spectra of Sway Motions in Beam Waves and Beam Wind

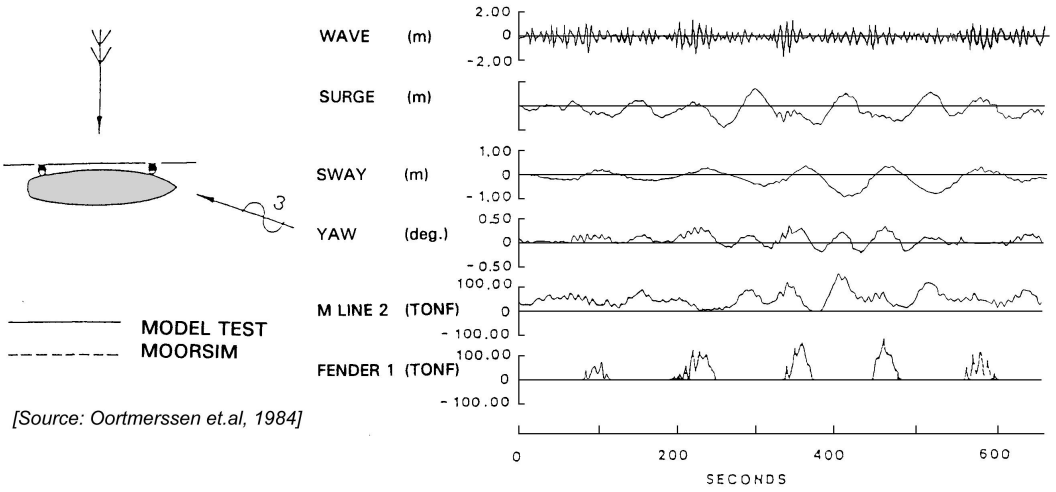

Figure 9.19: Behavior in Bow-Quartering Waves and Beam Wind

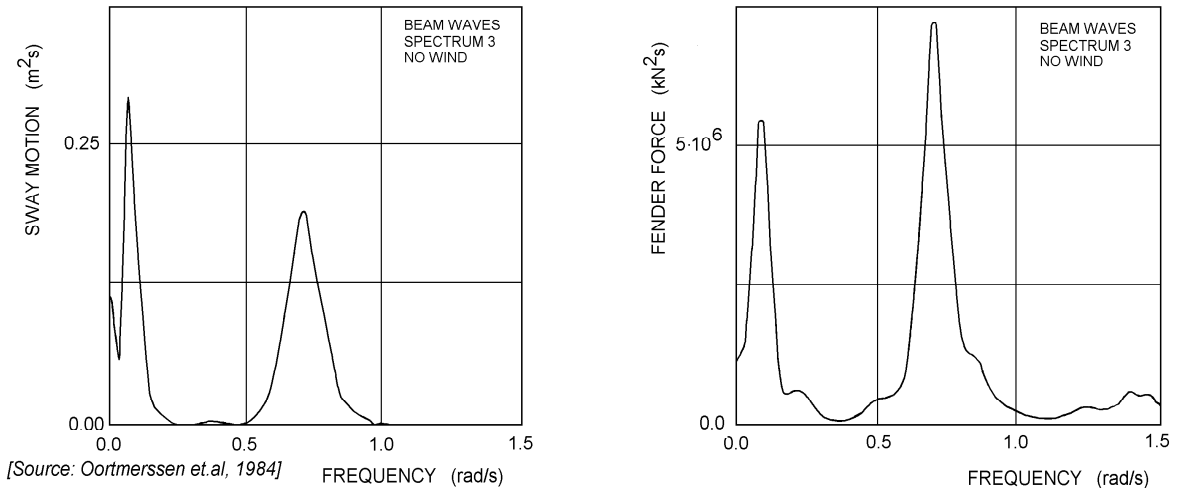

Figure 9.20: Spectra of Sway Motions and Fender Forces in Beam Waves without Wind

tion forces. On the basis of experimental and theoretical results it is generally agreed that, for engineering purposes, the wave drift forces are second order wave forces. This means that the forces are quadratic functions of the height of the incident waves.

[Pinkster, 1976] and [Pinkster, 1977] introduced a computation method based on direct integration of all pressure contributions on the wetted hull of the body. This method is also exact within potential theory.
[Faltinsen and Loken, 1978b] and [Faltinsen and Loken, 1978a] applied a similar method to the two dimensional case of cylinders in beam waves. They succeeded in giving a complete solution which includes the mean wave drift force in regular waves and the low frequency oscillating wave drift force in regular wave groups.
[Pinkster and Hooft, 1978] and [Pinkster, 1979] use a method of direct integration - for three-dimensional cases - the mean and low frequency part of the wave drift forces using an approximation for the force contribution due to the second order non-linear potential.
In general it has been found that for voluminous bodies, such as ships, methods based on potential theory give good results when compared with model test results. Discrepancies occur at wave frequencies near, for instance, roll resonance. In such cases viscous effects - not accounted for by potential theory - become important. For relatively slender objects such as some semi-submersibles, viscous effects may become important at all frequencies; see for instance [Dev, 1996] for the relevant work in this field.
This section deals, almost entirely, with the wave drift exciting forces and moments as determined by [Pinkster, 1980].

9.3.1 Second Order Wave Forces

Expressions for the second order wave force and moment will be deduced in this section based on the **direct integration method** of pressures on the hull. This method is straightforward and gives insight in the mechanism by which waves and the body interact to produce the force. First, the boundary conditions for the various potentials are treated; special attention is given to the boundary conditions at the body.

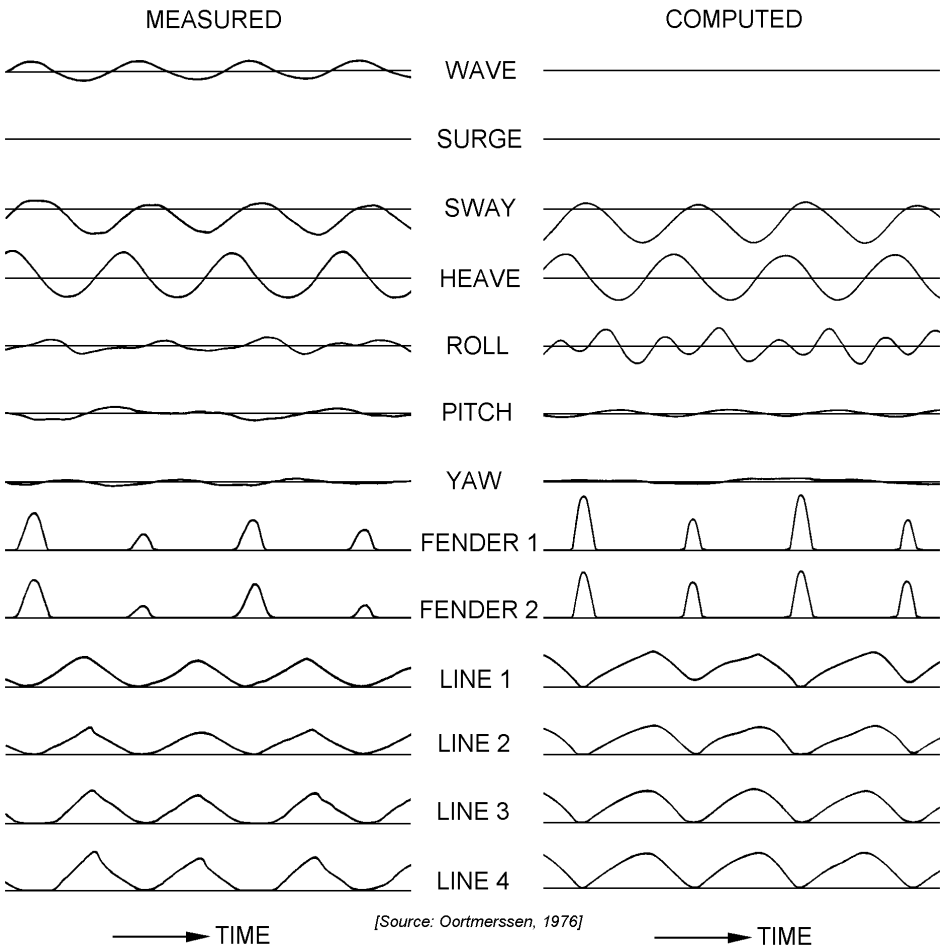

Figure 9.21: Measured and Computed Ship Motions and Mooring Forces

The theory is developed using perturbation methods. This means that all quantities such as wave height, motions, potentials, pressures etc., are assumed to vary only very slightly relative to some initial static value and may all be written in the following form:

$$X = X^{(0)} + \varepsilon X^{(1)} + \varepsilon^2 X^{(2)} \tag{9.1}$$

where $X^{(0)}$ denotes the static value, $X^{(1)}$ indicates the first order oscillatory variation, $X^{(2)}$ the second order variation. The parameter ε is some small number, with $\varepsilon \ll 1$, which denotes the order of oscillation. First order in this case means linearly related to the wave height and second order means that the quantity depends on the square of the wave height. In the following, quantities are of second order if preceded by ε^2. If, as in many cases, the ε^2 is discarded, this is due to the fact that the expression contains only second order quantities. In such instances second order quantities are recognized by the superscript $^{(2)}$ or by the fact that a component is the product of two first order quantities with superscript $^{(1)}$. For instance, the pressure component $-\frac{1}{2}\left(\nabla\Phi^{(1)}\right)^2$ should be recognized as a second order quantity.

The derivation of the second order wave forces and moments is based at first on the assumption that the body is floating in small amplitude waves. It is furthermore assumed that the body is only allowed to move in response to the first order hydrodynamic forces

at frequencies within the wave frequency region. Frequencies outside this region or higher orders of motion are not permitted. This means that expressions obtained for the second order wave forces contain only the wave exciting forces.

Coordinate Systems

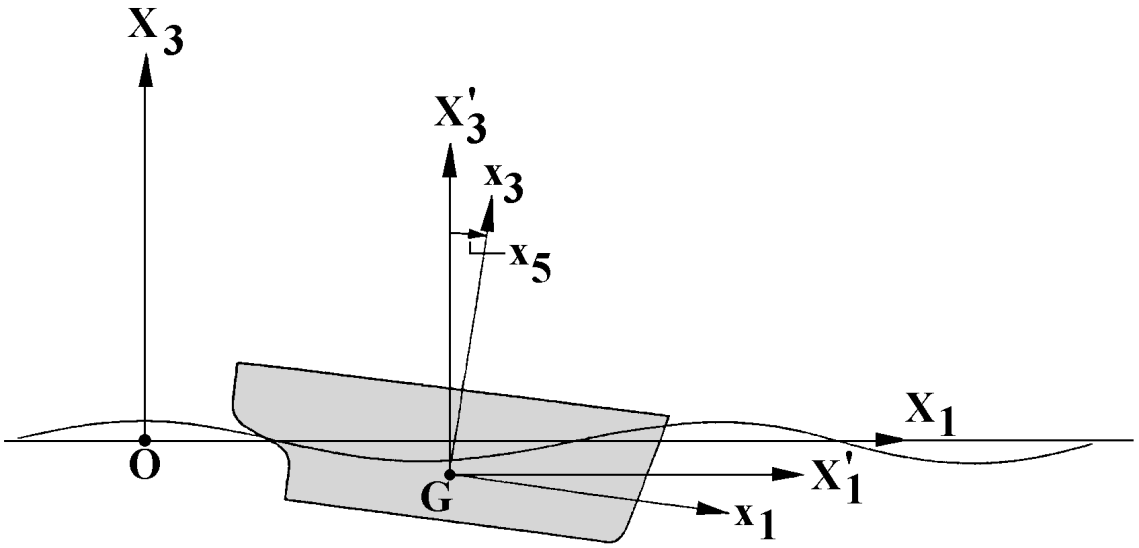

Figure 9.22: System of Coordinate Axes

Use is made here of three systems of coordinate axes (see figure 9.22):

- The first system of coordinate axes O-(X_1, X_2, X_3) is a right-handed **earth-bound axes system** with origin O, the X_1- and X_2-axes in the mean free surface of the sea and the X_3-axis positive upwards.
  A point in space has position or displacement vector $\vec{X} = (X_1, X_2, X_3)$.

- The second system is a right-handed system of G-(x_1, x_2, x_3) **body-bound axes system** with as origin the centre of gravity, G, of the body, the positive x_1- axis in the longitudinal direction (bow) and the positive x_3-axis upwards. In the mean position of the oscillating vessel this axes system is parallel to the earth-bound O-(X_1, X_2, X_3) system.
  The hull surface is uniquely defined in this system of axes. A point on the body surface has position vector $\vec{x} = (x_1, x_2, x_3)$ in the body-bound axes system. The orientation of a surface element in this system of coordinates is defined by the outward pointing normal vector $\vec{n} = (n_1, n_2, n_3)$.

- The third system of coordinates G-(X'_1, X'_2, X'_3) is a **moving axes system** with its origin in the mean position of the center of gravity, G, of the body. Its axes are always **parallel** to the axes of the earth-bound O-(X_1, X_2, X_3) system. So this axes system does not translate or rotate with the ship's motions; it translates only with the forward ship speed which is **not** present here..

The roll, pitch and yaw motions about the body-bound axes of the structure are given by the Eulerian angles x_4, x_5 and x_6, respectively.

First and Second Order Wave Loads

The **first order** wave loads have been defined in the chapter 7. There, the "body-in-waves" has no motions (zero order) in the earth-bound axis system. The waves are approaching a restrained body. Thus, first order fluid motions and resulting first order fluid forces have been considered there.
For the determination of the **second order** wave loads, the "body-in-waves" is carrying out a first order harmonic motion, **forced** by first order wave loads. The waves are approaching a harmonic oscillating body. Then, second order fluid motions and resulting second order fluid forces have to be considered too.

Body Motions

If the body has small amplitude motions resulting from the first order oscillatory wave forces, the resultant displacement vector $\vec{X} = (X_1, X_2, X_3)$ of a point on the body - relative to the earth-bound system of axes - is also a small first order quantity:

$$\vec{X} = \varepsilon \vec{X}^{(1)} \tag{9.2}$$

with:

$$\vec{X}^{(1)} = \vec{X_G}^{(1)} + R^{(1)} \cdot \vec{x} \tag{9.3}$$

where $\vec{X_G}^{(1)}$ is the oscillatory first order motion vector of the center of gravity of the body, $\vec{x} = (x_1, x_2, x_3)$ is the position vector of the point on the body in the body-bound axes system and $R^{(1)}$ is the linearized rotation transformation matrix, defined as:

$$R^{(1)} = \begin{bmatrix} 0 & -x_6^{(1)} & +x_5^{(1)} \\ +x_6^{(1)} & 0 & -x_4^{(1)} \\ -x_5^{(1)} & +x_4^{(1)} & 0 \end{bmatrix} \tag{9.4}$$

in which $x_4^{(1)}$, $x_5^{(1)}$ and $x_6^{(1)}$ are the first order roll, pitch and yaw motions of the structure. Similarly, the velocity $\vec{V}$ of a point on the body relative to the earth-bound system of axes, O-(X_1, X_2, X_3), is also a first order quantity and follows from:

$$\vec{V} = \varepsilon \vec{V}^{(1)} = \dot{\vec{X}} = \varepsilon \dot{\vec{X}}^{(1)} \tag{9.5}$$

with:

$$\dot{\vec{X}}^{(1)} = \vec{V}^{(1)} = \dot{\vec{X}}_G^{(1)} + \dot{R}^{(1)} \cdot \vec{x} \tag{9.6}$$

where:

$$\dot{R}^{(1)} = \begin{bmatrix} 0 & -\dot{x}_6^{(1)} & +\dot{x}_5^{(1)} \\ +\dot{x}_6^{(1)} & 0 & -\dot{x}_4^{(1)} \\ -\dot{x}_5^{(1)} & +\dot{x}_4^{(1)} & 0 \end{bmatrix} \tag{9.7}$$

in which $\dot{x}_4^{(1)}$, $\dot{x}_5^{(1)}$ and $\dot{x}_6^{(1)}$ are the first order roll, pitch and yaw angular velocities of the structure.
Note that $\vec{X}$ and $\vec{V}$ and their derivatives are the (oscillatory) motions of the body; so far they are not the motions of the fluid.
The orientation of surface elements of the body relative to the G-(x_1, x_2, x_3) body-bound axes are denoted by the outward pointing normal vector $\vec{n}$. When the body is carrying out small first order motions, the orientation of a surface element relative to the fixed O-(X_1, X_2, X_3) or G-(X_1', X_2', X_3') system of axes becomes:

$$\vec{N} = \vec{n} + \varepsilon \vec{N}^{(1)} \tag{9.8}$$

with:

$$\vec{N}^{(1)} = R^{(1)} \cdot \vec{n} \tag{9.9}$$

where the linearized rotation transformation matrices, $R^{(1)}$, follows from equation 9.4.

Fluid Motions

The fluid domain is - just as when determining the hydromechanical coefficients in chapter 7 - bounded by: 1) the surface of the body, 2) the free sea surface, 3) the sea bed and 4) a vertical cylinder with an infinite radius. Assuming that the fluid is inviscid, irrotational, homogeneous and incompressible, the fluid motion may be described by means of the velocity potential Φ:

$$\Phi = \varepsilon \Phi^{(1)} + \varepsilon^2 \Phi^{(2)} + ... \tag{9.10}$$

The potentials are defined relative to the earth-bound system of axes, O-(X_1, X_2, X_3).
As has been pointed out in chapter 7, the (linearized) first order potential $\Phi^{(1)}$ consists of the sum of potentials associated with the undisturbed incoming waves, $\Phi_w^{(1)}$, the diffracted waves, $\Phi_d^{(1)}$, and waves due to the first order body motions, $\Phi_b^{(1)}$, respectively; thus:

$$\Phi^{(1)} = \Phi_w^{(1)} + \Phi_d^{(1)} + \Phi_b^{(1)} \tag{9.11}$$

Continuity Condition

Both the first and the second order potentials must satisfy the equation of continuity within the fluid domain; the Laplace equation (see chapter 7) has to be fulfilled by both potentials as well:

$$\nabla^2 \Phi^{(1)} = 0 \qquad \text{and} \qquad \nabla^2 \Phi^{(2)} = 0 \tag{9.12}$$

Sea Bed Boundary Condition

Both potentials must satisfy the boundary condition at the horizontal sea bed, too:

$$\frac{\partial \Phi^{(1)}}{\partial X_3} = 0 \qquad \text{and} \qquad \frac{\partial \Phi^{(2)}}{\partial X_3} = 0 \qquad \text{for:} \quad X_3 = -h \tag{9.13}$$

where h is the water depth in the O-(X_1, X_2, X_3) axis system.

Free Surface Boundary Condition

In order to derive the boundary condition at the mean free surface use has to be made of the Bernoulli equation and the assumption that fluid elements in the free surface remain there at all times (no-leak condition); see chapter 7. A Taylor expansion can be used to transform the boundary conditions at the actual moving free surface ($X_3 = \zeta$) into boundary conditions at the mean free surface ($X_3 = 0$); see also chapter 5.
Then the **homogeneous** boundary condition becomes:

$$g \cdot \frac{\partial \Phi^{(1)}}{\partial X_3} + \frac{\partial^2 \Phi^{(1)}}{\partial t^2} = 0 \tag{9.14}$$

For the **particular solution** of the boundary condition of $\Phi^{(2)}$, only the final result - which is very complex to solve as will be explained later - is given here:

$$g \cdot \frac{\partial \Phi^{(2)}}{\partial X_3} + \frac{\partial^2 \Phi^{(2)}}{\partial t^2} = -2\left(\vec{\nabla}\Phi^{(1)} \cdot \vec{\nabla}\frac{\partial \Phi^{(1)}}{\partial t}\right) + \frac{\partial \Phi^{(1)}}{\partial t} \cdot \left(\frac{\partial^2 \Phi^{(1)}}{\partial X_3^2} + \frac{1}{g} \cdot \frac{\partial^2}{\partial t^2}\left(\frac{\partial \Phi^{(1)}}{\partial X_3}\right)\right) \tag{9.15}$$

This equation will be used further on in this chapter.

Body Boundary Condition

In general the boundary condition on the body is that no fluid passes through the hull (no-leak condition); the relative velocity between the fluid and the hull in the direction of the normal to the hull must be zero; see chapter 7.
This boundary condition has to be satisfied **at the instantaneous position of the hull surface**; thus the fluid motions in the direction of the normal on the body, $\vec{\nabla}\Phi \cdot \vec{N}$, have to be equal to the body motion in this normal direction, $\vec{V} \cdot \vec{N}$:

$$\vec{\nabla}\Phi \cdot \vec{N} = \vec{V} \cdot \vec{N} \tag{9.16}$$

or taking into account equations 9.5, 9.8 and 9.10:

$$\left(\varepsilon\vec{\nabla}\Phi^{(1)} + \varepsilon^2\vec{\nabla}\Phi^{(2)}\right) \cdot \left(\vec{n} + \varepsilon\vec{N}^{(1)}\right) = \left(\varepsilon\vec{V}^{(1)}\right) \cdot \left(\vec{n} + \varepsilon\vec{N}^{(1)}\right) \tag{9.17}$$

Grouping similar powers of ε results in the first and second order body boundary conditions. The boundary conditions for the first order potential, $\varepsilon\Phi^{(1)}$, on the body is as follows:

$$\vec{\nabla}\Phi^{(1)} \cdot \vec{n} = \vec{V}^{(1)} \cdot \vec{n} \tag{9.18}$$

The boundary condition for the second order potential on the body, $\varepsilon^2\Phi^{(2)}$, states that:

$$\vec{\nabla}\Phi^{(2)} \cdot \vec{n} = \left(\vec{V}^{(1)} - \vec{\nabla}\Phi^{(1)}\right) \cdot \vec{N}^{(1)} \tag{9.19}$$

in which the first part, $\vec{V}^{(1)} \cdot \vec{N}^{(1)}$, represents the body motions and the second part, $\vec{\nabla}\Phi^{(1)} \cdot \vec{N}^{(1)}$, the fluid motions.
Equations 9.18 and 9.19 have to be satisfied at the instantaneous position of the surface of the body. Assuming that the motions are small, and applying a Taylor expansion,

similar conditions may be stipulated for the potentials **at the mean position of the hull surface**.
The first order boundary condition then becomes:

$$\vec{\nabla}\Phi^{(1)} \cdot \vec{n} = \vec{V}^{(1)} \cdot \vec{n} \tag{9.20}$$

and the second order boundary condition becomes:

$$\vec{\nabla}\Phi^{(2)} \cdot \vec{n} = -\left(\vec{X}^{(1)} \cdot \vec{\nabla}\right) \cdot \left(\vec{\nabla}\Phi^{(1)} \cdot \vec{n}\right) + \left(\vec{V}^{(1)} - \vec{\nabla}\Phi^{(1)}\right) \cdot \vec{N}^{(1)} \tag{9.21}$$

in which the last term is the difference of the two velocity vectors along the hull surface caused by the first order change of the direction normal.
The potentials and their derivatives in equations 9.20 and 9.21 have to be evaluated at the mean position of the body.

Substitution of equation 9.11 in boundary condition 9.20 - so splitting the potential in three parts - yields the following:

$$\left(\vec{\nabla}\Phi_w^{(1)} + \vec{\nabla}\Phi_d^{(1)} + \vec{\nabla}\Phi_b^{(1)}\right) \cdot \vec{n} = \vec{V}^{(1)} \cdot \vec{n} \tag{9.22}$$

It is customary to decompose this equation into two components:

- Diffraction component:

$$\left(\vec{\nabla}\Phi_w^{(1)} + \vec{\nabla}\Phi_d^{(1)}\right) \cdot \vec{n} = 0 \qquad \text{(see chapter 7)} \tag{9.23}$$

$$\text{or} \tag{9.24}$$

$$\vec{\nabla}\Phi_d^{(1)} \cdot \vec{n} = -\vec{\nabla}\Phi_w^{(1)} \cdot \vec{n} \tag{9.25}$$

- Motion component:

$$\vec{\nabla}\Phi_b^{(1)} \cdot \vec{n} = \vec{V}^{(1)} \cdot \vec{n} \tag{9.26}$$

The methods in use to solve for the unknown first order potentials $\Phi_w^{(1)}$, $\Phi_d^{(1)}$ and $\Phi_b^{(1)}$ have already been discussed in chapters 5 and 7.

Substitution of the first order potential $\Phi^{(1)}$ from 9.11 in the non-homogeneous second order free surface boundary condition of equation 9.15 shows that the second order potential includes in the most general form the following components:

$$\begin{aligned} \Phi^{(2)} = \quad & \Phi_d^{(2)} \\ & + \Phi_{ww}^{(2)} + \Phi_{dd}^{(2)} + \Phi_{bb}^{(2)} + \Phi_{wd}^{(2)} + \Phi_{wb}^{(2)} + \Phi_{db}^{(2)} + \Phi_{dw}^{(2)} + \Phi_{bw}^{(2)} + \Phi_{bd}^{(2)} \end{aligned} \tag{9.27}$$

The first potential on the right-hand side of equation 9.27, $\Phi_d^{(2)}$, is a potential which satisfies the homogeneous boundary condition:

$$g \cdot \frac{\partial \Phi_d^{(2)}}{\partial X_3} + \frac{\partial^2 \Phi_d^{(2)}}{\partial t^2} = 0 \tag{9.28}$$

and $\Phi_d^{(2)}$ is therefore an "ordinary" potential which satisfies the linearized free surface condition.

The last nine components on the right-hand side of equation 9.27 are potentials which are particular solutions to the type of boundary condition as given in equation 9.18.
For instance for $\Phi_{ww}^{(2)}$:

$$g \cdot \frac{\partial \Phi_{ww}^{(2)}}{\partial X_3} + \frac{\partial^2 \Phi_{ww}^{(2)}}{\partial t^2} = -2 \left(\vec{\nabla} \Phi_w^{(1)} \cdot \vec{\nabla} \frac{\partial \Phi_w^{(1)}}{\partial t} \right) + \frac{\partial \Phi_w^{(1)}}{\partial t} \left(\frac{\partial^2 \Phi_w^{(1)}}{\partial X_3^2} + \frac{1}{g} \cdot \frac{\partial^2}{\partial t^2} \left(\frac{\partial \Phi_w^{(1)}}{\partial X_3} \right) \right) \quad (9.29)$$

Equation 9.27 can be written simplified by letting $\Phi_w^{(2)}$ represent the sum of the last nine components on the right-hand side of the equation, so that:

$$\Phi^{(2)} = \Phi_d^{(2)} + \Phi_w^{(2)} \quad (9.30)$$

This $\Phi_w^{(2)}$ may be regarded as the second order equivalent of the first order undisturbed incoming wave potential $\Phi_w^{(1)}$.
Substitution of equation 9.30 in the second order boundary condition 9.21 yields:

$$\left(\vec{\nabla} \Phi_w^{(2)} + \vec{\nabla} \Phi_d^{(2)} \right) \cdot \vec{n} = \quad - \left(\vec{X}^{(1)} \cdot \vec{\nabla} \right) \cdot \vec{\nabla} \Phi^{(1)} \cdot \vec{n} \quad + \left(\vec{V}^{(1)} - \vec{\nabla} \Phi^{(1)} \right) \cdot \vec{N}^{(1)} \quad (9.31)$$

or for the diffraction potential:

$$\vec{\nabla} \Phi_d^{(2)} \cdot \vec{n} = \quad - \vec{\nabla} \Phi_w^{(2)} \cdot \vec{n} \quad - \left(\vec{X}^{(1)} \cdot \vec{\nabla} \right) \cdot \vec{\nabla} \Phi^{(1)} \cdot \vec{n} \quad + \left(\vec{V}^{(1)} - \vec{\nabla} \Phi^{(1)} \right) \cdot \vec{N}^{(1)} \quad (9.32)$$

If the right-hand side of this equation is known, $\Phi_d^{(2)}$ can be solved for the entire structure using numerical methods.

In general, however, $\Phi_w^{(2)}$ in equation 9.32 presents **a problem due to the complexity** of the surface boundary condition expressed by equation 9.15.
[Faltinsen and Loken, 1978a] have found exact solutions of this problem for two-dimensional cases, applicable to vessels in beam seas. [Newman, 1993] has developed numerical methods to solve for the second order potential for the three-dimensional case. [Pinkster, 1980] suggest an approximation for $\Phi_d^{(2)}$ which is applicable to three-dimensional problems.
In a later section of this chapter it will be shown that the second order potential $\Phi_d^{(2)}$ accounts only for a part of the second order wave forces.

Boundary Conditions at Infinity

A radiation condition for the potentials $\Phi_w^{(1)}$, $\Phi_b^{(1)}$ and $\Phi_d^{(2)}$ - which states that at a great distance from the body the waves associated with these potentials move outwards - must be satisfied. This restriction imposes a uniqueness which would not otherwise be present. Since the components of $\Phi_w^{(2)}$ are particular solutions to the free surface boundary condition 9.15 - which is defined over the complete free surface - a radiation condition need not be imposed on this term.

Symmetry Condition

The symmetry conditions, as discussed in chapter 5 and 7, are not taken into account here. The structure can have any arbitrary under water form.

Pressure at a Point within the Fluid

If the velocity potential Φ is known, the fluid pressure at a point is determined using the (non-linear) Bernoulli equation (see chapter 5):

$$p = -\rho g X_3 - \rho \frac{\partial \Phi}{\partial t} - \frac{1}{2}\rho \left(\vec{\nabla}\Phi\right)^2 \tag{9.33}$$

Assuming that this point is carrying out small - first order - wave frequency motions, $\vec{X}^{(1)}$, about a mean position, $\vec{X}^{(0)}$, and applying a Taylor expansion to the pressure in its mean position, yields:

$$p = p^{(0)} + \varepsilon p^{(1)} + \varepsilon^2 p^{(2)} \tag{9.34}$$

where:

- Hydrostatic pressure:
$$p^{(0)} = -\rho g X_3^{(0)} \tag{9.35}$$
- First order pressure:
$$p^{(1)} = -\rho g X_3^{(1)} - \rho \frac{\partial \Phi^{(1)}}{\partial t} \tag{9.36}$$
- Second order pressure:
$$p^{(2)} = -\frac{1}{2}\rho \left(\vec{\nabla}\Phi^{(1)}\right)^2 - \rho \frac{\partial^2 \Phi^{(2)}}{\partial t^2} - \rho \left(\vec{X}^{(1)} \cdot \vec{\nabla} \frac{\partial \Phi^{(1)}}{\partial t}\right) \tag{9.37}$$

The derivatives of the potentials in the above equations have to be evaluated at the mean position of the point.
It has been assumed that the point is moving within the fluid domain. The same expression can be used to determine the pressure on a point on the hull of the body. This means that derivatives of the potentials are taken at the mean position of the hull. This position is actually alternately within and outside the actual fluid domain. This appears to be permissible if the potential functions are sufficiently "smooth" at the boundaries; see [Joseph, 1973]. This is assumed to be satisfied in this case.

Direct Pressure Integration

Since in general one is concerned with the slow wave drift force induced motions of bodies in the horizontal plane, the wave drift force should be determined in the G-(x, y, z) coordinate system.
The fluid force exerted on the body, relative to the G-(x, y, z) system of axes - which is the system with axes parallel to the axes of the earth-bound system, O-(X_1, X_2, X_3) - follows from:

$$\vec{F} = -\iint_S p \cdot \vec{N} \cdot dS \tag{9.38}$$

where S is the instantaneous wetted surface and $\vec{N}$ is the instantaneous normal vector to the surface element dS relative to the $G(x, y, z)$ system of axes. The normal vector, $\vec{N}$, is given by equation 9.8 and the pressure, p, by equation 9.34.
The **instantaneous wetted surface**, S, is split into two parts: **a constant part**, S_0, up to the static hull waterline and **an oscillating part**, s, the splash zone between the static hull waterline and the wave profile along the body; see figure 9.23.

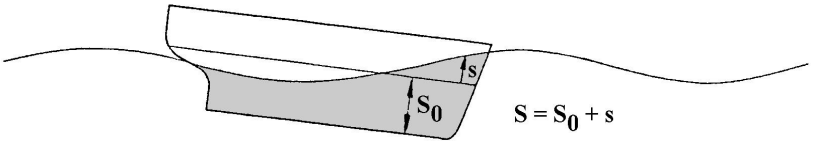

Figure 9.23: Wetted Surface

Substitution of all this in 9.38 yields for the fluid force exerted on the body:

$$\begin{aligned} \vec{F} &= -\iint_{S_0} \left(p^{(0)} + \varepsilon p^{(1)} + \varepsilon^2 p^{(2)}\right) \cdot \left(\vec{n} + \varepsilon \vec{N}^{(1)}\right) \cdot dS \\ &\quad -\iint_{s} \left(p^{(0)} + \varepsilon p^{(1)} + \varepsilon^2 p^{(2)}\right) \cdot \left(\vec{n} + \varepsilon \vec{N}^{(1)}\right) \cdot dS \end{aligned} \tag{9.39}$$

which can be written as follows:

$$\vec{F} = \vec{F}^{(0)} + \varepsilon \vec{F}^{(1)} + \varepsilon^2 \vec{F}^{(2)} + O(\varepsilon^3) \tag{9.40}$$

with:

$$\vec{F}^{(0)} = -\iint_{S_0} \left(p^{(0)} \cdot \vec{n}\right) \cdot dS \tag{9.41}$$

$$\begin{aligned} \varepsilon \vec{F}^{(1)} &= -\iint_{S_0} \left(p^{(0)} \cdot \varepsilon \vec{N}^{(1)}\right) \cdot dS - \iint_{S_0} \left(\varepsilon p^{(1)} \cdot \vec{n}\right) \cdot dS \\ &\quad -\iint_{s} \left(p^{(0)} \cdot \vec{n}\right) \cdot dS \end{aligned} \tag{9.42}$$

$$\begin{aligned} \varepsilon^2 \vec{F}^{(2)} &= -\iint_{S_0} \left(\varepsilon p^{(1)} \cdot \varepsilon \vec{N}^{(1)}\right) \cdot dS - \iint_{S_0} \left(\varepsilon^2 p^{(2)} \cdot \vec{n}\right) \cdot dS \\ &\quad -\iint_{s} \left(p^{(0)} \cdot \varepsilon \vec{N}^{(1)}\right) \cdot dS - \iint_{s} \left(\varepsilon p^{(1)} \cdot \vec{n}\right) \cdot dS \end{aligned} \tag{9.43}$$

Thus the fluid force is split here into three parts:
- a hydrostatic fluid force, $\vec{F}^{(0)}$,
- a first order oscillatory fluid force, $\vec{F}^{(1)}$,

- a second order fluid force, $\vec{F}^{(2)}$.

The **hydrostatic fluid force**, $\vec{F}^{(0)}$, follows from integration of the hydrostatic pressure, $p^{(0)}$, over the mean wetted surface, S_0, as given in equation 9.41:

$$\begin{aligned} \vec{F}^{(0)} &= -\iint_{S_0} \left(p^{(0)} \cdot \vec{n}\right) \cdot dS \\ &= \rho g \iint_{S_0} \left(X_3^{(0)} \cdot \vec{n}\right) \cdot dS \\ &= (0, 0, \rho g \nabla) \end{aligned} \tag{9.44}$$

which yields only a vertical force contribution, $F_3^{(0)}$, (no horizontal components):

$$\begin{aligned} F_3^{(0)} &= \rho g \iint_{S_0} (X_3 \cdot n_3) \cdot dS \\ &= \rho g \nabla \end{aligned} \tag{9.45}$$

in which ∇ is here the volume of displacement.

The **first order oscillatory fluid force**, $\vec{F}^{(1)}$, follows from equation 9.42:

$$\begin{aligned} \vec{F}^{(1)} &= -\iint_{S_0} \left(p^{(0)} \cdot \vec{N}^{(1)}\right) \cdot dS - \iint_{S_0} \left(p^{(1)} \cdot \vec{n}\right) \cdot dS \\ &\quad - \iint_{s} \left(p^{(0)} \cdot \vec{n}\right) \cdot dS \end{aligned} \tag{9.46}$$

which includes three integral terms:

1. Products of the hydrostatic pressures, $p^{(0)}$, and the first order oscillatory components of the normal vector, $\vec{N}^{(1)}$, which give first order force contributions over the constant part, S_0, of the wetted surface:

$$\begin{aligned} \vec{F}_A^{(1)} &= -\iint_{S_0} \left(p^{(0)} \cdot \vec{N}^{(1)}\right) \cdot dS \\ &= \rho g \iint_{S_0} \left(X_3^{(0)} \cdot \vec{N}^{(1)}\right) \cdot dS \end{aligned} \tag{9.47}$$

   which is - after using equation 9.9 (linear rotation-transformation) - equal to:

$$\begin{aligned} \vec{F}_A^{(1)} &= \rho g \iint_{S_0} \left(X_3^{(0)} \cdot \left\{R^{(1)} \cdot \vec{n}\right\}\right) \cdot dS \\ &= R^{(1)} \cdot (0, 0, \rho g \nabla) \end{aligned} \tag{9.48}$$

   This force component is caused by the rotating body axes; roll and pitch motions result in horizontal forces.

2. Products of the first order pressures, $p^{(1)}$, and the normal vector, $\vec{n}$, which give also first order force contributions over the constant part, S_0, of the wetted surface:

$$\vec{F}_B^{(1)} = -\iint_{S_0} \left(p^{(1)} \cdot \vec{n}\right) \cdot dS \tag{9.49}$$

3. Products of the hydrostatic pressures, $p^{(0)}$, and the normal vector, $\vec{n}$, which give (in principle) first order force contributions because of its integration over the oscillatory part, s, of the wetted surface.

$$\vec{F}_C^{(1)} = -\iint_s \left(p^{(0)} \cdot \vec{n}\right) \cdot dS = 0 \tag{9.50}$$

This term is zero because the hydrostatic pressure at the oscillating surface, $p^{(0)}$, is zero because it has to be determined at $X_3 = 0$.

Thus, the total first order fluid force follows from adding equations 9.48, 9.49 and 9.50:

$$\vec{F}^{(1)} = R^{(1)} \cdot (0, 0, \rho g \nabla) - \iint_{S_0} \left(p^{(1)} \cdot \vec{n}\right) \cdot dS \tag{9.51}$$

The **second order fluid force**, $\vec{F}^{(2)}$, follows from equation 9.43:

$$\begin{aligned} \vec{F}^{(2)} \;=\; & -\iint_{S_0} \left(p^{(1)} \cdot \vec{N}^{(1)}\right) \cdot dS - \iint_{S_0} \left(p^{(2)} \cdot \vec{n}\right) \cdot dS \\ & - \iint_{s} \left(p^{(0)} \cdot \vec{N}^{(1)}\right) \cdot dS - \iint_{s} \left(p^{(1)} \cdot \vec{n}\right) \cdot dS \end{aligned} \tag{9.52}$$

which includes four integral terms:

1. Products of the first order pressures, $p^{(1)}$, and the first order oscillatory components of the normal vector, $\vec{N}^{(1)}$, give second order force contributions over the constant part, S_0, of the wetted surface:

$$\vec{F}_A^{(2)} = -\iint_{S_0} \left(p^{(1)} \cdot \vec{N}^{(1)}\right) \cdot dS \tag{9.53}$$

When using equation 9.9 for $\vec{N}^{(1)}$ and equation 9.51 for the first order fluid force, one can write:

$$\begin{aligned} \vec{F}_A^{(2)} &= -R^{(1)} \cdot \iint_{S_0} \left(p^{(1)} \cdot \vec{n}\right) \cdot dS \\ &= R^{(1)} \cdot \left\{\vec{F}^{(1)} - R^{(1)} \cdot (0, 0, \rho g \nabla)\right\} \\ &= R^{(1)} \cdot \left\{\vec{F}^{(1)} - R^{(1)} \cdot (0, 0, mg)\right\} \end{aligned} \tag{9.54}$$

Equation 9.54 shows that a second order force along the earth-bound axes follows from the rotation of the first order fluid force and the gravitational force acting on the body; both relative to the body axes system. The last term deliver horizontal forces caused by the roll and pitch motions.
According to Newton's law, one may state that:

$$\vec{F}^{(1)} - R^{(1)} \cdot (0, 0, \rho g \nabla) = m \cdot \overrightarrow{\ddot{X}}_G^{(1)} \tag{9.55}$$

from which it follows that:

$$\vec{F}_A^{(2)} = R^{(1)} \cdot \left\{ \vec{F}^{(1)} + R^{(1)} \cdot (0, 0, \rho g \nabla) \right\} = m \cdot R^{(1)} \cdot \vec{\ddot{X}}_G^{(1)} \tag{9.56}$$

2. Products of the second order pressures, $p^{(2)}$, and the normal vector, $\vec{n}$, also give second order force contributions over the constant part, S_0, of the wetted surface:

$$\vec{F}_B^{(2)} = -\iint_{S_0} \left(p^{(2)} \cdot \vec{n} \right) \cdot dS \tag{9.57}$$

This part, $\vec{F}_B^{(2)}$, involves a straightforward integration of the second order pressure $p^{(2)}$ as given in equation 9.37 over the constant part, S_0, of the wetted surface of the body:

$$\vec{F}_B^{(2)} = \iint_{S_0} \left\{ \frac{1}{2}\rho \left(\vec{\nabla}\Phi^{(1)} \right)^2 + \rho \frac{\partial \Phi^{(2)}}{\partial t} + \rho \vec{X}^{(1)} \cdot \vec{\nabla} \frac{\partial \Phi^{(1)}}{\partial t} \right\} \cdot \vec{n} \cdot dS \tag{9.58}$$

3. Products of the hydrostatic pressures, $p^{(0)}$, and the first order oscillatory components of the normal vector, $\vec{N}^{(1)}$, give (in principle) second order force contributions because of its integration over the oscillatory part, s, of the wetted surface.

$$\vec{F}_C^{(2)} = -\iint_{s} \left(p^{(0)} \cdot \vec{N}^{(1)} \right) \cdot dS \tag{9.59}$$

Using equation 9.9 yields:

$$\vec{F}_C^{(2)} = -R^{(1)} \cdot \iint_{s} \left(p^{(0)} \cdot \vec{n} \right) \cdot dS = 0 \tag{9.60}$$

This term is zero because the hydrostatic pressure at the oscillating surface, $p^{(0)}$, is zero because it has to be determined at $X_3 = 0$.

4. Products of the first order pressures, $p^{(1)}$, and the normal vector, $\vec{n}$, give second order force contributions because of its integration over the oscillatory part, s, of the wetted surface.

$$\vec{F}_D^{(2)} = -\iint_{s} \left(p^{(1)} \cdot \vec{n} \right) \cdot dS \tag{9.61}$$

This part, $\vec{F}_D^{(2)}$, with an integration over the oscillating part, s, of the wetted surface, is found by substituting the expression for the first order pressure $p^{(1)}$ as given in equation 9.36 in here and writing the surface element dS as:

$$dS = dX_3 \cdot dl \tag{9.62}$$

in which dl is a differential length along the water line.
Also taking into account that the dynamic part of the pressure in the fluid at the waterline is:

$$-\rho \frac{\partial \Phi^{(1)}}{\partial t} = \rho g \zeta^{(1)} \tag{9.63}$$

this integral for $\vec{F}_D^{(2)}$ becomes:

$$\vec{F}_D^{(2)} = -\int_{wl}\int_{X_{3wl}^{(1)}}^{\zeta^{(1)}} \rho g \left(-X_3 + \zeta^{(1)}\right) \vec{n} \cdot dX_3 \cdot dl \tag{9.64}$$

The relative wave height, $\zeta_r^{(1)}$, is defined by a superposition of the first order wave elevation, $\zeta^{(1)}$, and the first order vertical motion of the hull at the water line, $X_{3wl}^{(1)}$:

$$\zeta_r^{(1)} = \zeta^{(1)} - X_{3wl}^{(1)} \tag{9.65}$$

This results in:

$$\vec{F}_D^{(2)} = -\oint_{wl} \frac{1}{2}\rho g \left(\zeta_r^{(1)}\right)^2 \cdot \vec{n} \cdot dl \tag{9.66}$$

Finally, the **total second order fluid force** is found from the separate contributions in equations 9.56, 9.58, 9.60 and 9.66:

$$\begin{aligned}
\vec{F}^{(2)} &= \vec{F}_A^{(2)} + \vec{F}_B^{(2)} + \vec{F}_D^{(2)} \qquad \left(\text{Remember: } \vec{F}_C^{(2)} = 0\right) \\
&= m \cdot R^{(1)} \cdot \ddot{\vec{X}}_G^{(1)} \\
&\quad + \iint_{S_0} \left\{ \frac{1}{2}\rho \left(\vec{\nabla}\Phi^{(1)}\right)^2 + \rho\frac{\partial \Phi^{(2)}}{\partial t} + \rho \vec{X}^{(1)} \cdot \vec{\nabla}\frac{\partial \Phi^{(1)}}{\partial t} \right\} \cdot \vec{n} \cdot dS \\
&\quad - \oint_{wl} \frac{1}{2}\rho g \left(\zeta_r^{(1)}\right)^2 \cdot \vec{n} \cdot dl
\end{aligned} \tag{9.67}$$

Notice that the added resistance of a ship in waves (also a second order phenomenon), as obtained by [Boese, 1970] in chapter 8, consists of two of these second order contributions:

$$R_{aw} = \vec{F}_A^{(2)} + \vec{F}_D^{(2)} \qquad \text{according to [Boese, 1970]} \tag{9.68}$$

Both of these contributions are related to products of two first order terms, as used in the linear theory in chapter 8. Of course, the contribution of $\vec{F}_B^{(2)}$ is missing in the linear theory there; this term includes the second order pressures.

9.3.2 Second Order Wave Moments

The moment of the fluid forces about the axes of the $G(X_1', X_2', X_3')$ system of coordinates follows from:

$$\vec{M} = -\iint_S p \cdot \left(\vec{X}' \times \vec{N}\right) \cdot dS \tag{9.69}$$

The derivation is analogous to that followed for the force and the final expression for the second order wave moment is:

$$\begin{aligned}\vec{M}^{(2)} &= I \cdot R^{(1)} \cdot \vec{\ddot{X}}_G^{(1)} \\ &+ \iint_{S_0} \left\{ \frac{1}{2}\rho \left(\vec{\nabla}\Phi^{(1)} \right)^2 + \rho \frac{\partial \Phi^{(2)}}{\partial t} + \rho \cdot \vec{X}^{(1)} \cdot \vec{\nabla} \frac{\partial \Phi^{(1)}}{\partial t} \right\} \cdot (\vec{x} \times \vec{n}) \cdot dS \\ &- \oint_{wl} \frac{1}{2}\rho g \left(\zeta_r^{(1)} \right)^2 \cdot (\vec{x} \times \vec{n}) \cdot dl \end{aligned} \tag{9.70}$$

in which I is the mass moment of inertia about the considered body axis of the structure.

9.3.3 Quadratic Transfer Functions

In this section it will be shown that equations 9.67 and 9.70 which are, in waves, functions of time, may be used to compute quadratic transfer functions for the mean and low frequency force and moment components. These in turn will allow determination of the wave drift forces and moments in the frequency domain, and after taking double Fourier transforms, allow prediction of the forces in the time domain, see [Dalzell, 1976] and [Kim and Breslin, 1976].

The procedure to obtain the quadratic transfer functions of the forces will first be **illustrated** by taking the low frequency part of the longitudinal component of the last part of equation 9.67 which refers to the force contribution due to the relative wave height:

$$F_1^{(2)} = F_1^{(2)}(t) = - \oint_{wl} \frac{1}{2}\rho g \left(\zeta_r^{(1)}(t,l) \right)^2 \cdot n_1 \cdot dl \tag{9.71}$$

In irregular long-crested waves, the elevation - to first order of the incoming, undisturbed waves - referred to the mean position of the centre of gravity of the floating body may be written as:

$$\zeta^{(1)}(t) = \sum_{i=1}^{N} \zeta_i^{(1)} \cdot \cos\left(\omega_i t + \tilde{\varepsilon}_i\right) \tag{9.72}$$

The first order relative wave height at a point l on the waterline of the body may be written as follows:

$$\zeta_r^{(1)}(t,l) = \sum_{i=1}^{N} \zeta_i^{(1)} \cdot \zeta_{r_i}^{(1)'}(l) \cdot \cos(\omega_i t + \tilde{\varepsilon}_i + \varepsilon_{r_i}(l)) \tag{9.73}$$

Substitution of 9.73 in equation 9.71 leads to:

$$\begin{aligned} F_1^{(2)}(t) &= \sum_{i=1}^{N}\sum_{j=1}^{N} \zeta_i^{(1)}\zeta_j^{(1)} P_{ij} \cdot \cos\left\{(\omega_i - \omega_j)t + (\tilde{\varepsilon}_i - \tilde{\varepsilon}_j)\right\} \\ &+ \sum_{i=1}^{N}\sum_{j=1}^{N} \zeta_i^{(1)}\zeta_j^{(1)} Q_{ij} \cdot \sin\left\{(\omega_i - \omega_j)t + (\tilde{\varepsilon}_i - \tilde{\varepsilon}_j)\right\} \end{aligned} \tag{9.74}$$

The high frequency terms (sum frequency terms) have been disregarded in this equation. In equation 9.74 P_{ij} and Q_{ij} are the components of the time independent quadratic transfer function with:

$$P_{ij} = \oint_{wl} \frac{1}{4}\rho g \zeta_{r_i}^{(1)'}(l) \cdot \zeta_{r_j}^{(1)'}(l) \cdot \cos\{\varepsilon_{r_i}(l) - \varepsilon_{r_j}(l)\} \cdot n_1 \cdot dl \tag{9.75}$$

$$Q_{ij} = \oint_{wl} \frac{1}{4}\rho g \zeta_{r_i}^{(1)'}(l) \cdot \zeta_{r_j}^{(1)'}(l) \cdot \sin\{\varepsilon_{r_i}(l) - \varepsilon_{r_j}(l)\} \cdot n_1 \cdot dl \tag{9.76}$$

Taking now the low frequency part of the square of the wave elevation given by equation 9.72 results in:

$$\left(\zeta_{LF}^{(1)}(t)\right)^2 = \sum_{i=1}^{N}\sum_{j=1}^{N} \frac{1}{2}\zeta_i^{(1)}\zeta_j^{(1)} \cdot \cos\{(\omega_i - \omega_j)t + (\tilde{\varepsilon_i} - \tilde{\varepsilon_j})\} \tag{9.77}$$

Comparison with equation 9.74 shows that P_{ij} and Q_{ij} are transfer functions which give that part of the wave drift force which is in-phase and out-of-phase respectively with the low frequency part of the square of the incident waves.
It will be clear that similar developments can be made for other contributions to the wave drift forces which are dependent on products of first order quantities.

Approximation for Second Order Potential Contribution

As mentioned in a previous section, the contribution to the drift forces due to the second order potential presents special problems due to the non-linear nature of the free-surface condition and the complexity of the body boundary conditions. This section discusses a method to approximate the effect of the second order potential.
The approximation is based on the assumption that the major part of the low frequency second order force due to the second order potential is the wave exciting force component due to the contribution $\Phi_{ww}^{(2)}$ of the undisturbed incoming waves to the second order potential. This assumes that the first order diffraction and body motion potentials $\Phi_d^{(1)}$ and $\Phi_b^{(1)}$ are small relative to the undisturbed wave potential $\Phi_w^{(1)}$. This means that the right-hand side of the free surface boundary condition of equation 9.15 only involves terms associated with the first order velocity potential $\Phi_w^{(1)}$ of the undisturbed incoming waves. The second order potential which satisfies this boundary condition and the boundary condition at the sea bed as well as the equation of continuity has been given by [Bowers, 1975].
We now consider a regular wave group travelling in the positive X_1-direction consisting of two regular waves with frequencies ω_i and ω_j with $\omega_i > \omega_j$.
The first order velocity potential associated with these waves is:

$$\Phi_w^{(1)} = -\sum_{i=1}^{N} \frac{\zeta_i^{(1)}\, g\, \cosh k_i\,(X_3 - h)}{\omega_i\, \cosh k_i\, h} \cdot \sin(k_i\, X_1 - \omega_i\, t + \tilde{\varepsilon_i}) \tag{9.78}$$

The low frequency component of the second order potential associated with these waves is as follows:

$$\Phi_{ww}^{(2)} = - \sum_{i=1}^{N}\sum_{j=1}^{N} \zeta_i^{(1)}\zeta_j^{(1)} \cdot A_{ij} \cdot \frac{\cosh\{(k_i - k_j)(X_3 - h)\}}{\cosh(k_i - k_j)\, h}\,.$$

$$\cdot \sin\{(k_i - k_j)X_1 - (\omega_i - \omega_j)t + (\tilde{\varepsilon_i} - \tilde{\varepsilon_j})\} \tag{9.79}$$

in which A_{ij} is a coefficient depending on ω_i and ω_j and on the water depth h:

$$A_{ij} = \frac{g}{2} \cdot \frac{B_{ij} + C_{ij}}{(\omega_i - \omega_j)^2 - (k_i - k_j)g \cdot \tanh(k_i - k_j)\, h} \tag{9.80}$$

in which:

$$B_{ij} = \frac{k_i^2}{\omega_i \cosh^2 k_i h} - \frac{k_j^2}{\omega_j \cosh^2 k_j h} \tag{9.81}$$

$$C_{ij} = \frac{2k_i k_j \cdot (\omega_i - \omega_j) \cdot (1 + \tanh k h \tanh k_j h)}{\omega_i \omega_j} \tag{9.82}$$

The low frequency component of this second order potential represents a long wave which is induced by the presence of the regular wave group. The phase of this long wave - relative to the wave group - is such that it has a trough where the wave group attains its maximum wave elevation and a crest where it attains its minimum elevation. This is shown in figure 9.24.

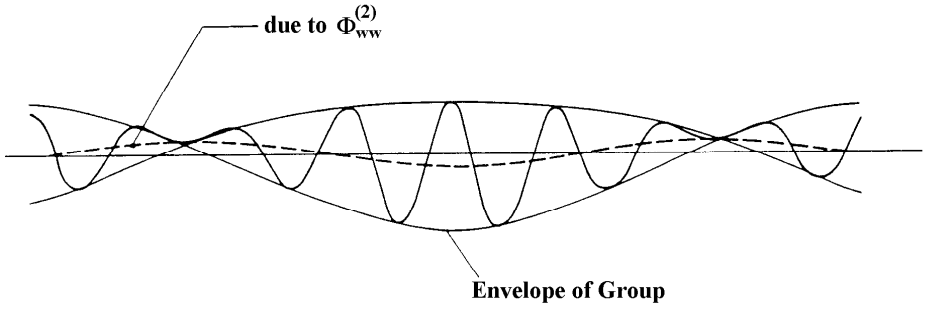

Figure 9.24: Wave due to Second Order Potential in a Regular Wave Group

The potential associated with such a wave does not satisfy the boundary condition on the body which for the simplified case is assumed to be equivalent to the normal first order boundary condition. This means that contributions due to products of first order quantities are neglected in the right-hand-side of equation 9.32.
The second order diffraction potential $\Phi_d^{(2)}$ in equation 9.36 satisfies the equation of continuity, the boundary condition at the sea floor, the radiation condition and the homogeneous free surface condition:

$$g \cdot \frac{\partial \Phi}{\partial X_3} + \frac{\partial^2 \Phi}{\partial t^2} = 0 \tag{9.83}$$

This last relationship gives rise to the well known dispersion relationship:

$$\omega^2 = kg \cdot \tanh kh \tag{9.84}$$

The incoming waves due to the low frequency second order potential have a wave number equal to $k_i - k_j$ and a wave frequency equal to $\omega_i - \omega_j$. These waves do not satisfy the dispersion equation 9.84.

If the incoming waves have a frequency of $\omega_i - \omega_j$ then the diffracted waves have the same frequency; the wave number will follow from the relationship:

$$(\omega_i - \omega_j)^2 = k\,g \cdot \tanh\, k\,h \tag{9.85}$$

In order to simplify the situation we allow the diffracted waves to have the same wave number $k_i - k_j$ as the incoming waves. This means that differences will occur in the diffracted waves further away from the body. Close to the body the situation will be similar since the boundary condition at the body still has to be satisfied. The reason for this assumption regarding the wave number of the diffracted waves will be apparent from the following.

The problem has been reduced to a situation where one has to determine the wave exciting force on the body due to a wave which has a velocity potential given by equation 9.79. The diffracted waves have the same wave number as the incoming waves. This is solved by considering the ordinary first order wave exciting force $F^{(1)}$ on the body in a regular wave with wave number equal to $k_i - k_j$ in an ordinary gravity field. For such a case the associated wave frequency ω will be in accordance with the dispersion relationship equation 9.84. The frequency of this wave can be made equal to the frequency $\omega_i - \omega_j$ of the second order waves by selecting a different value for the acceleration of gravity:

$$g_{ij} = \frac{(\omega_i - \omega_j)^2}{(k_i - k_j) \cdot \tanh(k_i - k_j)h} \tag{9.86}$$

Since the wave exciting force is proportional to the acceleration of gravity, the initial force $F^{(1)}$ in a wave with frequency ω, which follow from equation 9.84, becomes a second order wave force with frequency $\omega_i - \omega_j$ by simply applying the factor:

$$n_{ij} = \frac{g_{ij}}{g} \tag{9.87}$$

to the initial force.

This does not complete the transformation however, since besides satisfying the requirement that wave number and wave frequency be equal, the amplitude of the potentials must also be equal. After alteration of the acceleration of gravity, the transformed potential of the first order wave is:

$$\Phi = -\frac{\zeta_a^{(1)}\, g_{ij}}{(\omega_i - \omega_j)} \cdot \frac{\cosh\{(k_i - k_j)(X_3 - h)\}}{\cosh(k_i - k_j)\, h} \cdot \sin\left\{(k_i - k_j)X_1 - (\omega_i - \omega_j)t + (\tilde{\varepsilon_i} - \tilde{\varepsilon_j})\right\} \tag{9.88}$$

The amplitude of the second order potential is given in equation 9.79. Equality of the amplitudes means that:

$$\frac{\zeta_a^{(1)}\, g_{ij}}{(\omega_i - \omega_j)} = \zeta_i^{(1)}\, \zeta_j^{(1)} \cdot A_{ij} \tag{9.89}$$

This means that the first order wave amplitude must be selected so that:

$$\zeta_a^{(1)} = \zeta_i^{(1)}\, \zeta_j^{(1)} \cdot \frac{A_{ij}(\omega_i - \omega_j)}{g_{ij}} \tag{9.90}$$

The first order force $F^{(1)}$ is determined for a value of unity for the wave amplitude ζ_a. Since forces are proportional to the wave amplitude, equation 9.90 gives a second correction factor

which has to be applied to the force $F^{(1)}$ in order to give the required second order force $F^{(2)}$:

$$F_{ij}^{(2)} = n_{ij} \cdot \frac{\zeta_i^{(1)} \zeta_j^{(1)} \cdot A_{ij} (\omega_i - \omega_j)}{g_{ij}} \cdot F^{(1)} \tag{9.91}$$

which, taking into account equation 9.87, gives:

$$F_{ij}^{(2)} = f_{ij} \cdot F^{(1)} \tag{9.92}$$

where:

$$f_{ij} = \frac{\zeta_i^{(1)} \zeta_j^{(1)} \cdot A_{ij} (\omega_i - \omega_j)}{g} \tag{9.93}$$

Equation 9.92 transforms a first order wave force into a second order wave force. As can be seen from this equation, the second order force becomes a function of two frequencies ω_i and ω_j. This approximation for the second order force can also be expressed in terms of contributions to the coefficients P_{ij} and Q_{ij}.

Wave Drift Forces in Regular Wave Groups

From the previous sections it was seen that the total wave drift forces may thus be expressed in terms of transfer functions which are a function of two frequencies.
The most elementary sea state which gives low frequency wave drift forces is one which consists of two regular waves with amplitude, frequency and random phase of $\zeta_1, \omega_1, \varepsilon_1$ and $\zeta_2, \omega_2, \varepsilon_2$ respectively, with $\omega_1 > \omega_2$.

$$\zeta(t) = \zeta_1 \cdot \cos(\omega_1 t + \varepsilon_1) + \zeta_2 \cdot \cos(\omega_2 t + \varepsilon_2) \tag{9.94}$$

The wave drift force in such a case is:

$$\begin{aligned} F^{(2)}(t) = \quad & \zeta_1^2.P_{11} + \zeta_2^2.P_{22} \\ & + \zeta_1\zeta_2(P_{12} + P_{21}) \cdot \cos\{(\omega_1 - \omega_2)t + (\varepsilon_1 - \varepsilon_2)\} \\ & + \zeta_1\zeta_2(Q_{12} - Q_{21}) \cdot \sin\{(\omega_1 - \omega_2)t + (\varepsilon_1 - \varepsilon_2)\} \end{aligned} \tag{9.95}$$

The frequency of the low frequency part of the wave drift force is equal to the difference between the frequencies of the regular wave components. This is the frequency of the regular wave group which is the result of superposition of two regular waves (see figure 9.25). It is noted that the constant part of the wave drift force is the sum of the constant parts due to each of the wave components. The amplitude of the quadratic transfer function is:

$$|T_{ij}| = \sqrt{P_{ij}^2 + Q_{ij}^2} \tag{9.96}$$

Since P_{ij} and Q_{ij}, etc. never occur in isolation, it can be so arranged that certain symmetry relations are valid:

$$P_{ij} = P_{ji} \tag{9.97}$$

$$Q_{ij} = -Q_{ji} \tag{9.98}$$

$$|T_{ij}| = |T_{ji}| \tag{9.99}$$

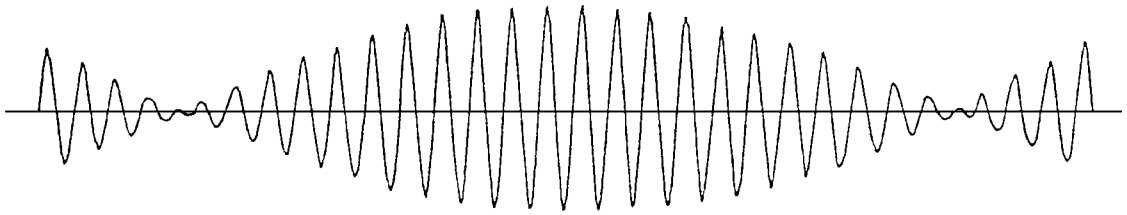

Figure 9.25: Regular Wave Group

Frequency Domain Calculation of Mean and Low Frequency Drift Force

The mean drift force in irregular waves with spectral density $S_{\zeta\zeta}(\omega)$ is found by putting $\omega_1 = \omega_2$ in equation 9.74:

$$F^{(2)}_{1_{mean}} = \sum_{i=1}^{N} \zeta_i^{(1)^2} \cdot P_{ii} \tag{9.100}$$

which, taking into account that:

$$\zeta_i^{(1)^2} = 2 \cdot S_\zeta(\omega_i) \cdot d\omega_i \qquad \text{(see chapter 5)} \tag{9.101}$$

results in:

$$F^{(2)}_{1_{mean}} = 2 \int_0^\infty S_\zeta(\omega) \cdot P(\omega, \omega) \cdot d\omega \tag{9.102}$$

where $P(\omega, \omega)$ is known as the mean drift force coefficient in regular waves.
By using equation 9.74 with $i = j$, $P(\omega, \omega$ is also written as:

$$P(\omega, \omega) = \frac{F_1}{\zeta_a^2}(\omega) \tag{9.103}$$

Similarly it can be shown that the spectral density of the low frequency part of the wave drift force is:

$$S_F(\mu) = 8 \int_0^\infty S_\zeta(\omega_1) \cdot S_\zeta(\omega_2) \cdot |T(\omega_1, \omega_2)|^2 \cdot d\omega \tag{9.104}$$

where $\omega_1 - \omega_2 = \mu$ is the low frequency and $\mid T(\omega_1, \omega_2) \mid$ is the amplitude of the quadratic transfer function.
Equation 9.104 can also be written as:

$$S_F(\mu) = 8 \int_0^\infty S_\zeta(\omega + \mu) \cdot S_\zeta(\omega) \cdot |T(\omega + \mu, \omega)|^2 \cdot d\omega \tag{9.105}$$

9.3.4 Computed Results of Wave Drift Forces

The expression for the wave drift forces and moments given by equations 9.67 and 9.70 have been evaluated at MARIN, using a three-dimensional singularity distribution computer program, see [Pinkster, 1977] and [Pinkster, 1980]. The computations have been performed for a number of the cases and the results have been compared with some analytical solutions and results of model tests. All results are for zero forward speed.

Mean Drift Forces in Regular Waves

Figure 9.26 compares the computed horizontal drift force on a free floating hemisphere to an analytical result given by [Kudou, 1977].
Figure 9.27 compares the computed mean vertical drift force on a long free floating submerged cylinder in beam seas to two-dimensional analytical results given by [Ogilvie, 1963].
Figure 9.28 compares the computed mean horizontal drift force on a long free floating cylinder in beam seas to two-dimensional results given by [Faltinsen and Loken, 1979] based on Maruo's theory.
Figure 9.30 (see also [Pinkster, 1979] and [Pinkster, 1980]) compares the computed mean drift force on a rectangular barge and a semi-submersible in head seas to results of measurements carried out at MARIN. The vessels are shown in figure 9.29. In general it can be said that the computations compare favorably with analytical solutions and results of model tests.

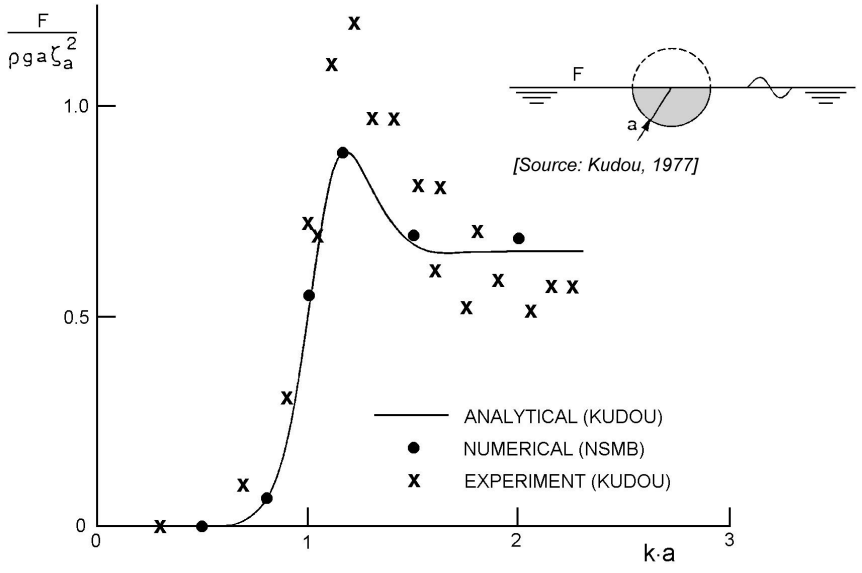

Figure 9.26: Mean Horizontal Wave Drift Forces on a Floating Sphere

Components of Mean Wave Drift Forces

This section gives results of calculations which reveals the importance of various contributions to the mean drift forces as given by equation 9.67; this yields after re-arranging the terms in this equation in a sequence as given by [Pinkster, 1980]:

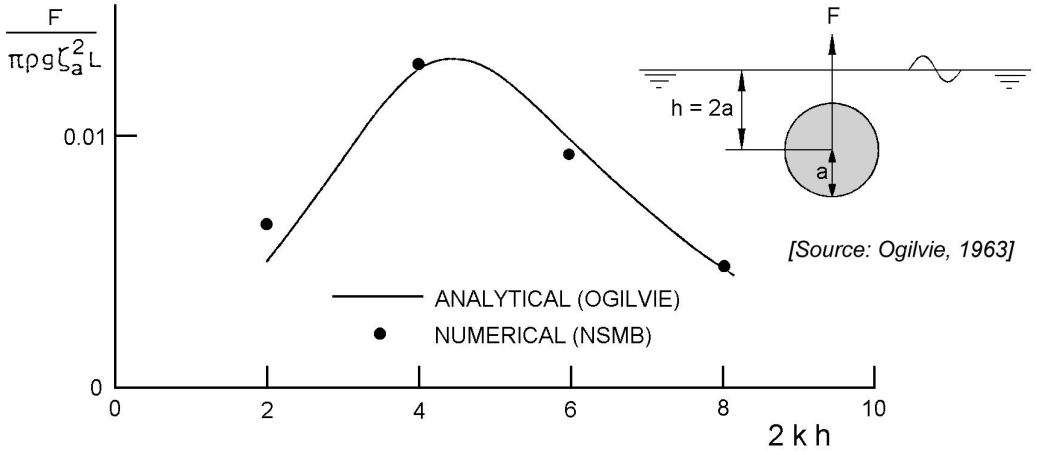

Figure 9.27: Mean Vertical Wave Drift Forces on a Submerged Cylinder

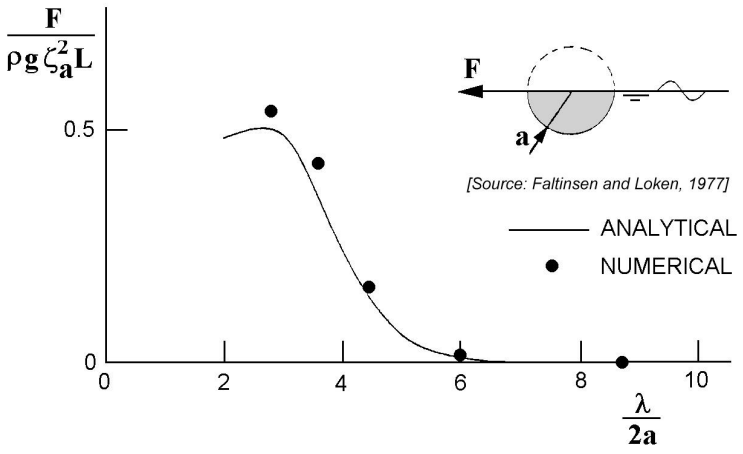

Figure 9.28: Mean Horizontal Wave Drift Forces on a Cylinder

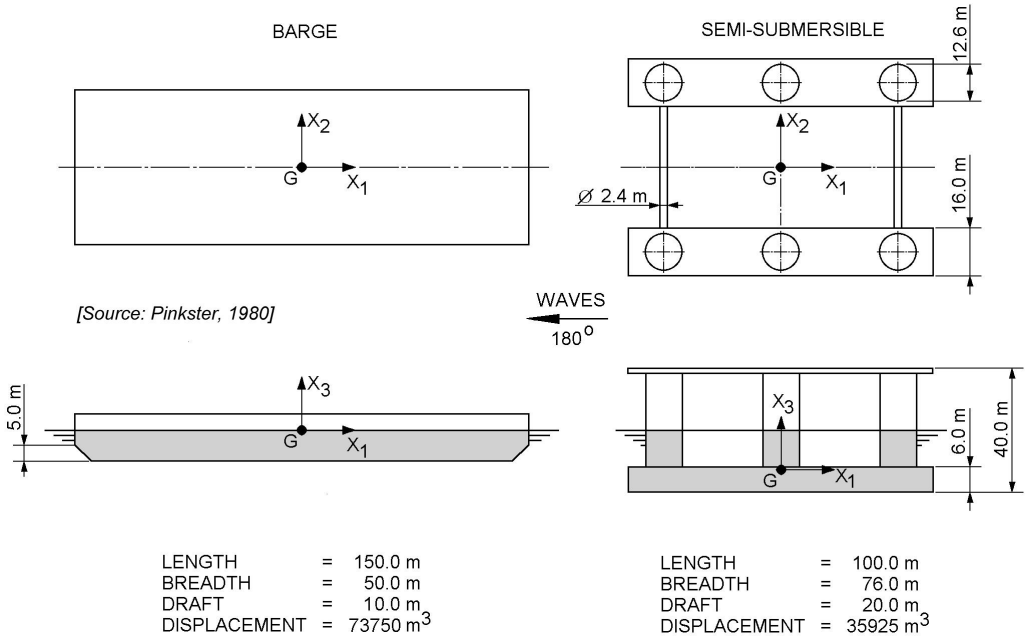

Figure 9.29: Vessels used for Experiments

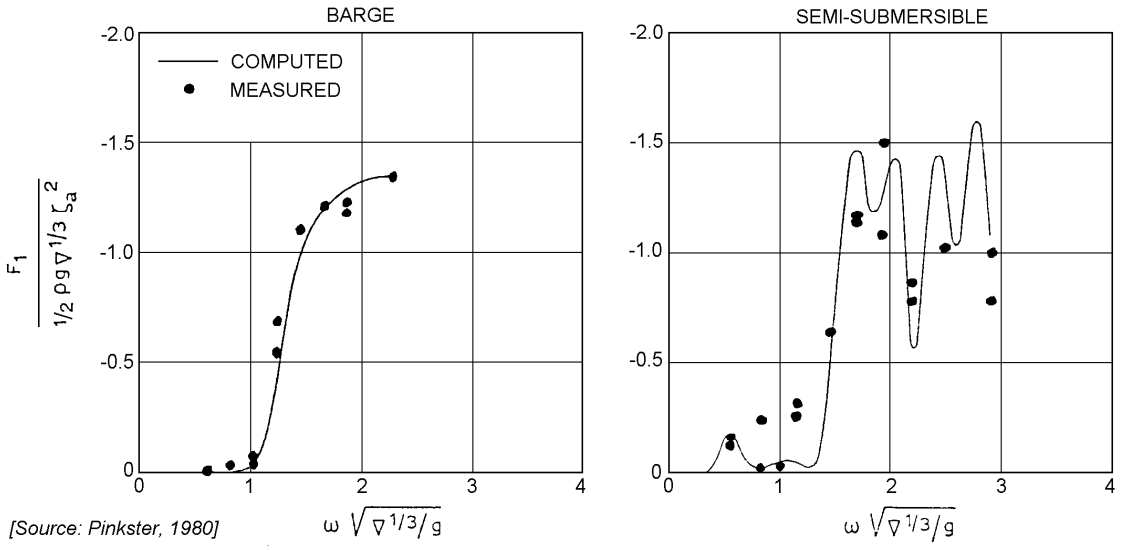

Figure 9.30: Mean Surge Drift Forces in Regular Head Waves

$$\begin{aligned}
\vec{F}^{(2)} &= -\frac{1}{2}\rho g \oint_{wl} \left(\zeta_r^{(1)}\right)^2 \cdot \vec{n} \cdot dl \\
&+\frac{1}{2}\rho \iint_{S_0} \left(\vec{\nabla}\Phi^{(1)}\right)^2 \cdot \vec{n} \cdot dS \\
&+\rho \iint_{S_0} \vec{X}^{(1)} \cdot \vec{\nabla}\frac{\partial \Phi^{(1)}}{\partial t} \cdot \vec{n} \cdot dS \\
&+m \cdot R^{(1)} \cdot \ddot{\vec{X}}_G^{(1)} \\
&+\rho \iint_{S_0} \frac{\partial \Phi^{(2)}}{\partial t} \cdot \vec{n} \cdot dS
\end{aligned} \tag{9.106}$$

Figure 9.31 gives the five components of the computed mean surge drift force on a rectangular barge and a semi-submersible in head waves.

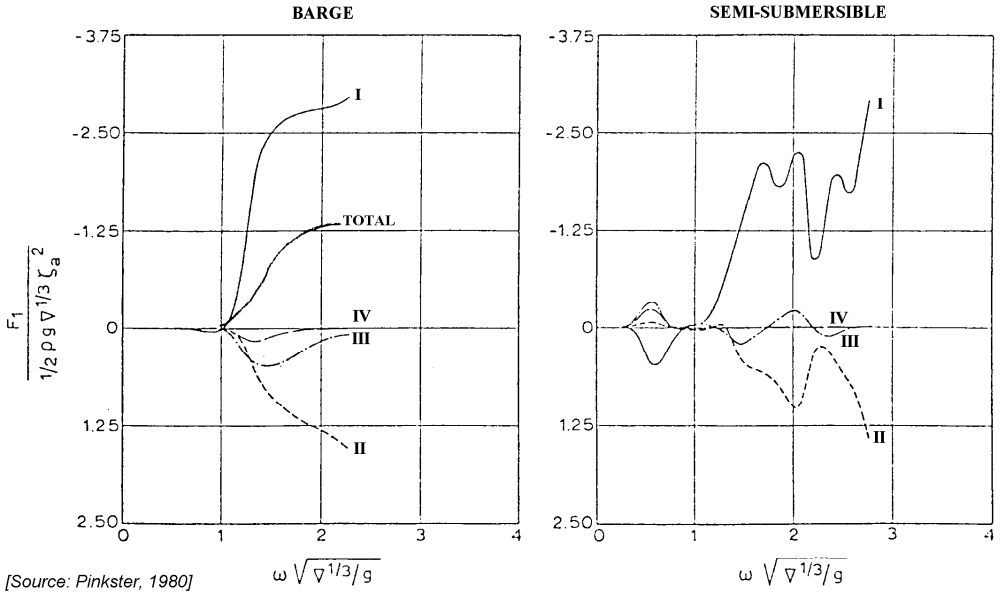

Figure 9.31: Components of Computed Mean Surge Drift Forces

The numerals in these figures refer to the following components of the mean force:

I: Relative wave height contribution:

$$-\frac{1}{2}\rho g \oint_{wl} \left(\zeta_r^{(1)}\right)^2 \cdot n_1 \cdot dl$$

II: Pressure drop due to velocity squared:

$$\frac{1}{2}\rho \iint_{S_0} \left(\vec{\nabla}\Phi^{(1)}\right)^2 \cdot n_1 \cdot dS \tag{9.107}$$

III: Pressure due to product of gradient of first order pressure and first order motion:

$$\rho \iint_{S_0} \left(\vec{X}^{(1)} \cdot \vec{\nabla} \Phi^{(1)} \right) \cdot n_1 \cdot dS \tag{9.108}$$

IV: Contribution due to product of pitch motion and heave inertia force:

$$m \cdot x_5^{(1)} \cdot \ddot{X}_{3_G}^{(1)} \tag{9.109}$$

V: Contribution due to the second order potential $\Phi^{(2)}$, which is zero in regular waves:

$$\rho \iint_{S_0} \frac{\partial \Phi^{(2)}}{\partial t} \cdot \vec{n} \cdot dS \tag{9.110}$$

The results in figure 9.31 show that in general contribution I due to the relative wave height is dominant, while the three remaining terms II, III and IV tend only to reduce somewhat the effect of contribution I. For high frequencies (to the right in the figures) terms III and IV vanish since the body motions - on which these terms are dependent - reduce to zero in short waves. This leaves only the terms I and II.
For the semi-submersible in figure 9.31 it is apparent that it is the wave drift forces acting on the columns which form the greater part of the total horizontal wave drift forces.
Figure 9.32 shows the computed contributions to the mean horizontal drift force on the floating sphere. In this case only contributions I, II and III play a part. As the frequency increases again only contributions I and II remain.
Figure 9.33 shows the computed contributions to the vertical force on the submerged cylinder in beam seas. Since there is no waterline, only contributions II and III play a role. For high frequencies only II remains.

9.3.5 Low Frequency Motions

In view of the analogy which exists between the low frequency waves, the drift forces and the low frequency part of the square of the elevations of the incident waves as indicated by equations 9.74 and 9.77, we will look at some aspects of the waves. This will give some indications regarding the properties of the low frequency wave drift forces.
The irregular waves are assumed to behave as a random Gaussian process. Thus, the wave elevation in a fixed point in irregular waves, may be written as follows:

$$\zeta(t) = \sum_{i=1}^{N} \zeta_i \cdot \sin\left(\omega_i t + \tilde{\varepsilon}_i\right) \tag{9.111}$$

where $\tilde{\varepsilon}_i$ is a random phase angle.
In amplitude modulated form this becomes:

$$\zeta(t) = A(t) \cdot \sin\left(\omega_0 t + \varepsilon(t)\right) \tag{9.112}$$

where:

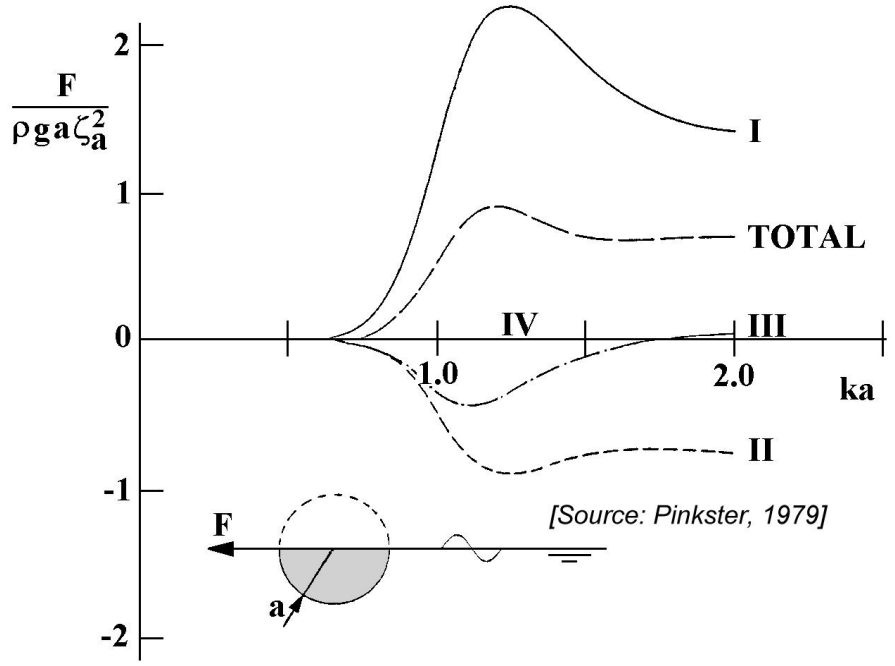

Figure 9.32: Components of Computed Mean Horizontal Drift Forces on a Sphere

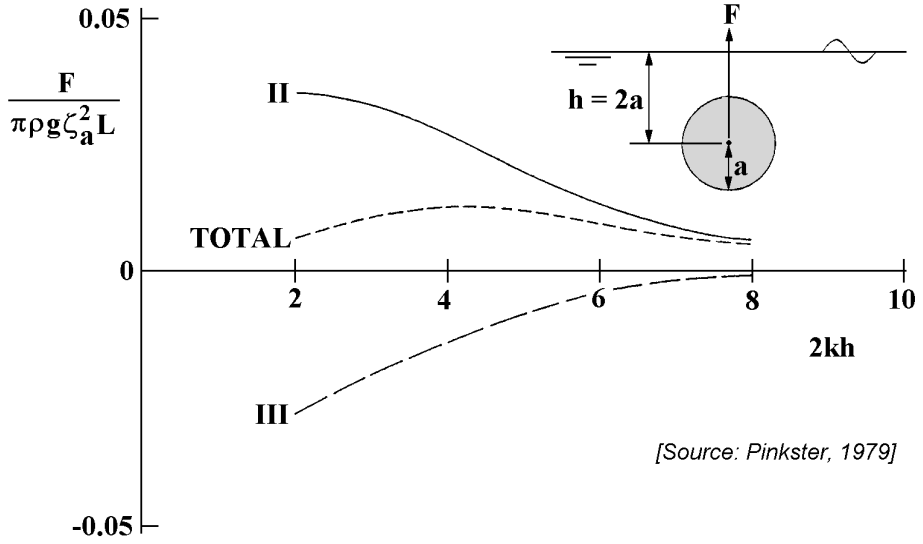

Figure 9.33: Components of Computed Mean Vertical Drift Forces on a Submerged Cylinder

$$\begin{aligned} A(t) = &= \text{wave envelope} = \sqrt{\sum_{i=1}^{N}\sum_{i=1}^{N}\zeta_i\zeta_j \cdot \cos\{(\omega_i-\omega_j)t + (\tilde{\varepsilon_i}-\tilde{\varepsilon_j})\}} \\ \varepsilon(t) &= \text{slowly varying phase angle} \\ \omega_0 &= \text{some centrally chosen fixed wave frequency} \end{aligned}$$

The behavior of the wave envelope, $A(t)$, contains information with respect to the grouping of waves. Squaring the wave elevation, $\zeta(t)$, and taking only the low frequency part gives:

$$\begin{aligned} \zeta_{lf}^2(t) &= \frac{1}{2}\sum_{i=1}^{N}\sum_{j=1}^{N}\zeta_i\zeta_j \cdot \cos\{(\omega_i-\omega_j)t + (\tilde{\varepsilon_i}-\tilde{\varepsilon_j})\} \\ &= \frac{1}{2}A^2(t) \end{aligned} \tag{9.113}$$

This shows that the low frequency part of the square of the wave elevation also contains information on wave grouping.
From equation 9.113 it follows that:

$$A^2(t) = 2\zeta_{lf}^2(t) \tag{9.114}$$

Based on the assumption that the wave elevations are normally distributed, it can be shown that the spectral density, $S_g(\mu)$ of $A^2(t)$, is related to the normal wave spectrum, $S_\zeta(\omega)$, in the following way:

$$S_g(\mu) = 8\int_0^\infty S_\zeta(\omega)\cdot S_\zeta(\omega+\mu)\cdot d\omega \tag{9.115}$$

The distribution function of $A^2(t)$ is, for a narrow-banded spectrum:

$$f(A^2) = \frac{1}{2m_0}\cdot e^{-\frac{A^2}{2m_0}} \tag{9.116}$$

where:

$$m_0 = \int_0^\infty S_\zeta(\omega)\cdot d\omega \tag{9.117}$$

This is the Rayleigh distribution for wave heights used in chapter 5.
From the above, it follows that knowledge of $S_\zeta(\omega)$ and the assumption that the wave elevation is normally distributed is sufficient to calculate the spectral density and distribution function of $A^2(t)$. From this relationship it follows that the spectral density and distribution may also be calculated from the low frequency part of the square of the record of the wave elevation measured in the basin. If the waves are completely random then the spectral density and distribution obtained from and based on the normal (first) spectrum of the waves should correspond with the spectral density and distribution of $2\zeta_{lf}^2$ calculated directly from the wave record.
The distribution function $p(A^2)$ and $p(2\zeta_{lf}^2)$ and the spectral density of the waves and of A^2 and $2\zeta_{lf}^2$ are shown in figure 9.34 and figure 9.35 respectively for an irregular wave train generated in a basin of MARIN.
From equation 9.114 it follows that the wave envelope is related to the low-pass filtered square of the wave elevation:

$$A(t) = \sqrt{2}\cdot\zeta_{lf}(t) \tag{9.118}$$

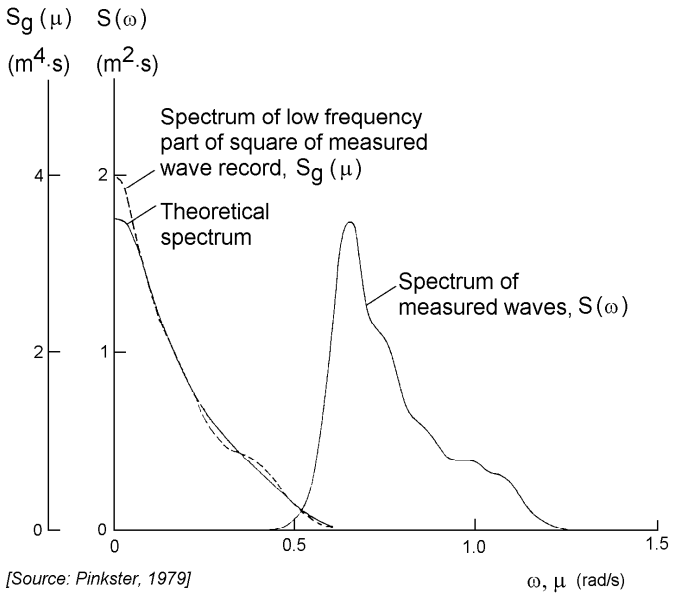

Figure 9.34: Wave Spectra and Low-Frequency Part of the Square of a Wave Record

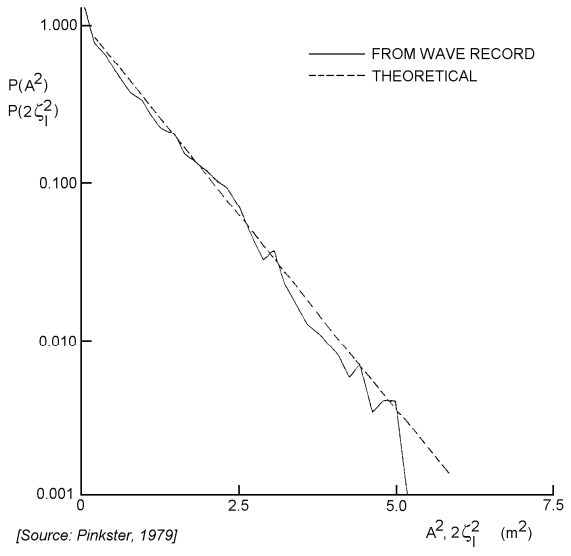

Figure 9.35: Distribution Function of Low-Frequency Part of the Square of a Wave Record

In order to show that this operation does indeed represents the wave envelope, results are plotted in figure 9.36 showing the wave elevation $\zeta(t)$ and the corresponding wave envelope $A(t)$ calculated in accordance with equation 9.118. Also shown in the same figure is the record of the wave elevation $\zeta(t)$ divided by the envelope $A(t)$.
According to equation 9.112:

$$\sin\left(\omega_0 t + \varepsilon(t)\right) = \frac{\zeta(t)}{A(t)} \tag{9.119}$$

From this it is seen that the signal oscillates between $+1$ and -1 with varying frequency. From figure 9.36 it is seen that generally this agrees quite well with theory. The slowly varying nature of the frequency can be seen quite clearly.
In the foregoing, both the behavior of the envelope $A(t)$ and the square of the envelope have been treated. More attention should, however, be given to the behavior of the square of the envelope in view of the analogy between this quantity and the low frequency second order wave drifting forces.

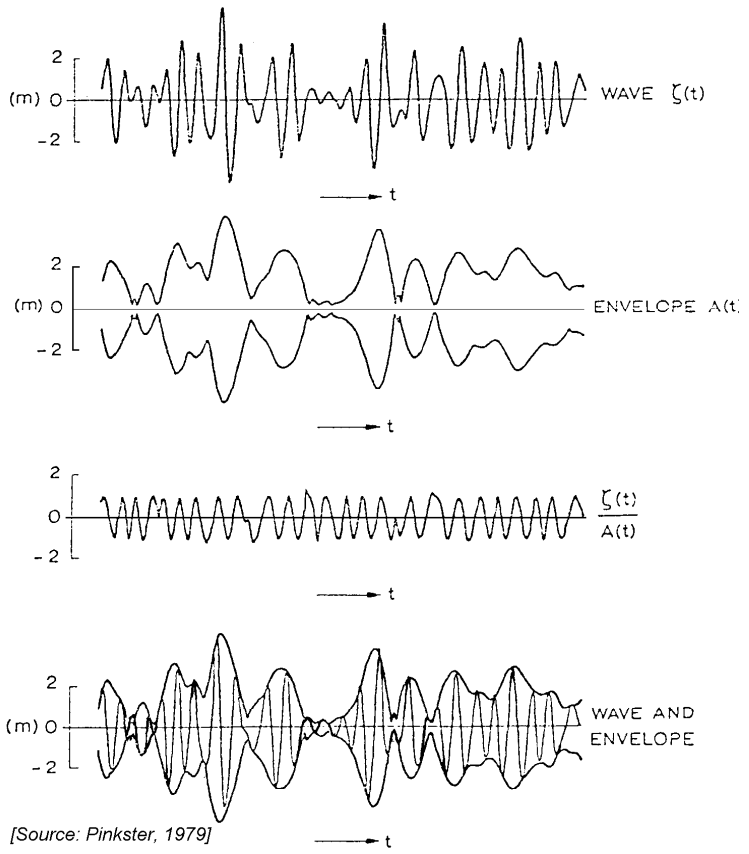

Figure 9.36: Irregular Waves and Wave Enveloppe

The similarity between the low frequency surge and sway drift forces on a tanker in bow quartering waves and the low frequency part of the square of the incident waves is apparent in figure 9.37. These results were measured during model tests.
The distribution function of the low frequency surge drift force in irregular waves measured on a tanker in head seas is given in figure 9.38.

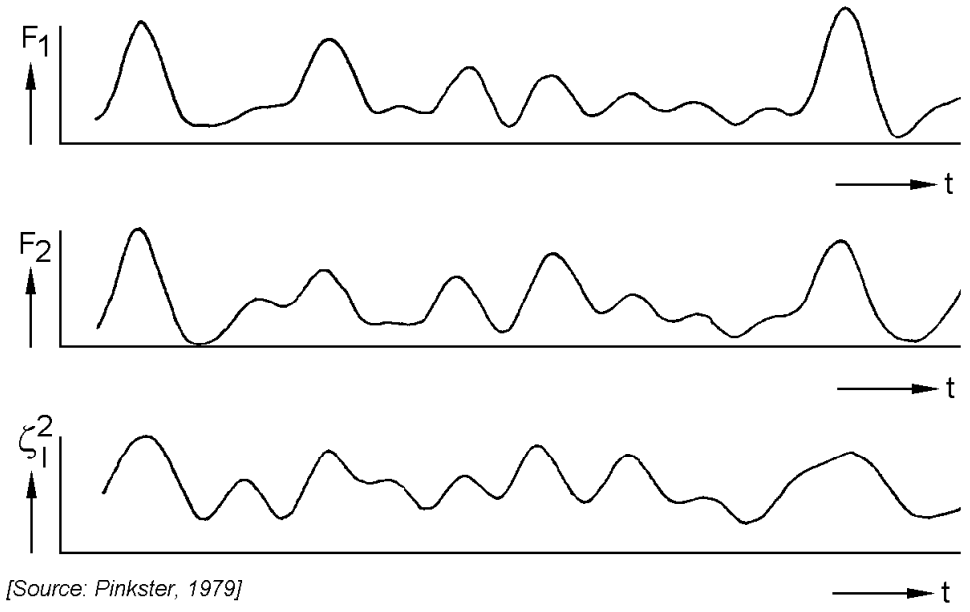

Figure 9.37: Low-Frequency Surge and Sway Drift Forces on a Tanker and Low-Frequency Part of Wave Height Squared

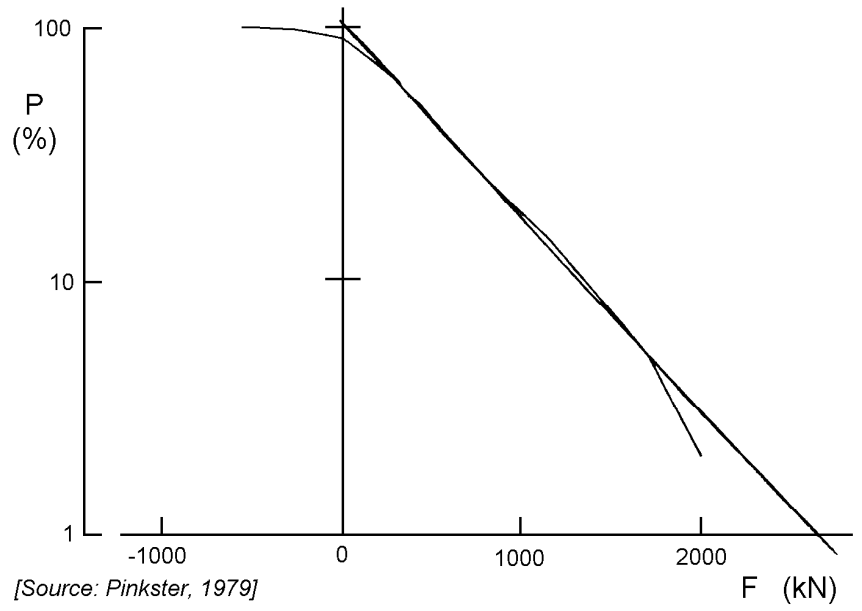

Figure 9.38: Distribution Function of the Low-Frequency surge Drift Forces on a Tanker in Irregular Head Waves

It is seen that this resembles an exponential distribution valid for the low frequency part of the square of the wave height.
In the beginning of this chapter, results were given on the wave drift forces on a tanker moored in shallow water. In such cases, the influence of the second order potential $\Phi^{(2)}$ on the wave drift forces become more pronounced. Results were also given on the low frequency "set-down" waves associated with the second order potential of the undisturbed incoming waves.

9.3.6 Simple Frequency Domain Method

A simple qualitative model is introduced in this section. It yields insight about the influence of mean and low frequency wave drift forces in irregular waves on the motions of a moored vessel. This model, simple though it may seem, has proved to be a very useful tool to explain and to predict low frequency motions of such vessels.
If a vessel is moored by means of a mooring system with linear restoring characteristics, the low frequency surge or sway motions may be approximated by the following equation of motion:

$$(m+a)\ddot{x} + b\dot{x} + cx = F^{(2)}(t) \tag{9.120}$$

where:

$m+a$	=	virtual mass
b	=	damping coefficient
c	=	restoring coefficient
$F^{(2)}(t)$	=	time dependent low frequency wave drift force

The mean displacement from the zero position due to the mean wave drift force is found from:

$$X_{mean} = \frac{F^{(2)}_{mean}}{c} \tag{9.121}$$

where $F^{(2)}_{mean}$ is given by equation 9.102 and equation 9.103.
The root-mean-square of the low frequency part of the motion is found from:

$$m_{0x} = \sigma_x^2 = \int_0^\infty \left|\frac{x_a}{F_a}(\mu)\right|^2 \cdot S_f(\mu) \cdot d\mu \tag{9.122}$$

where:

$S_f(\mu)$	=	spectral density of the wave drift force given by equation 9.105
$\lvert\frac{x_a}{F_a}(\mu)\rvert$	=	frequency dependent motion amplitude response function

The motion amplitude response function follows from:

$$\left|\frac{x_a}{F_a}(\mu)\right| = \frac{1}{\sqrt{\{c-(m+a)\mu^2\}^2 + b^2\mu^2}} \tag{9.123}$$

see chapter 6.

For slightly damped systems, which applies to many cases of moored vessels, the following assumption may be made with respect to the spectral density of the low frequency drift force:

$$S_f(\mu) \approx S_f(\mu_e) \tag{9.124}$$

where μ_e is the natural frequency of the moored vessel defined by:

$$\mu_e = \sqrt{\frac{c}{m+a}} \tag{9.125}$$

This result implies that the major part of the motion response will be due to excitation near the natural frequency. In that case, equation 9.122 may be approximated by:

$$\sigma_x^2 = S_f(\mu_e) \cdot \int_0^\infty \left| \frac{x_a}{F_a}(\mu) \right|^2 \cdot d\mu \tag{9.126}$$

If the natural frequency of the system is close to zero, the following approximation can also be applied:

$$S_f(\mu_e) \approx S_f(0) \tag{9.127}$$

From equation 9.105 it follows that:

$$S_f(0) = 8 \int_0^\infty S_\zeta^2(\omega) \cdot |T(\omega,\omega)|^2 \cdot d\omega \tag{9.128}$$

Since $Q(\omega,\omega) = 0$ (from equation 9.98) and taking into account equation 9.103 this becomes:

$$S_f(0) = 8 \int_0^\infty S_\zeta^2(\omega) \cdot \left| \frac{F}{\zeta_a^2}(\omega) \right|^2 \cdot d\omega \tag{9.129}$$

In this case the mean-square of the low frequency part of the motions can be written as follows:

$$\sigma_x^2 = S_f(0) \int_0^\infty \left| \frac{x_a}{F_a}(\mu) \right|^2 \cdot d\mu \tag{9.130}$$

Taking into account equation 9.123 this becomes:

$$\sigma_x^2 = \frac{\pi}{2bc} \cdot S_f(0) \tag{9.131}$$

which reveals the remarkable fact that the virtual mass $(m+a)$ of the vessels has no direct bearing on the mean or the low frequency motion.
From equation 9.131, it is seen that besides the exciting force, the most important factors determining the motions appear to be the damping b and the stiffness c of the mooring system. The trend suggested by equation 9.131 is also seen in results given by [Remery and Hermans, 1972] on the influence of the parameter c on the RMS value of the low frequency surge motion of a barge moored in head seas.
The general characteristic of the mooring force as expressed by the mean-square of the mooring force cx is found by multiplying equation 9.131 by c^2:

$$\sigma_{mf}^2 = \frac{\pi c}{2b} \cdot S_f(0) \tag{9.132}$$

This reveals that as the stiffness c of a mooring system increases, so does the RMS value of the low frequency mooring force.
It must be remembered that equations 9.131 and 9.132 can only be used in an indicative way. In many cases the mooring system will not be linear, or the number of degrees of freedom of the moored vessel will be too great to allow such simplifications as made here. We refer to [Oortmerssen, 1976b] and [Wichers, 1988] for more details concerning simulation techniques for moored vessels.

9.4 Remarks

The theory relating to second order wave drift forces has been treated in this chapter. Some results of computations have been compared with results derived analytically and by means of model tests. These results apply to the mean drift forces in regular waves, which can be used to estimate the mean and low frequency drift forces in irregular waves.
The low frequency part of the wave drift forces should theoretically, be determined by considering the drift forces in regular wave groups. In such cases the second order potential also contributes to the force, see [Pinkster, 1980]. [Faltinsen and Loken, 1979] have indicated that, for vessels floating in beam seas, the sway drift forces calculated using only information on the mean drift forces in regular waves gives results which are sufficiently accurate for engineering purposes. Results given by [Pinkster and Hooft, 1978] and [Pinkster, 1979] on the low frequency drift forces on a barge and a semi-submersible in head waves generally confirms the conclusion provided the frequency of interest is low. Frequencies of interest for moored vessels are the natural frequencies of the horizontal motions induced by the presence of the mooring system. In some cases the natural frequencies of vertical motions can also be of interest from the point of view of vertical motions induced by the low frequency wave drift forces.
It can be shown that, in at least one case, the mean wave drift forces in regular waves cannot be used to estimate the low frequency drift forces in irregular waves. This case concerns the low frequency sway drift force on a free floating, submerged cylinder in beam seas. According to [Ogilvie, 1963], the mean wave drift force in regular waves is zero for all wave frequencies. This means that the low frequency wave drift force in irregular waves estimated using only the mean wave drift force will be zero as well. Computations carried out using the method given by [Pinkster, 1979] which determines the low frequency force in regular wave groups show that this will not be true. The table below presents amplitudes of low-frequency sway drift forces in regular wave groups on a submerged cylinder in beam waves, with its center one diameter below the mean free surface:

$\frac{F_{2_{ij}}}{\pi\rho g L \zeta_1 \zeta_2}$

	$2k_ih$			
$2k_jh$	2	4	6	8
2	0.00	0.08	0.09	0.08
4		0.00	0.06	0.07
6			0.00	0.05
8				0.00

Chapter 10

STATION KEEPING

10.1 Introduction

Precise positioning and long term motion control of ships and other floating structures are important in offshore operations. Mooring systems and thrusters are major tools for maintaining a structure in position in current, wind and waves. The increasing application of large offshore structures has put high demands upon the design of these positioning arrangements. Important parameters in this respect are the large displacement of the structure, deep and hostile waters and the required round-the-year workability.
The external loads on the structure have been discussed in earlier chapters. This chapter treats some other important phenomena of station keeping problems of a floating structure, such as mooring systems, thruster performance and motion control.

10.2 Mooring Systems

Any mooring system is made of a number of lines (chain, wire or synthetic rope) with their upper ends attached to different points of the floating structure and their lower ends anchored at the sea bed.
The cables are constructed from steel chain, rope or a combination of both. The ropes are available in constructions from steel and natural or synthetic fibres. Multi-component cable lines - cables composed of two or more lengths of different material - are used to get a heavy chain at the sea bed and a lighter rope close to the water surface. This results in an optimal combination of stiffness and total weight. The tension forces in the cables are dependent on the cable weight, its elastic properties and the mooring system.

Typical and important types of mooring systems are:

- Catenary Line Mooring
  This are the oldest and still most common mooring systems. It derives its restoring force primarily by lifting and lowering the weight of the mooring line, at least in the static sense. Generally, this yields a hard spring system with a force increasing more than directly proportional to the displacement. In a spread mooring system as given in figure 10.1, several pre-tension anchor lines are arrayed around the structure to

[0] J.M.J. Journée and W.W. Massie, *"OFFSHORE HYDROMECHANICS"*, First Edition, January 2001, Delft University of Technology. For updates see web site: http://www.shipmotions.nl.

hold it in the desired location. The normal case is that the anchors can be easily moved, which implies that these anchors can not be loaded by too large vertical forces. To ensure that the anchors are kept in position, it is necessary that a significant part of the anchor line lie on the sea bed.

- Taut Line Mooring
  The mooring system has a pattern of taut, light-weight lines radiating outward. The lines have a low net submerged weight, which means that the catenary action has been eliminated. The system gets its restoring force as a function of horizontal displacement primarily from elastic stretch of the line itself. Synthetic fibers are most common for this type of mooring.

- Tension Leg Mooring
  This special mooring system is used for tension leg platforms (TLP), as has been shown in chapter 9. The buoyancy of this platform exceeds its weight and a net downward force is supplied by the vertically tensioned mooring, secured by dead-weight or anchor piles. These mooring lines provide essentially total restraint against vertical movements of the platform in water depths of about 1 km or less. When the floating object is horizontally displaced from its equilibrium position, the restoring force on the object results from the horizontal component of the mooring leg tension.

The pre-tension in the cable is often established by the use of winches on the floating structure. The winches pull on the cables to establish the desired cable configuration. As the structure moves in response to unsteady environmental loads, the tension in the cable changes due to varying cable geometry. Thus, the mooring cables have an effective stiffness which - combined with the motions of the structure - introduce forces depending on the mooring cable characteristics.

Offshore mooring systems are discussed in detail by [Massie, 1997]. The mooring forces on the floating structure are an input in the equations of motion of the structure in the time domain. Two methods to obtain these forces on the structure - a static approach and a simple dynamic approach - are given here. The positions of the anchor point and the suspension point as well as the length of the cable line and its strain characteristics are supposed to be known in these methods.
The hydromechanical interaction between waves and currents and the moving mooring or towing line can lead to significant forces. Sometimes they even exceed the net gravity force on the line. This is discussed in detail in chapter 12. The axial resistance of a line in the water is much lower than its transverse (cylinder drag) resistance. See chapter 4 for an indication of this. Hydrodynamic interaction introduces hysteresis damping in a mooring system.

10.2.1 Definitions

Consider a cable with an un-stretched length L, at the lower end attached to an anchor point, A, and at the upper end attached to a suspension point, B, on a floating structure. In an earth-bound right-handed coordinate system, S-(X_1, X_2, X_3), with the origin somewhere in the fluid (S is often taken in the still water plane) and the vertical axis positive upwards, the anchor point, A, is given by (X_{1A}, X_{2A}, X_{3A}) and the suspension point, B, of the cable on the floating structure is given by (x_{bB}, y_{bB}, z_{bB}); see figure 10.1.

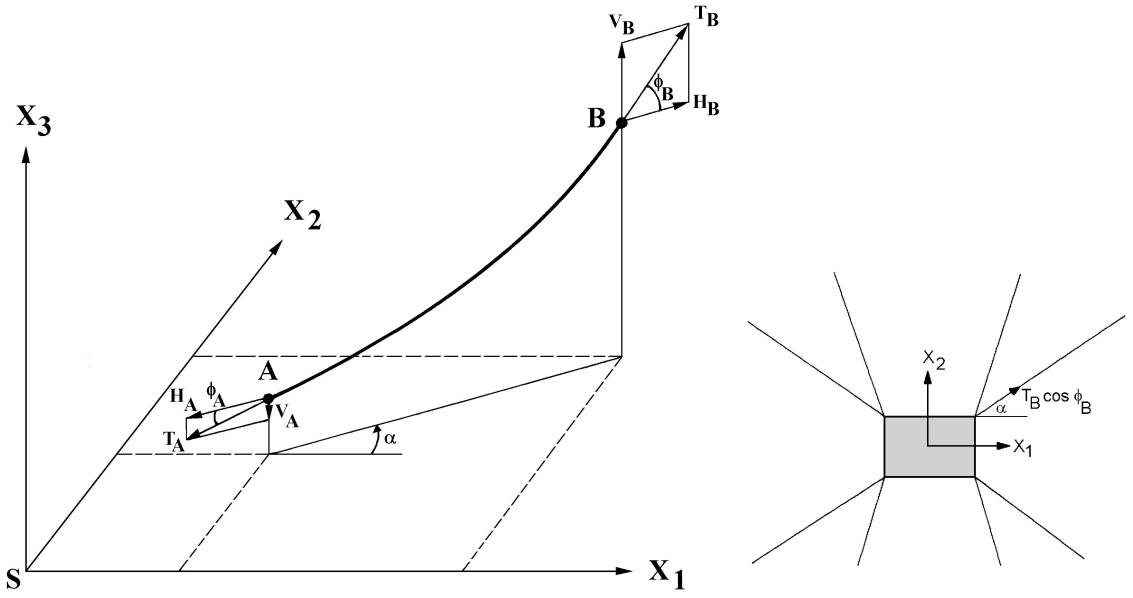

Figure 10.1: Cable Line in an Earth-Bound Axes System

The center of gravity, G, of the structure is given by (X_{1G}, X_{2G}, X_{3G}). A steadily translating coordinate system is given by G-(x_1, x_2, x_3), with roll, pitch and yaw angles x_4, x_5 and x_6 about these axes.
In the body-bound system of axes, G-(x_b, y_b, z_b), the suspension point, B, of the cable on the floating structure is defined by (x_{bB}, y_{bB}, z_{bB}).
In the earth-bound system of axes, the components of this suspension point, (X_{1B}, X_{2B}, X_{3B}), on the moving structure are found by:

$$\begin{aligned}
X_{1B} = X_{1G} \quad & +x_{bB} \cdot (+\cos x_5 \cdot \cos x_6) \\
& +y_{bB} \cdot (-\cos x_4 \cdot \sin x_6 + \sin x_4 \cdot \sin x_5 \cdot \cos x_6) \\
& +z_{bB} \cdot (+\sin x_4 \cdot \sin x_6 + \cos x_4 \cdot \sin x_5 \cdot \cos x_6) \\
\\
X_{2B} = X_{2G} \quad & +x_{bB} \cdot (+\cos x_5 \cdot \sin x_6) \\
& +y_{bB} \cdot (+\cos x_4 \cdot \cos x_6 + \sin x_4 \cdot \sin x_5 \cdot \sin x_6) \\
& +z_{bB} \cdot (-\sin x_4 \cdot \cos x_6 + \cos x_4 \cdot \sin x_5 \cdot \sin x_6) \\
\\
X_{3B} = X_{3G} \quad & +x_{bB} \cdot (-\sin x_5) \\
& +y_{bB} \cdot (+\sin x_4 \cdot \cos x_5) \\
& +z_{bB} \cdot (+\cos x_4 \cdot \cos x_5)
\end{aligned} \tag{10.1}$$

or in a linearized form as used in previous chapters:

$$\begin{aligned}
X_{1B} &= X_{1G} + x_{bB} - y_{bB} \cdot x_6 + z_{bB} \cdot x_5 \\
X_{2B} &= X_{2G} + x_{bB} \cdot x_6 + y_{bB} + z_{bB} \cdot x_4 \\
X_{3B} &= X_{3G} - x_{bB} \cdot x_5 + y_{bB} \cdot x_4 + z_{bB}
\end{aligned} \tag{10.2}$$

10.2.2 Static Catenary Line

Consider now this cable with an un-stretched length L, at the lower end attached to an anchor point, A, and at the upper end attached to a suspension point, B, in a vertical plane through this cable line. A two-dimensional sketch of this catenary anchor line is shown in figure 10.2.

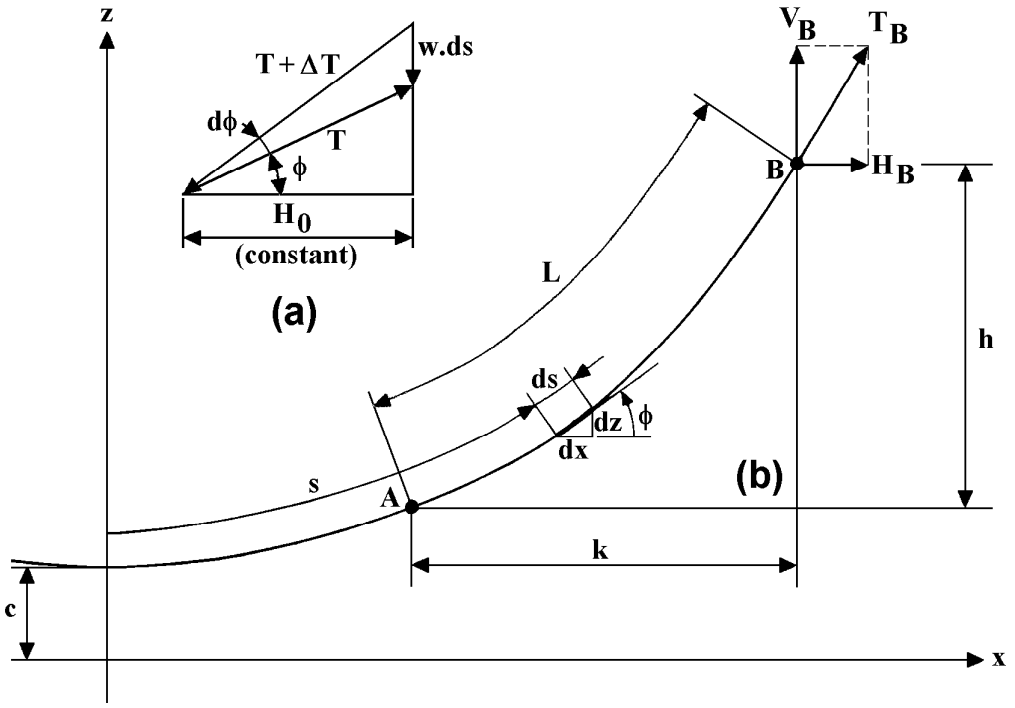

Figure 10.2: Cable Curve Symbols

For obtaining the equations of a static cable line, reference can be given to a number of papers in this field; for instance [Massie, 1997] and [Korkut and Hebert, 1970].

Inelastic Cable Line

Suppose: the length of the cable, L, is known and the relative positions of two - in principle arbitrary - points A and B on the cable are defined by the distances k and h. The anchor point is defined in a new 2-D coordinate system (see figure 10.2) by (x_A, z_A) and the suspension point on the structure is defined by (x_B, z_B) with:

$$x_B = x_A + k \qquad \text{and} \qquad z_B = z_A + h \tag{10.3}$$

The position of the origin of the axis system (x, z) relative to the cable line follows from two unknown coefficients, C_1 and C_2, as will be explained in the following.
When defining:

$$u = \frac{dz}{dx} \quad \text{and} \quad c = \frac{H_0}{w} \tag{10.4}$$

in which w is the weight per unit length of the cable in water (see also figure 10.2-a), it can be found that:

$$ds = \sqrt{1 + u^2} \cdot dx$$

$$\begin{aligned} du &= d\left(\frac{dz}{dx}\right) = d\left(\tan\phi\right) = \frac{w \cdot ds}{H_0} = \frac{ds}{c} \\ du &= \frac{\sqrt{1+u^2}}{c} \cdot dx \qquad \text{or:} \qquad dx = c \cdot \frac{du}{\sqrt{1+u^2}} \end{aligned} \tag{10.5}$$

With this, an integral equation will be obtained:

$$\int dx = c \cdot \int \frac{du}{\sqrt{1+u^2}} \tag{10.6}$$

Integration of this equation provides:

$$x = c \cdot \ln\left(u + \sqrt{1+u^2}\right) + C_1 = \frac{c}{\sinh u} + C_1 \tag{10.7}$$

or:

$$u = \sinh\left(\frac{x}{c} - C_1\right) \tag{10.8}$$

Herein, the constant C_1 will be zero because the origin in figure 10.2 is chosen in such a way that the derivative $u = dz/dx$ is zero for x is zero, so:

$$u = \sinh\left(\frac{x}{c}\right) \tag{10.9}$$

Then the equation of the cable curve can be written as:

$$z = \int_0^x u \cdot dx = c \cdot \cosh\left(\frac{x}{c}\right) + C_2 \tag{10.10}$$

The origin in figure 10.2 is chosen in such a way that $C_2 = 0$, thus:

$$z = c \cdot \cosh\left(\frac{x}{c}\right) \tag{10.11}$$

This means that $z = c$ for $x = 0$.
Also, the distance s can be obtained:

$$s = \int_0^x \sqrt{1+u^2} \cdot dx = \int_0^x \sqrt{1+\sinh^2\left(\frac{x}{c}\right)} \cdot dx \tag{10.12}$$

or:

$$s = c \cdot \sinh\left(\frac{x}{c}\right) \tag{10.13}$$

Combining equations 10.11 and 10.13 provides a simple relation between z and s:

$$z^2 - s^2 = c^2 \tag{10.14}$$

from which after some algebra for the points A and B on the cable line follows:

$$\sqrt{L^2 - h^2} = c\sqrt{2} \cdot \sinh\left(\frac{k}{2c}\right) \tag{10.15}$$

The values k, h and L are known, so the value of c has to be found from this equation in an iterative manner.

But, after expanding the sinh-expression in series:

$$\sinh\left(\frac{k}{2c}\right) = \frac{k}{2c} + \frac{k^3}{48c^3} + ... \tag{10.16}$$

and neglecting the higher order terms in here, the value of c can be found directly:

$$c = \sqrt{\frac{k^3}{24 \cdot \left(\sqrt{2\left(L^2 - h^2\right)} - k\right)}} \tag{10.17}$$

The relative position of the anchor point, x_A, can be found after some algebra by writing down $L + h$ with equations 10.13 and 10.11. A substitution of $x_M = x_A + k/2$ and $\sinh\{k/(2c)\}$ from equation 10.15 in here provides x_A. Then, z_A follows from x_A and equation 10.11. The coordinates of the suspension point, x_B and z_B, follow from those of the anchor point and equation 10.3.

$$\begin{aligned} x_A &= c \cdot \ln\left(\sqrt{\frac{L+h}{2\left(L-h\right)}}\right) - \frac{k}{2} & x_B &= x_A + k \\ z_A &= c \cdot \cosh\left(\frac{x_A}{c}\right) & z_B &= z_A + h \end{aligned} \tag{10.18}$$

On a flat horizontal sea bed, the magnitude of x_A should always be positive. If from calculations follows that x_A is negative, the cable is lying on the sea bed. In this case the length of the free hanging part of the cable has to be determined by an iterative method until $x_A = 0$ has been reached. This point will become the new anchor point of the cable line. Then, the distance between the old and the new anchor point plus the length of the free hanging part of the cable is equal to the total length of the cable.

Finally, in any cross section of the cable, the forces are given by:

$$H = w \cdot c \qquad V = w \cdot s \qquad T = w \cdot z \tag{10.19}$$

Then, the cable force components in the anchor point and the suspension point are:

$$\begin{aligned} H_A &= w \cdot c & H_B &= H_A \\ V_A &= w \cdot c \cdot \sinh\left(\frac{x_A}{c}\right) & V_B &= w \cdot c \cdot \sinh\left(\frac{x_B}{c}\right) \\ T_A &= \sqrt{H_A^2 + V_A^2} & T_B &= \sqrt{H_B^2 + V_B^2} \\ \phi_A &= \arctan\left\{\sinh\left(\frac{x_A}{c}\right)\right\} & \phi_B &= \arctan\left\{\sinh\left(\frac{x_B}{c}\right)\right\} \end{aligned} \tag{10.20}$$

Elastic Cable Line

In the previous, the elongation of the cable due to the tension force in the cable has not been taken into account. For this, the cable characteristics have to be defined. These characteristics are given here by the following relation between the tension force, T, in the cable and the specific strain of the cable, ε:

$$\begin{aligned} T &< T_{lin}: & T &= \frac{(EA)^2}{4 \cdot T_{lin}} \cdot \varepsilon^2 \\ T &> T_{lin}: & T &= -T_{lin} + EA \cdot \varepsilon \end{aligned} \tag{10.21}$$

with:

E	=	elasticity modulus of the cable
A	=	cross sectional area of the cable
$\varepsilon = \Delta L \,/\, L$	=	specific strain of the cable
T_{lin}	=	tension force in the cable at the boundary between the linear and the non-linear elasticity

These force-strain characteristics are shown in figure 10.3.

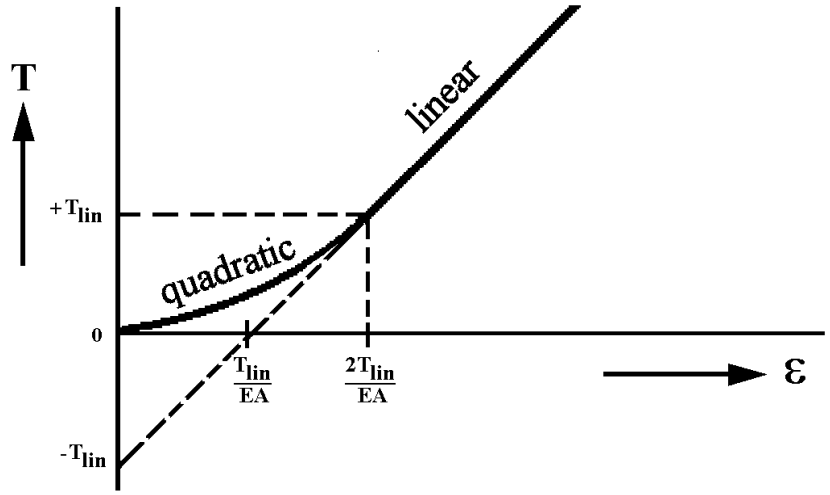

Figure 10.3: Cable Line Characteristics

Thus, $T_{lin} = 0$ provides the characteristics of a linear spring and a very large value of T_{lin} results in a quadratic force-strain relation. With these cable characteristics, the effect of an elongation of the cable can be taken into account.
The actual length of the cable is given by:

$$L = L_0 + \Delta L_0 \tag{10.22}$$

in which L_0 is the length of the not-loaded cable and ΔL_0 is the elongation due to the tension force in the cable.
First, the cable curve algorithms have to be solved for a cable length equal to the length of the not-loaded cable, so: $\Delta L_0 = 0$. This results in a known distribution of the tension forces $T(s)$ in the cable. With the cable characteristics, the distribution of the strain of the cable $\varepsilon(s)$ can be determined.
Then, the new total elongation follows from:

$$\Delta L_0 = \int_0^L \varepsilon(s) \cdot ds \tag{10.23}$$

This integration can be carried out numerically by dividing the cable length into n (for instance $n = 20$) line elements. The integration provides a new length L of the cable and the calculation procedure has to be repeated with this new length. A numerical procedure, such as a 'Regula Falsi' method, can be used to obtain a balance.
If a significant part of the cable is lying on the horizontal sea bed, then a certain friction of the cable over the sea bed can be taken into account.

Figure 10.4 shows an example of results of static catenary line calculations for an anchored platform. Figure 10.4-a shows the platform anchored by two anchor lines of chain at 100 m water depth. Figure 10.4-b shows the horizontal forces at the suspension points of both anchor lines as a function of the horizontal displacement of the platform. Finally, figure 10.4-c shows the relation between the total horizontal force on the platform and its horizontal displacement. This figure shows clearly the non-linear relation between the horizontal force on the platform and its horizontal displacement.

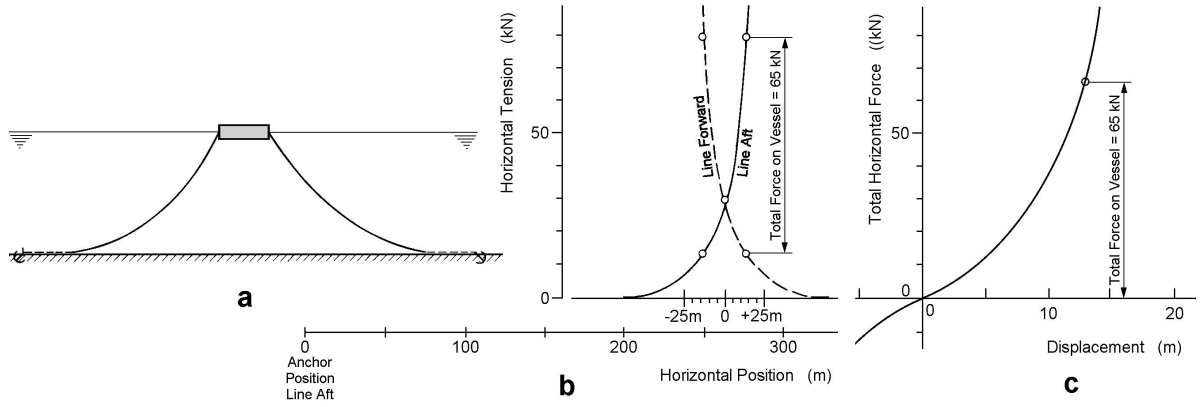

Figure 10.4: Horizontal Forces on a Platform as Function of its Horizontal Displacement

10.2.3 Dynamic Effects

In practical situations, the dynamic behavior of cable lines may contribute to the maximum tension significantly. Important parameters in this respect are the non-linear static load excursion, the low-frequency (pre-)tension and the amplitude and frequency of the exciting upper end oscillation. So far, the non-linear static load excursion has been accounted for but the dynamic behavior of the cable line has been ignored.
The prime dynamic tension increase, originated from the normal drag forces related to large global cable line motions at the middle sections. Long periods of slackness - even at low frequencies of oscillation - can occur due to 'flying' of the line under the influence of gravity and drag only. With increasing frequencies, the drag and the inertia equals the gravity forces resulting in an 'elevated equilibrium' of the line and the normal motions of the upper section of the line yields lower tension values. Inertia effects becomes of importance at higher frequencies, especially for steel wires and multi-component lines. Also, currents and waves will influence the hydrodynamic drag on the mooring lines.

Lumped Mass Method

[Van den Boom, 1985] describes a technique which implies that the behavior of a continuous line is modelled as a set of concentrated masses connected by massless springs. This involves the lumping of all effects of mass, external forces and internal reactions at a finite number of points along the line. By applying the equations of dynamic equilibrium (stress/strain) to each mass, a set of discrete equations of motion is derived. These equations may be solved in the time domain using finite difference techniques. Small effects of material damping, bending and torsional moments are ignored.

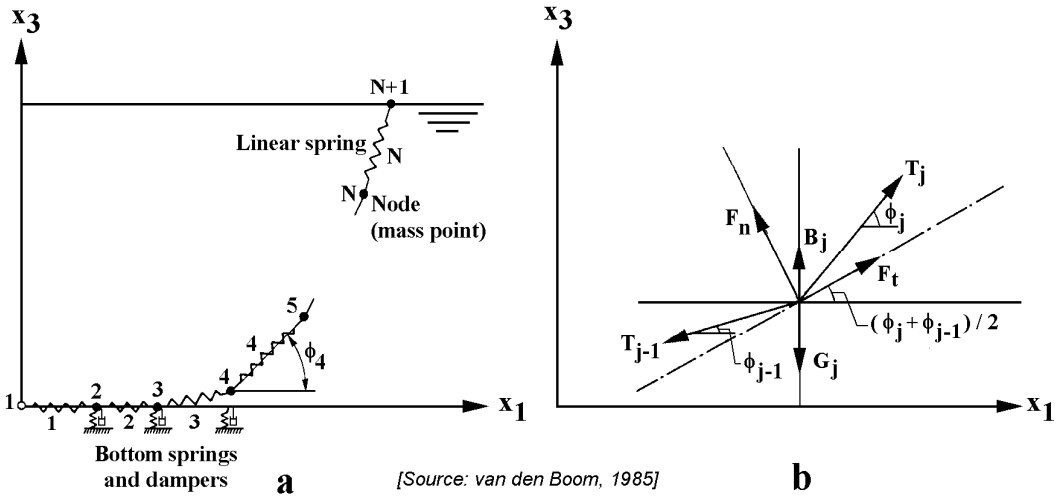

Figure 10.5: Discretization and Definitions for Lump Mass Method

Following the paper of [Van den Boom, 1985], the discretization of the mooring line can be obtained by lumping all forces to a finite number of nodes - so-called 'lumped masses' - as given in figure 10.5-a. The finite segments connecting the nodes are considered as massless springs accounting for the tangential elasticity of the line. The line is assumed to be fully flexible in bending directions. The hydrodynamic forces are defined in a local system of coordinates (tangential and normal direction) at each mass, as given in figure 10.5-b.
In order to derive the equations of motion of the j-th lumped mass, Newton's law is written in global coordinates:

$$([M_j] + [m_j(\tau)]) \cdot \vec{\ddot{x}}_j(\tau) = \vec{F}_j(\tau) \tag{10.24}$$

where $[M_j]$ is the inertia matrix, $[m_j(\tau)]$ is the hydrodynamic inertia matrix, τ is the time, $\vec{x}_j(\tau)$ is the displacement vector and $\vec{F}_j(\tau)$ is the external force vector.
The hydrodynamic inertia matrix, $[m_j(\tau)]$ can be obtained from the normal and tangential fluid forces by directional transformations:

$$[m_j(\tau)] = a_j^n \cdot \left[\Lambda_j^n(\tau)\right] + a_j^t \cdot \left[\Lambda_j^t(\tau)\right] \tag{10.25}$$

where a_j^n and a_j^t represent the normal (superscript n) and tangential (superscript t) hydrodynamic mass:

$$\begin{aligned} a_j^n &= \rho \cdot C_M^n \cdot \frac{\pi}{4} \cdot D_j^2 \cdot l_j \\ a_j^t &= \rho \cdot C_M^t \cdot \frac{\pi}{4} \cdot D_j^2 \cdot l_j \end{aligned} \tag{10.26}$$

In here, C_M^n and C_M^t are the non-dimensional normal and tangential hydrodynamic mass coefficients.
$\left[\Lambda_j^n\right]$ and $\left[\Lambda_j^t\right]$ are directional matrices given below for the two-dimensional case:

$$\left[\Lambda_j^n\right] = \begin{pmatrix} \sin^2\vec{\phi}_j & -\sin\vec{\phi}_j\cos\vec{\phi}_j \\ -\sin\vec{\phi}_j\cos\vec{\phi}_j & \cos^2\vec{\phi}_j \end{pmatrix}$$

$$\begin{aligned}\left[\Lambda_j^t\right] &= \begin{pmatrix} \cos^2\vec{\phi}_j & \sin\vec{\phi}_j\cos\vec{\phi}_j \\ \sin\vec{\phi}_j\cos\vec{\phi}_j & \sin^2\vec{\phi}_j \end{pmatrix} \\ \vec{\phi}_j &= \frac{\vec{\phi}_j + \vec{\phi}_{j-1}}{2} \end{aligned} \tag{10.27}$$

The nodal force vector, $\vec{F}$, contains contributions from the segment tension, T, the drag force, $\vec{F}_D$, buoyancy and weight, $\vec{F}_W$, and soil forces, $\vec{F}_S$:

$$\vec{F}_j(\tau) = T_j(\tau)\cdot\overrightarrow{\Delta x}_j(\tau) - T_{j-1}(\tau)\cdot\overrightarrow{\Delta x}_{j-1}(\tau) + \vec{F}_{D_j}(\tau) + \vec{F}_{W_j}(\tau) + \vec{F}_{S_j}(\tau) \tag{10.28}$$

where $\overrightarrow{\Delta x}_j(\tau)$ is the segment basis vector $(\vec{x}_{j+1} - \vec{x}_j)/l_j$, in which l_j is the original segment length.
The drag force, $\vec{F}_D$, (see chapter 4) may be derived from the normal and tangential force components:

$$\begin{aligned}\vec{F}_{D_j}(\tau) &= [\quad(\tau)]\cdot\vec{f}_{D_j}(\tau) \\ f_{D_j}^n(\tau) &= \frac{1}{2}\rho\cdot C_D^n\cdot D_j\cdot l_j\cdot u_j^n(\tau)\cdot\left|u_j^n(\tau)\right| \\ f_{D_j}^t(\tau) &= \frac{1}{2}\rho\cdot C_D^t\cdot D_j\cdot l_j\cdot u_j^t(\tau)\cdot\left|u_j^t(\tau)\right| \\ \vec{u}_j(\tau) &= [\Gamma_j(\tau)]\cdot\left(c_j - \dot{\vec{x}}_j(\tau)\right) \end{aligned} \tag{10.29}$$

where

$\vec{f}_{D_j}$	=	drag force in local coordinates
$\vec{u}_j$	=	relative fluid velocity in local coordinates
c_j	=	current vector in global coordinates
ρ	=	fluid density
D	=	characteristic segment diameter
l	=	segment length
C_D	=	non-linear (quadratic) 2-D damping (or drag) coefficient
C_D^n	=	normal drag coefficient
C_D^t	=	tangential drag coefficient

The directional matrices $[\quad_j(\tau)]$ and $[\Gamma_j(\tau)]$ are used to transform the global drag forces and velocities into local drag forces and velocities:

$$[\quad_j] = [\Gamma_j] = \begin{pmatrix} -\sin\vec{\phi}_j & \cos\vec{\phi}_j \\ \cos\vec{\phi}_j & \sin\vec{\phi}_j \end{pmatrix} \tag{10.30}$$

C_M is a 2-D non-dimensional hydrodynamic mass coefficient. The 2-D quadratic drag coefficient C_D has been discussed in chapter 4. The hydrodynamic mass and drag coefficients C_M and C_D - as they are used in the so-called Morison equations - will be discussed in more detail in chapter 12.
[Van den Boom, 1985] has derived the fluid reactive force coefficients a^n, a^t, C_D^n and C_D^t from forced oscillation tests and free hanging tension tests with model chain and wire

sections. A volumetric diameter, defined by $d_c = 2\sqrt{\nabla/\pi l}$ (with ∇ is segment volume and l is segment length), proved to be an accurate parameter in the dimensionless hydrodynamic coefficients. From the model tests it was concluded that frequency-independent coefficients can be used for normal mooring chains and wires.
Dynamic sea bed reaction forces do not affect the behavior of the line and can be modelled as critical damped springs to prevent numerical instabilities. Tangential soil friction forces may be of importance when the line part on the bottom is extremely long and transverse soil reactive forces may be of importance for 3-D problems. Both soil effects are neglected here, thus the vertical force component, F_{S3_j}, equals:

$$\begin{aligned} F_{S3_j} &= -b_j \cdot \dot{x}_{3_j} - c_j \cdot x_{3_j} \qquad \text{for: } x_{3_j} < 0 \\ F_{S3_j} &= 0 \qquad\qquad\qquad\qquad\quad \text{for: } x_{3_j} > 0 \end{aligned} \tag{10.31}$$

The time domain relations between nodal displacements, velocities and accelerations are approximated by finite difference methods such as the Houbolt scheme which is described by [Bathe and Wilson, 1976]:

$$\begin{aligned} \vec{\dot{x}}_j\,(\tau+\Delta\tau) &= \frac{1}{6\Delta\tau}\cdot\{11\vec{x}_j\,(\tau+\Delta\tau) - 18\vec{x}_j\,(\tau) + 9\vec{x}_j\,(\tau-\Delta\tau) + 2\vec{x}_j\,(\tau-2\Delta\tau)\} \\ \vec{\ddot{x}}_j\,(\tau+\Delta\tau) &= \frac{1}{\Delta\tau^2}\cdot\{2\vec{x}_j\,(\tau+\Delta\tau) - 5\vec{x}_j\,(\tau) + 4\vec{x}_j\,(\tau-\Delta\tau) - \vec{x}_j\,(\tau-2\Delta\tau)\} \end{aligned}$$

or:

$$\vec{x}_j\,(\tau+\Delta\tau) = \frac{5}{2}\vec{x}_j\,(\tau) - 2\vec{x}_j\,(\tau-\Delta\tau) + \frac{1}{2}\vec{x}_j\,(\tau-2\Delta\tau) + \frac{1}{2}\Delta\tau^2\,\vec{\ddot{x}}_j\,(\tau+\Delta\tau) \tag{10.32}$$

The segment tension $T_j\,(\tau+\Delta\tau)$ is derived from the node positions by a Newton-Raphson iteration using the additional equation for the constitutive stress-strain relation:

$$\vec{\psi}_j\,(\tau) = l_j^2 \cdot \left\{ \vec{\Delta x}_j\,(\tau) - \left(1 + \frac{T_j\,(\tau)}{E_j \cdot A_j}\right)^2 \right\} \tag{10.33}$$

$$\vec{T}^{k+1}\,(\tau+\Delta\tau) = \vec{T}^{k}\,(\tau+\Delta\tau) - \left[\Delta\psi^k\,(\tau)\right]^{-1} \cdot \vec{\psi}^{\,k}\,(\tau) \tag{10.34}$$

where $\vec{\psi} = \left(\psi_1, ..., \psi_j, ..., \psi_N\right)$ is segment length error vector, $\vec{T}^k = (T_1, ..., T_j, ..., T_N)$ is tentative segment tension vector at the k-th iteration and $\Delta\psi = \partial\psi/\partial T$ is the length error derivative matrix obtained from equations 10.32 and 10.33.
For each time step the system of equation 10.34 should be solved until acceptable convergence of $T^k\,(\tau+\Delta\tau)$ is obtained. The initial tentative tension can be taken equal to the tension in the previous step. Each node j is connected to the adjacent nodes $j-1$ and $j+1$, hence equation 10.34 represents a three-diagonal $(N \times 3)$ system. Such equations may be efficiently solved by the so-called Thomas algorithm.
[Van den Boom, 1985] claims that - certainly for engineering applications - the Lumped Mass Method (LMM) does provide efficient and accurate predictions of dynamic line motions and tensions.

10.2.4 Experimental Results

[Kwan, 1990] checked results of calculations in the time domain - which include dynamic effects - against results of measurements. First, he carried out model tests. Then, - to eliminate potential questions about the scale effects of model tests - a full scale measurement was carried out in 1984 on a drill ship.. Some of his results are shown in figure 10.6.

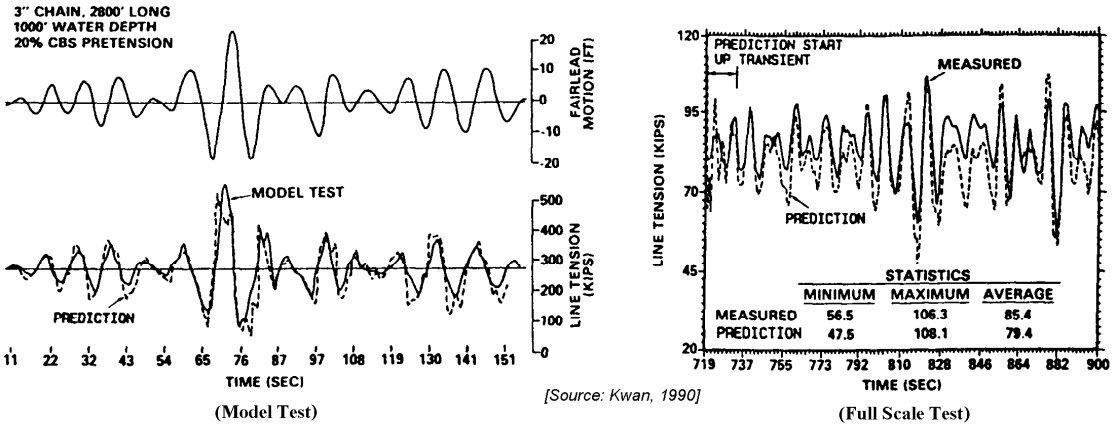

Figure 10.6: Comparison of Predicted and Measured Line Tensions

[Kwan, 1990] concluded that - in general - the predicted line tensions compare well with the model test and full scale measurement results.

10.2.5 Suspension Point Loads

Now, the components of the cable forces in the suspension point, B, in the vertical plane through the cable line are known; they can be derived in the earth-bound (X_1, X_2, X_3)-system of axes by:

$$\begin{aligned} T_{X_{1B}} &= +T_B \cdot \cos\phi_B \cdot \cos\alpha \\ T_{X_{2B}} &= +T_B \cdot \cos\phi_B \cdot \sin\alpha \\ T_{X_{3B}} &= -T_B \cdot \sin\phi_B \end{aligned} \tag{10.35}$$

where T_B, ϕ_B and α are defined in figure 10.1.
The angle of the cable forces in the horizontal plane in the (X_1, X_2, X_3)-system of axes is given by:

$$\alpha = \arctan\left\{\frac{X_{3B} - X_{3A}}{X_{1B} - X_{1A}}\right\} \qquad \text{with: } 0 \leqslant \alpha \leqslant 2\pi \tag{10.36}$$

Then, the forces and moments on the structure in the steadily translating axes system G-(x_1, x_2, x_3) are:

$$\begin{aligned} F_{x_{1\text{CABLE}}} &= +T_{X_{1B}} \cdot \cos x_6 + T_{X_{2B}} \cdot \sin x_6 \\ F_{x_{2\text{CABLE}}} &= -T_{X_{1B}} \cdot \sin x_6 + T_{X_{2B}} \cdot \cos x_6 \\ F_{x_{3\text{CABLE}}} &= +T_{X_{3B}} \\ F_{x_{4\text{CABLE}}} &= +T_{X_{2B}} \cdot (X_{3B} - X_{3G}) + T_{X_{3B}} \cdot (X_{2B} - X_{2G}) \\ F_{x_{5\text{CABLE}}} &= +T_{X_{1B}} \cdot (X_{3B} - X_{3G}) - T_{X_{3B}} \cdot (X_{1B} - X_{1G}) \\ F_{x_{6\text{CABLE}}} &= -T_{X_{3B}} \cdot (X_{2B} - X_{2G}) + T_{X_{2B}} \cdot (X_{1B} - X_{1G}) \end{aligned} \tag{10.37}$$

10.3 Thrusters

Thrusters may be used - in combination with a mooring system or alone - to keep the vessel in its desired position.

10.3.1 Characteristics

From open water propeller tests - see chapter 4 - with fixed pitch propellers (FPP) and controllable pitch propellers (CPP), one can get a first estimate of the thruster characteristics. An FPP prevails, from an energy efficiency point of view. An example of the difference in power consumption of an FPP versus a CPP is shown in figure 10.7.

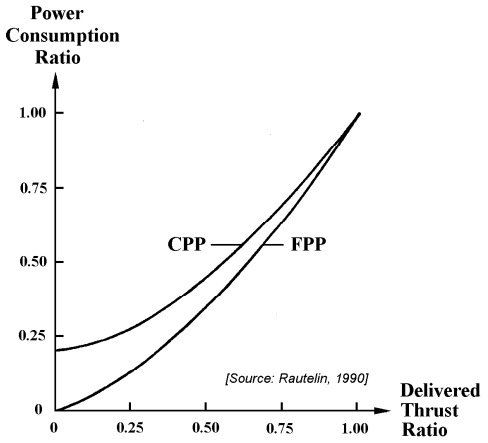

Figure 10.7: Power Consumption of FPP Versus CPP

In typical marine applications, there is always first the question of whether to use direct drive by diesel engine or an electrical drive but in offshore DP applications the diesel drive is rarely considered. For electrical drive, the three main solutions are:
- a constant speed AC motor drive (1- or 2-speed), which requires a CPP,
- a variable speed DC motor drive, which works with an FPP and
- a variable speed frequency converter and AC motor drive, with an FPP.

It derives from the CPP curve that there is a need to improve the efficiency of the thruster performance at part loads from that of a single speed drive. The 2-speed drive already looks much better - on paper - but due to its limited thrust developing capacity at the lower speed, the higher speed tends to be used more for safety's sake in practise. So that, when the energy efficiency at typical DP load area is of prime importance, variable speed (rpm) with an FPP is the ideal solution. This requirement has been mostly met by DC drives so far.

To make an AC motor speed variable, the supply frequency to the motor must be varied, hence the name of the frequency converter. There are basically three types of converters (see figure 10.8):
- the current source converter, which supplies current from the DC link in step form,
- the voltage source, which supplies stepped voltage and
- the pulse width modulated (PMW) type, which simulates the output waveform by supplying a number of pulses of varying width.

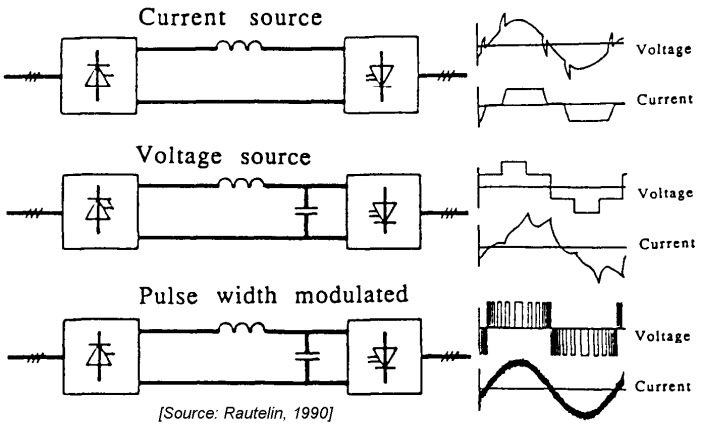

Figure 10.8: Frequency Converter Principles

Frequency converter drives are good solutions for industrial variable speed drives. Pipelaying vessel 'Lorelay' - operated since 1986 by Allseas Marine Contractors S.A. - was the first DP offshore vessel fully designed around AC variable speed FPP propulsion and thruster drives of PMW type. These drives may offer in many ways a solution which can improve the performance of station keeping and the drive system reliability.

10.3.2 Loss of Efficiency

A thruster in isolation will lose efficiency due to an interaction the hull and by the presence of current and waves. Also thruster-thruster interaction can play a significant role.

Coanda Effect

An important thruster-hull interaction effect is the **Coanda effect**. This phenomenon and its effect on the efficiency of the thruster is clearly explained by [Faltinsen, 1990] as follows.

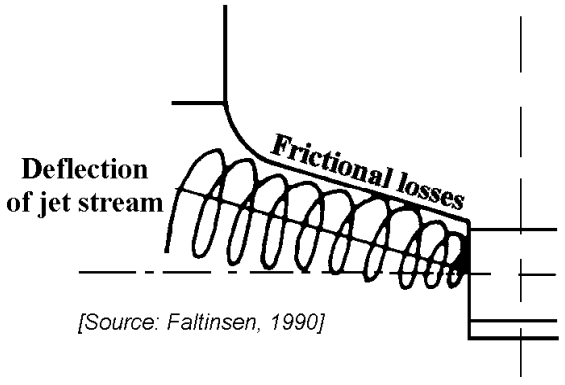

Figure 10.9: Coanda Effect of a Stern Skeg Tunnel Thruster

The thruster slip stream will be attracted by the hull - as shown in figure 10.9 - with loss of thrust as a consequence. This propeller slip stream can be represented by a circular jet, which acts like a line of sinks This means that water is entrained in the jet from

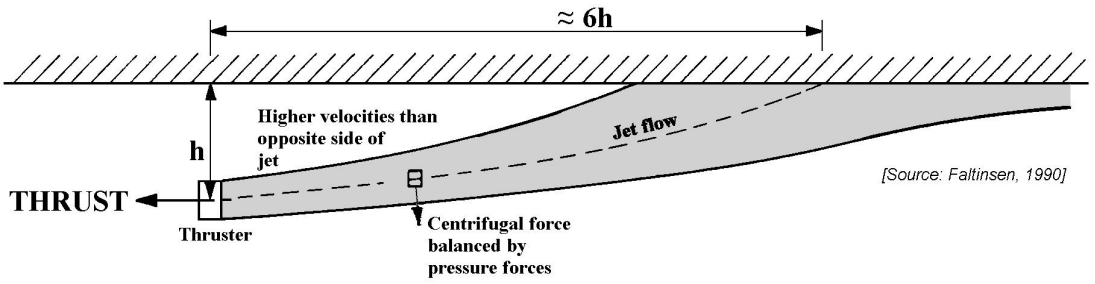

Figure 10.10: Coanda Effect in a Propeller Slip Stream

outside the jet. If the boundary had not been there, the entrained velocity would have been directed radially toward the center of the jet; the entrained velocity is only a function of the radius. If a boundary is present, the velocity will be at a maximum between the jet and the boundary. High velocity means low pressure. This means a pressure difference across the jet with a resultant force towards the boundary. This force will attract the jet towards the wall. The attraction force has to be in balance with the centrifugal force of the jet flow and this balance determines the position of the jet relative to the wall. This principle is shown in figure 10.10.

For a thin jet - initially at a distance h from an infinitely long parallel wall - it takes roughly $6h$ to hit the wall. This information can be used as a rough tool for avoiding the propeller slip stream coming into contact with the hull.

However, one should realize that this approximation of the propeller slip stream by a thin jet is a strong idealization. The jet must have a radius comparable to the propeller radius. Close to the propeller the flow is not jet-like. It actually takes a distance from the thruster of about $6D$ (6 times the diameter of the propeller) before the propeller slip stream develops into a fully turbulent jet-like flow. The jet will spread as a function of the distance from the thruster. If we consider a free jet - so a jet not in presence of a boundary - the points in a jet where the velocity is half the maximum velocity will spread with an angle of about $5°$. This spreading may cause the propeller slip stream to be in contact with the hull before the above attraction effect has fully developed. When the propeller stream clings to the hull, it behaves like a wall jet. The wall jet may very well separate from the hull again. This depends on the local radius of curvature of the hull. If a sharp corner is present the propeller stream will separate and there will be no significant thrust loss.

It is to difficult to estimate theoretically what the loss due to the Coanda effect is. According to [Faltinsen, 1990], limited full scale experience from a supply ship indicates that the Coanda effect may cause a 30-40 % loss of thrust for a given power. In that case the propeller stream followed the ship hull all the way up to the free surface. If the propeller stream had been separated from some point on the hull surface, it is expected that this would have caused a smaller loss.

For semi-submersibles, the Coanda effect for a thruster on one pontoon, may cause the propeller stream to hit another pontoon. The loss due to this can roughly be estimated by considering the propeller stream to be an incident current on the other pontoon.

Another case for a semi-submersible would be if the thruster is aligned longitudinally along the pontoon. Due to the long distance, the propeller slip stream is likely to be completely attracted to the pontoon. The boundary flow between the wall jet and the pontoon will cause shear forces. According to [Faltinsen, 1990], this may amount to 10-15 % loss of

power.
A practical solution to avoid the Coanda effect can be found in tilting the thruster nozzle over about 5 degrees in a downwards direction. Then, the propeller slip stream will not be attracted by the hull in that amount and - in the case of a semi-submersible- hitting the other pontoon by the propeller slip stream can be avoided. As a consequence of this, a decrease of the loss of thrust for a given power can be expected.

Thruster-Thruster Interaction

For vessels where it is impossible to avoid placing the thrusters where the inflow and outflow fields may interfere, physical model tests are the only reliable way to define the effects. [English and Wilde, 1976] describe a series of experiments wherein thruster interaction effects were derived from physical model tests.
In some cases, tilting the thruster nozzle over about 5 degrees in a downwards direction can avoid or decrease thruster-truster interaction.

Current Effects

For tunnel thrusters, the thruster forces are affected by the flow of a current past the inlet and outlet. The loss of thrust is caused by deflection of the jet stream and by interactions between the jet stream and the hull which give rise to suction forces on the tunnel outlet of the vessel.
[Chislett and Bjorheden, 1966] studied the influence of forward speed of a 232 meter length ship on the effectiveness of a lateral-thrust device in turning the hull, which appeared to be of considerable magnitude. They showed results of model experiments on the percentage lost of side force and yaw moment of the thruster as a function of the velocity ratio: the forward ship speed - thruster jet speed ratio.
The thruster jet speed, V_{jet}, has been evaluated by the conservation of momentum in the fluid:

$$T_{\text{jet}} = \rho V_{\text{jet}}^2 \cdot \frac{\pi}{4} D_{\text{jet}}^2 \qquad \text{or:} \qquad V_{\text{jet}} = \sqrt{\frac{T_{\text{jet}}}{\rho \cdot \frac{\pi}{4} D_{\text{jet}}^2}} \tag{10.38}$$

where the thrust, T_{jet}, is that measured at zero forward speed. With known diameter, D_{jet}, this equation provides the jet speed, V_{jet}. This jet exit velocity was assumed to be independent of the forward ship speed; an assumption supported by additional torque measurements.
The measured forces, Y, and moments, N, on the ship are made dimensionless the jet exit velocity too:

$$Y' = \frac{Y}{\rho V_{\text{jet}}^2 \cdot \frac{\pi}{4} D_{\text{jet}}^2} \qquad \text{and} \qquad N' = \frac{N}{\rho V_{\text{jet}}^2 \cdot \frac{\pi}{4} D_{\text{jet}}^2 \cdot x_T} \tag{10.39}$$

where x_T is the distance of the tunnel center from amidships.
Figure 10.11-a and 10.11-b and presents, for a number of propeller rates, these non-dimensional loads on the ship as a function of the velocity ratio.
Figure 10.11-a provides the loss of efficiency of the thruster due to the forward ship speed. At ship speeds less than about 3 knots, the lever arm of the moment, calculated from N/Y, appeared to be similar to x_T. At higher speeds this value increases, so the estimated

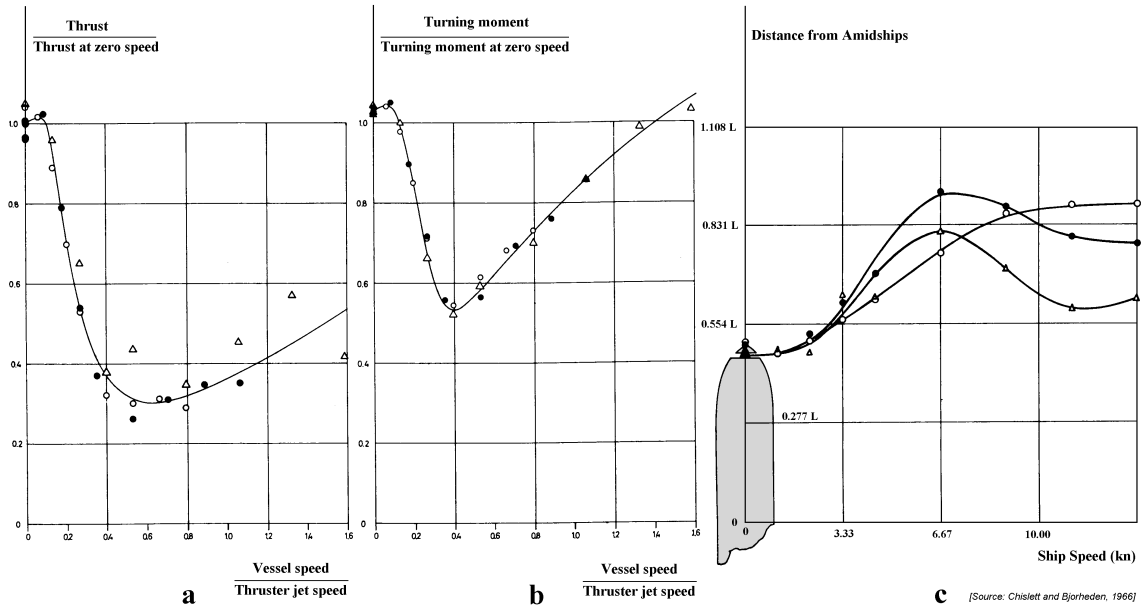

Figure 10.11: Effect of Forward Ship Speed on Bow Thruster Performance

moment will be conservative when using the measured forces from figure 10.11-a and x_T as the lever arm, see figure 10.11-c.

[Faltinsen, 1990] used these thrust reduction results of [Chislett and Bjorheden, 1966] to estimate the loss of efficiency of thrusters by currents. Together with the current velocity, figure 10.11-a provides the loss of efficiency of the thruster due to a current and the moment can be found with the lever arm x_T.
It has been found by [Edwards, 1985] that thrusters and particularly main propulsion units in the vicinity of the after body can create markedly different reaction forces and moments on vessels at oblique angles, particularly at high current speeds.

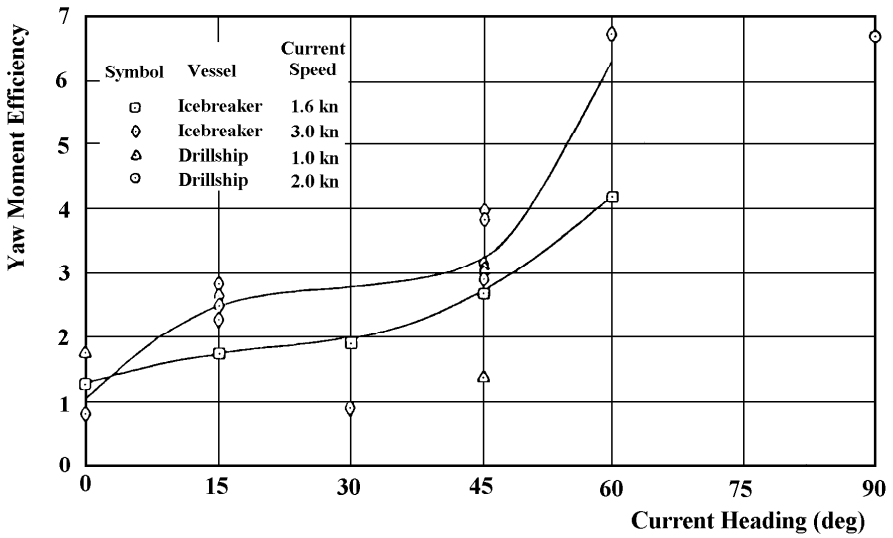

Figure 10.12: Starboard Main Propulsion Unit Yaw Moment Efficiency

This is illustrated in figure 10.12, where the effectiveness of a single main propulsion unit in producing yaw moment is plotted versus heading with respect to current direction. An effectiveness of 1.0 indicates a measured reaction moment equivalent to the calculated thrust times the moment arm, taking into account the observed advance ratio. It can be seen that the measured reaction moment is many times the ideal value. In essence the propeller operation has drastically changed the pressure distribution around the vessel, aligned obliquely to the flow from that with no propeller in operation. To a lower extent, this may be seen for through-hull thrusters placed at the extremity of the vessel. The only way to asses effects such as this is with physical model tests.

Wave Effects

[Minsaas et al., 1986] have argued that a similar effect to this must be present in waves. They did experiments with a fictitious bow thruster system in head waves. The ship sides were simulated by vertical plates parallel to the incident regular waves. The whole system was restrained from oscillating.
As treated in chapter 5, the wave velocity amplitude, V_p, at the propeller centre ($z = -h_p$) can be written as:

$$V_p = \zeta_a \omega \cdot e^{-kh_p} \tag{10.40}$$

By interpreting V_p as a current velocity they were able to predict trends in their experimental results. If a ship is moving in waves the problem becomes more complicated. The velocity across the propeller jet at the tunnel entrance is no longer V_p. This problem requires further research.
The presence of waves causes - even for a thruster with a constant propeller pitch or propeller speed setting - oscillating thrust and torque performances. Similar effects appear in the case of vertical and horizontal oscillations of the ship itself.

Free Surface Effects

When a thruster comes close to the free surface other problems appear. Depending on the thruster loading this may cause air ventilation with a serious loss of propeller thrust and torque.
Tests in still water were performed by [Minsaas et al., 1986], in order to study the effects of waves based on a quasi-steady assumption. As long as the thruster is not ventilating, this is legitimate, since the wave-induced motions occur with a much lower frequency than the propeller rotation. However, when the propeller is in a transient ventilating condition, there is also a frequency connected with the development of the ventilated area on the propeller blades. this wave-induced effect can not be simulated by means of results in calm water.
The tests in calm water were performed with different propeller axis submerges, h_p, relative to the free surface. By the quasi-steady assumption one can interpret h_p as the submergence of the instantaneous position of the wave surface, see figure 10.13. By averaging the propeller thrust and torque in time one can find the effect of the wave induced motions of the ship on the thruster characteristics.

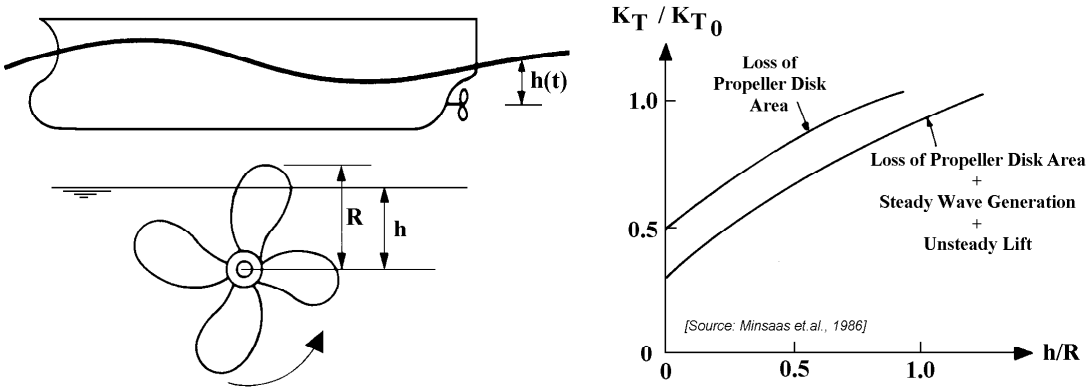

Figure 10.13: Effect of Waves on a Propeller, a Quasi-Steady Approximation

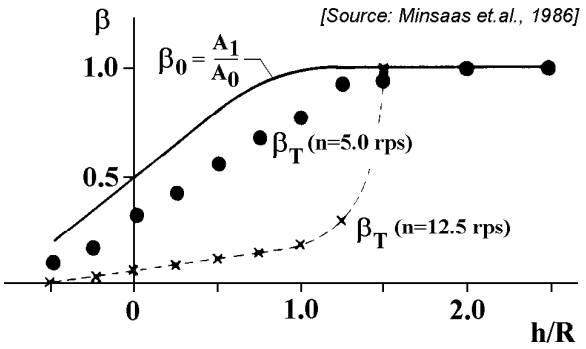

Figure 10.14: Lost of Thrust due to Bow Immersion in Calm Water

Typical model test results from calm water are shown in figure 10.14 where thrust is presented as a fraction of the thrust for a fully immersed propeller, $\beta_T = K_{T_{h/R}}/K_{T_0}$, and for different number of revolutions, n.

It is observed that the number of revolutions has a marked influence on the results. The effect of loss of effective propeller area is important. When $h/R < 1.0$ the ratio of the immersed disk area, A_1, and the total disk area, A_0, of the propeller is $\beta_0 = A_1/A_0$. If we assume that the thrust is proportional to A_1, β_0 gives the thrust reduction for small n-values as illustrated in figure 10.14. For large n-values we see that the thrust is very low for the small h/R-values. This is due to propeller ventilation. Qualitatively it can be explained as follows. Increased n means increased loading. This means large suction pressures on the propeller. The lower pressure is, the more likely it is that ventilation occurs. For $h/R = 1.0$-1.5 there is a very rapid variation in thrust. This is when ventilation starts. The behavior of β in waves is not quasi-steady when the propeller is in a transient ventilating state. The maximum thrust is reached later in time than maximum immersion. In most cases maximum thrust never reaches the same thrust value as when the propeller was fully immersed in static conditions.

[Minsaas et al., 1986] have tried to apply their experimental results for a ducted propeller and bow thruster in regular waves to thrust loss for different ships and sea states. An example for a 250 meter long ship is presented in figure 10.15.

The results will depend on propeller shaft submergence, h, propeller diameter, D, propeller

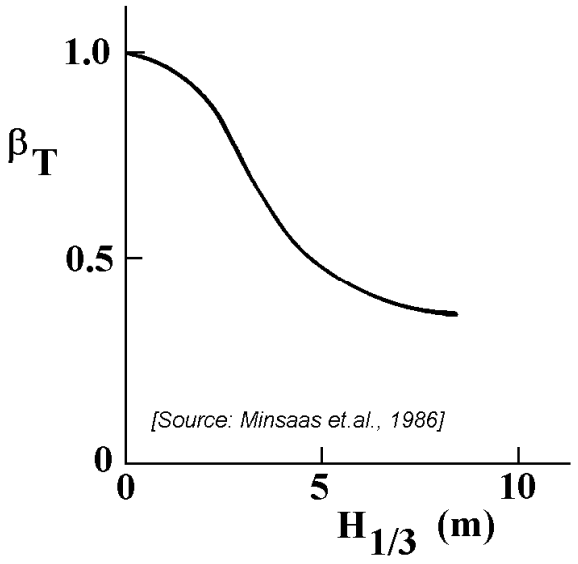

Figure 10.15: Thrust Reduction in Head Waves

pitch, propeller revolution, n, and hull form. The results in figure 10.15 show that even a large ship experiences considerable thrust losses in rough seas.

10.4 Dynamic Positioning

The 'Eureka' was the world's first automatically controlled dynamically positioned vessel. This semi-submersible was built by Shell Oil Company for exploration core drilling and began operation in the spring of 1961. With one thruster power for each of its 400 tons of displacement, it was very successful in taking cores up to 150 m in the sea floor. Averaging over two locations per day, it drilled as many as nine in a single day in water depths out to 1200 m. Comparably sized anchored vessels at the time could get one location in two to four days and were limited to only about 100 m of water.

Since this first operation of a dynamic position system, they have come a long way. Much larger thrusters are stationing much larger vessels in much deeper water. Taut wire position measurements has been given way to satellite positioning by Global Positioning Systems (GPS). The old single-thread analog systems are gone and the digital computers are provided in dual and now triple redundancy. Failure rates have gone from several per month and over 20 percent downtime in the first year to a present day Mean Time Between Failure (MTBF) of about three years for the best systems.

Development of a successful dynamic positioning system requires a means of checking out the performance of the entire system from the controls to the reaction of the vessel to the environmental and thruster forces on the hull. A complete simulation will yield the performance of the system by means of mathematical analysis before any hardware has been acquired. Then by means of the detailed system simulator, one can vary parameters on the control of the system, hardware characteristics, propeller design or even hull design to obtain the desired performance in the changing environment and also in response to sudden failure of a component of the system.

10.4.1 Control Systems

The brain of the dynamically positioned system is the **controller**. Basically, it measures the position of the vessel with respect to the intended position and directs power to the various thrusters to correct any position error.
In its simplest form, the controller will call for thrust in the direct opposite to the position error. Without some modulation of the thrust and provisioning of a 'dead band', the system would continually overshoot. Probably the simplest practical system consists of thrust and moment commands **proportional (P)** to the amount of position and heading error:

$$\vec{T} = f\,(X_1, X_2, X_6) \quad \text{(P-controller)} \tag{10.41}$$

The axes system is given in figure 10.16, with the origin, S, of the earth-bound axes system in the still water surface. Notify the right-handed axes system here, with the vertical axis, X_3, positive downwards, as it is often used by manoeuvreing researchers.

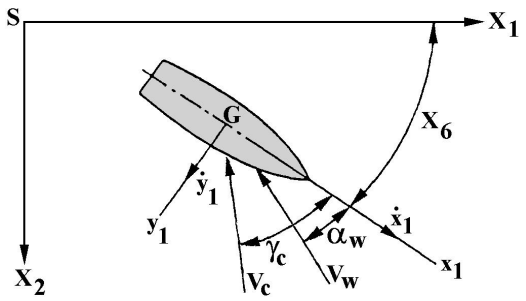

Figure 10.16: Dynamic Positioning Axes System

Even this simple controller needs one more level of complexity. In the event the thruster system is saturated, the controller must assign priority to heading control or position control. Usually heading priority is called for since the proper heading will minimize the relevant motions and thus the translational thrust requirements.
Using successive positioning error signals, one can determine the step-wise velocity of the vessel. System performance is greatly improved by adding velocity terms, the **derivative (D)** of the excursion, to the thrust equations:

$$\vec{T} = f\,\left(X_1, X_2, X_6,\ \dot{X}_1, \dot{X}_2, \dot{X}_6\right) \quad \text{(PD-controller)} \tag{10.42}$$

Finally in order to bring the vessel back to the zero position, the thrust must take into account the time over which external forces have been acted. A term is added to; the **integral (I)** of the excursion with time:

$$\vec{T} = f\,\left(X_1, X_2, X_6,\ \int (X_1, X_2, X_6)\,dt,\ \dot{X}_1, \dot{X}_2, \dot{X}_6\right) \quad \text{(PID-controller)}$$

The foregoing systems are all **feed-back** systems. A further refinement in performance can be achieved by adding a predictive or feed-forward component. This is particularly vital where significant time delays may be encountered. Examples of time delays are diesel-generator set power build-up, or even starting an additional thruster. The **feed-forward** elements may be wind velocity, V_w, and direction, α_w:

$$\vec{T} = f\left(X_1, X_2, X_6, \int (X_1, X_2, X_6)\, dt, \dot{X}_1, \dot{X}_2, \dot{X}_6, V_w, \alpha_w\right) \qquad \begin{matrix}\text{(PID-controller with} \\ \text{wind-feed-forward)}\end{matrix} \tag{10.43}$$

[Pinkster, 1978] suggested to extend the wind-feed-forward system with an intriguing wave-feed-forward system. He carried out model experiments in bow-quartering irregular waves ($H_{1/3} = 4.9$ m and $T_2 = 10.2$ s) and a stern-quartering current (1 knot). The wave-feed-forward system consisted of 8 ship-mounted wave probes. He showed that a wave-feed-forward system is capable to reduce the low-frequency part of the sway motion by about 70 % and the surge motion by about 50 %. The DP simulation procedure can be extended to include this factor, but the value of the simulation would depend primarily on the degree to which the simulated wave data represents possible actual wave measurements. So far, wave-feed-forward has not yet been incorporated in DP simulations.

The possibilities for evaluating the generalized function of eleven variables in equation 10.43 are limitless, hence the need for mathematical simulation.

10.4.2 Mathematical Model

For a dynamically positioned floating structure, only the horizontal low-frequency motions for surge ($k = 1$), sway ($k = 2$) and yaw ($k = 6$) are of interest. The thruster forces have to balance the mean wave, current and wind loads. Further, $\ddot{x}_k$, $\dot{x}_k$ and x_k are the slowly varying motions of the structure. It are the high-frequency motions of the waves that are neglected or filtered out, because it is generally impossible to have a system that can react to these high-frequency wave forces.

A general form of the three nonlinear coupled (Euler) equations of motion in the horizontal plane for surge, sway and yaw of a DP vessel - with an axes system as given in figure 10.16 - is given by:

$$\begin{aligned}
&(\rho\nabla + a_{11}) \cdot \ddot{x}_1(t) + b_{11} \cdot \dot{x}_1(t) + b_1^V \cdot \dot{x}_1(t) \cdot |\dot{x}_1(t)| - (\rho\nabla + a_{22}) \cdot \dot{x}_2(t) \cdot \dot{x}_6(t) = \\
&\qquad = F_1^W(t) + F_1^C(t) + F_1^{WD}(t) + F_1^R(t) + T_1(t) \\
&(\rho\nabla + a_{22}) \cdot \ddot{x}_2(t) + b_{22} \cdot \dot{x}_2(t) + b_2^V \cdot \dot{x}_2(t) \cdot |\dot{x}_2(t)| + (\rho\nabla + a_{11}) \cdot \dot{x}_1(t) \cdot \dot{x}_6(t) = \\
&\qquad = F_2^W(t) + F_2^C(t) + F_2^{WD}(t) + F_2^R(t) + T_2(t) \\
&(I_{66} + a_{66}) \cdot \ddot{x}_6(t) + b_{66} \cdot \dot{x}_6(t) + b_6^V \cdot \dot{x}_6(t) \cdot |\dot{x}_6(t)| - (a_{11} - a_{22}) \cdot \dot{x}_1(t) \cdot \dot{x}_2(t) = \\
&\qquad = F_6^W(t) + F_6^C(t) + F_6^{WD}(t) + F_6^R(t) + T_6(t)
\end{aligned} \tag{10.44}$$

where $\rho\nabla$ is the solid mass of the ship, I_{66} is the mass moment of inertia of the ship, a_{kk} is the hydrodynamic mass or inertia, b_{kk} is the hydrodynamic damping coefficient, b_k^V is the quadratic viscous drag force or moment coefficient, F_k^W is the wind force or moment, F_k^C is the current force or moment F_k^{WD} is the slow-drift wave excitation force or moment, $F_k^R(t)$ is the force or moment due to the riser and T_k is the thruster force or moment.

Notice the appearance here of a sway-yaw velocity coupling term in the surge equation, a surge-yaw velocity coupling term in the sway equation and a surge-sway velocity coupling term in the yaw equation. These three mass terms follow from a proper derivation of the nonlinear Euler equations of motion in the horizontal plane, which has been treated plentiful in the literature on manoeuvering, guidance and control of ships; for instance [Fossen, 1994].

The relative water velocity and direction - see figure 10.16 - are:

$$\begin{aligned} V_{C_R} &= \sqrt{\left(\dot{x}_1 + V_C \cos\gamma_C\right)^2 + \left(\dot{x}_2 + V_C \sin\gamma_C\right)^2} \\ \gamma_{C_R} &= \arctan\left(\frac{\dot{x}_2 + V_C \sin\gamma_C}{\dot{x}_1 + V_C \cos\gamma_C}\right) \end{aligned} \tag{10.45}$$

Then the current forces and moments can be obtained by:

$$F_k^C = R'_k\left(\gamma_{C_R}\right) \cdot V_{C_R}^2 \qquad \text{for}: \; k = 1, 2, 6 \tag{10.46}$$

where $R'_k\left(\gamma_{C_R}\right)$ is the resistance coefficient in the x_k-direction due to the relative water velocity in the γ_{C_R}-direction.
The vessel velocities along the fixed (global) axes (X_1, X_2) are related to the velocities along the local axes by the following transformation relations:

$$\begin{aligned} \dot{X}_1 &= \dot{x}_1 \cos x_6 - \dot{x}_2 \sin x_6 \\ \dot{X}_2 &= \dot{x}_2 \sin x_6 + \dot{x}_2 \cos x_6 \\ \dot{X}_6 &= \dot{x}_6 \end{aligned} \tag{10.47}$$

In addition, the excursions in surge sway and yaw are obtained from:

$$X_1 = \int \dot{X}_1 \cdot dt \qquad X_2 = \int \dot{X}_2 \cdot dt \qquad X_6 = \int \dot{X}_6 \cdot dt \tag{10.48}$$

The first-order differential equations governing thrust build-up with time of a DP system with a PID-controller can be written in the form:

$$\begin{aligned} T_1 + \tau_1 \cdot \frac{dT_1}{dt} &= -K_1^P \cdot X_1 - K_1^I \cdot \int_0^t X_1 \cdot dt - K_1^D \cdot \dot{X}_1 \\ T_2 + \tau_2 \cdot \frac{dT_2}{dt} &= -K_2^P \cdot X_2 - K_2^I \cdot \int_0^t X_2 \cdot dt - K_2^D \cdot \dot{X}_2 \\ T_6 + \tau_6 \cdot \frac{dT_6}{dt} &= -K_6^P \cdot X_6 - K_6^I \cdot \int_0^t X_6 \cdot dt - K_6^D \cdot \dot{X}_6 \end{aligned} \tag{10.49}$$

where τ_k are **time constants** and the right hand term and K_k^P, $K_k^I$and K_k^D are **gain constants** of the PID-controller.
Sometimes, a low-pass filter is used in the last term, $K_i^D \cdot \dot{X}_i$, which avoids undesirable effects of high frequencies.

10.4.3 Wind Feed-Forward

[McClure et al., 1990] give a practical example of the utility of a simulation with wind feed-forward for the response of a 189 meter length ship to a sudden squall. Their equations of motion are comparable to those given in 10.44. In each of their simulation runs, the ship was in equilibrium in 29 knots wind, half a knot current and a sea with a significant wave height of 4.5 meter. The squall is of 600 seconds duration with wind velocities of about 35 to 60 knots, see figure 10.17-a.

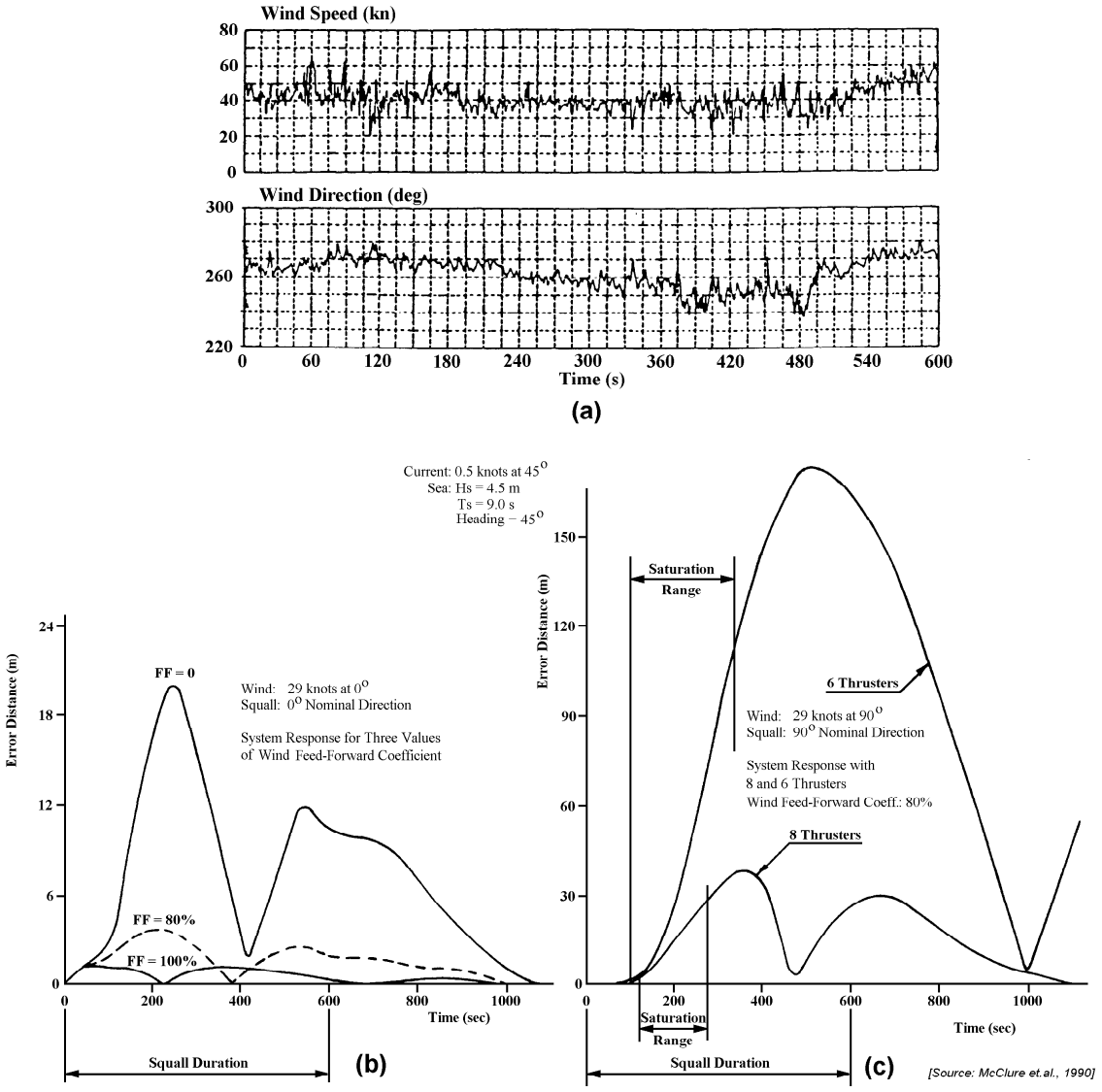

Figure 10.17: Squall Simulation with Head and Beam Wind

With the squall from directly ahead, the thrusters have sufficient capacity and the system behaves satisfactory. The benefit of wind feed-forward is illustrated in figure 10.17-b. Without wind feed-forward, the vessel moves 20 meter off station and overshoots 12 meter before setting down. Feed-forward can never be 100 % effective, so performance at 80 % effectiveness - which is a reasonable expectation - is also shown in this figure.
When the squall is imposed from the beam direction, the thrusters are momentarily loaded

to capacity and the system is 'saturated'. Figure 10.17-c illustrates the necessity of providing thrust in excess of the static balance. The curves shown represent in one case 3 thrusters available, 10,300 kWh, and in the other case 6 thrusters totalling 7725 kWh. Either system has more than enough thrust to exceed the equilibrium loading. Both cases include wind feed-forward at 80 % effectiveness. Note that the time during which the system is saturated is relatively brief, yet the system allows large drift and overshoot.

10.4.4 Gain Constants Estimate

For a DP system there has to be an allocation system that tells how the power should be distributed among the individual thruster units. If the thrusters are a part of a DP system with a PD-controller, an idealized simplification of the total thruster forces - with time constant $\tau \rightarrow 0$ - can be written as:

$$T_k = -K_k^P \cdot X_k - K_k^D \cdot \dot{X}_k \qquad \text{for: } k = 1, 2, 6 \tag{10.50}$$

[Faltinsen, 1990] proposes a simple method to get a feeling for the magnitude of the gain constants, K_k^D and K_k^P of the PD-controller of a dynamically positioned ship. An example is given here for surge, of which the simplified uncoupled equation of the slow-drift motion is given by:

$$(m_{11} + a_{11}) \cdot \ddot{x}_1 + b_{11} \cdot \dot{x}_1 = F_1^{SW} + F_1^W + T_1 \tag{10.51}$$

A substitution of equation 10.50 (with $x_1 = X_1$ and $\dot{x}_1 = \dot{X}_1$) in equation 10.51 provides equation 10.52 for surge of the DP vessel:

$$(m_{11} + a_{11}) \cdot \ddot{x}_1 + \left(b_{11} + K_1^D\right) \cdot \dot{x}_1 + K_1^P \cdot x_1 = F_1^{SW} + F_1^W \tag{10.52}$$

where m_{11} is the mass of the ship, a_{11} is the hydrodynamic mass, b_{11} is the hydrodynamic damping, F_1^{SW} is the slow-drift wave excitation force and F_1^W the gust force. The mean values of F_1^{SW} and F_1^W are supposed to be zero.
The gain constant K_1^P will be chosen so that the natural period in surge of the slowly oscillating ship is from 100-200 seconds. The damping coefficient, b_{11}, has been neglected by Faltinsen at this very low frequency and the gain constant K_1^D was set equal to about 60 % of the critical damping; so $\kappa = 0.60$, see chapter 6. The final real values will be decided after full scale sea tests with the DP system.
Thus, as a first estimate:

$$\begin{aligned} K_1^P &= \omega_0^2 \cdot (m_{11} + a_{11}) \qquad \text{where } \omega_0 = \frac{150}{2\pi}, \text{ for instance} \\ K_1^D &= 1.20 \cdot \sqrt{(m_{11} + a_{11}) \cdot K_1^P} \end{aligned} \tag{10.53}$$

With these equations, the variance of the slow-drift surge motion can be calculated in a way as has been done in chapter 6 for motions with frequencies in the wave-frequency range. Finally, the variance of the total thruster forces follow from equation 10.50.
For ships, the potential mass for surge can be approximated by 5-8 % of the ship's solid mass. The damping coefficient, b_{11}, has assumed to be zero here. This assumption is true for the potential damping but viscous effects can have some influence. In some papers, the use of a surge damping coefficient of about 5 % of the critical damping of a soft spring system is recommended.

10.4.5 Motion Reference Filtering

Suppose a simple uncoupled equation of motion for sway of a DP vessel, given by:

$$(m_{22} + a_{22}) \cdot \ddot{x}_2(t) + b_{22} \cdot \dot{x}_2(t) = F_2^D(t) + T_2(t) \tag{10.54}$$

where $F_2^D(t)$ is the total sway drift force and $T_2(t)$ is the total sway thruster force.
The use of a PD-controller means that the thruster force contains a part which is proportional (P) to the position error, $x_2(t)$, and a part which is proportional to the derivative (D) to time of this position error, the velocity $\dot{x}_2(t)$. To obtain 'smooth' input signals $x_2(t)$ and $\dot{x}_2(t)$, the measured reference signal, $x_2(t)$ - being obtained by systems such as Loran, GPS, a taut wire system or an acoustic system - has to be filtered; the wave frequency motions and the high frequency disturbances are filtered out. But, filtering - for instance by using a Kalman filter - necessarily introduces a time lag, τ. Due to this time lag, the thruster force is applied 'later':

$$T_2(t) = -K_2^P \cdot X(t-\tau) - K_2^D \cdot \dot{X}_2(t-\tau) \tag{10.55}$$

where τ is the time lag of the DP system between the filtered motion signals and the thruster reaction.
However, thruster forces are affected by the presence of waves. This holds that - in spite of filtering out of wave frequent motions - via the actual thruster forces wave frequent contributions will be introduced again in the system.
The displacement and velocity can be expanded in series:

$$\begin{aligned} X_2(t-\tau) &= X_2(t) - \frac{\partial\{X_2(t)\}}{\partial t} \cdot \tau + ... \\ \dot{X}_2(t-\tau) &= \dot{X}_2(t) - \frac{\partial\left\{\dot{X}_2(t)\right\}}{\partial t} \cdot \tau + ... \end{aligned} \tag{10.56}$$

These series can be simplified by assuming τ to be small relative to the natural period of the sway motion; thus a linearization is permitted:

$$\begin{aligned} X_2(t-\tau) &= X_2(t) - \dot{X}_2(t) \cdot \tau \\ \dot{X}_2(t-\tau) &= \dot{X}_2(t) - \ddot{X}_2(t) \cdot \tau \end{aligned} \tag{10.57}$$

so:

$$T_2(t) = +K_2^D \cdot \ddot{X}_2(t) \cdot \tau + \left\{-K_2^D + K_2^P \cdot \tau\right\} \cdot \dot{X}_2(t) - K_2^P \cdot X_2(t) \tag{10.58}$$

With $\ddot{x}_2 = \ddot{X}_2$, $\dot{x}_2 = \dot{X}_2$ and $x_2 = X_2$, the following expression is found from equation 10.54:

$$\left(m_{22} + a_{22} - K_2^D \cdot \tau\right) \cdot \ddot{x}_2(t) + \left(b_{22} + K_2^D - K_2^P \cdot \tau\right) \cdot \dot{x}_2(t) + K_2^P \cdot x_2(t) = F_2^D(t) \tag{10.59}$$

This equation shows that the effect of a time lag in the DP system is to reduce the mass term in the equation of motion and also to reduce the damping term.
Assuming that the total sway drift force, $F_2^D(t)$, can be characterized as a low frequency 'white noise' process with mean value $\overline{F_2^D}$ and the spectral density, S_f, the above equation

of motion can be solved in the frequency domain, as has been discussed at the end of chapter 9.
The results with respect to the variance of the sway velocity are as follows:

$$\sigma_{x_2}^2 = \frac{\pi}{2 \cdot (b_{22} + K_2^D - K_2^P \cdot \tau) \cdot K_2^P} \cdot S_f \tag{10.60}$$

$$\sigma_{\dot{x}_2}^2 = \frac{\pi}{2 \cdot (b_{22} + K_2^D - K_2^P \cdot \tau) \cdot (m_{22} + a_{22} - K_2^D \cdot \tau)} \cdot S_f \tag{10.61}$$

Since the sway motion and the sway velocity are not-correlated processes, the variance of the total thruster force is found to be as follows:

$$\sigma_{F_{2_T}}^2 = \left(K_2^P \cdot \sigma_{x_2}\right)^2 + \left(K_2^D \cdot \sigma_{\dot{x}_2}\right)^2 \tag{10.62}$$

The mean thruster force follows from:

$$\overline{T_2} = -\overline{F_2^D} \tag{10.63}$$

Because τ is in the nominator of equations 10.60, 10.61 and 10.62, it is obvious that an increased time lag, τ, results in increased variances, σ, of the motions together with also increased required thruster forces. This means that attention has to be paid to a careful choice and a proper use of the filtering technique.

10.4.6 Role of Model Tests

The role of model tests in the design process of a DP control system for a vessel is well described by [McClure et al., 1990]. Their view on this subject is summarized below.

Clearly, the availability of today's computing power and sophisticated graphics engines render the use of digital time domain, non-linear dynamic simulation programs the best alternative for validating band optimizing the design of modern DP systems. These simulation programs require reliable functional relationships between environmental parameters such as current speed, wind speed, wave height and period - together with their directions to the ships heading - and longitudinal force, side force and yaw moment. In addition to these environmental 'forcing functions' the performance of thrusters, rudders and main propulsors in providing reaction forces and moments in opposition to the environmental forces is required in terms of applied power, thruster orientation and proximity to other propulsion devices.
Despite the advancement of numerical models for the prediction of hydro- and aerodynamic forces on floating structures, they still do not posses sufficient precision for providing an adequate function for use in the dynamic simulators, particularly as the requirements to analyze the station keeping of permanent systems for deep water and hostile environments emerge.
The role of physical model experiments in DP system design, validation and optimization is analogous to their role in supporting maneuvering simulators for surface ships and submarines. This role can be viewed in comparison with the full physical simulation of a DP system at model scale in a similar way that the use of model tests and maneuvering simulators are compared with free-running maneuvering experiments. Both of these 'full physical simulations' are expensive, require physical reproduction of the controller and all

of its strategies and suffer from hydrodynamic and time scale effects. Large models are required to minimize scale effects on control appendage effectiveness and a thorough examination of the sensitivity to overall response to subtle changes in control algorithms is so time consuming as to be virtually impossible.
Nonetheless, some tests facilities have conducted experiments, where a 'complete' physical simulation of a DP system was undertaken. However, the opinion of [McClure et al., 1990] is that such simulations are useful, only to validate numerical codes and are not a viable design or optimization tool.

Nowadays, the efficient use of model tests to provide inputs required by numerical simulators are mainly restricted to the following aspects:

- Wind Forces and Moments
  The use of wind tunnel models to establish the longitudinal and lateral wind force coefficients for mono-hulls and semi-submersibles we well-known. Scale effects due to Reynolds number disparity between model and full scale are mitigated somewhat due to the bluffness of the elements of the above water portion of these vessels. While there exists published data for some classes of vessels, [OCIMF, 1977], it is advisable to conduct experiments to determine the aerodynamic coefficients when the configuration of the above water portion of the vessel departs significantly from that for which published data is available.

- Current Forces and Moments
  If it were possible to always maintain a nearly zero heading with respect to the current, such information would not be terribly important. However, the likelihood of misalignment between the direction of sea, wind and current can be high in tidal seas and estuaries and during squalls. So, in order to accurately analyze the response of a dynamically positioned vessel, it is necessary to understand the relationship between the coefficients of longitudinal and lateral forces and yaw moment and heading.
  Again, it would be useful to use existing systematic series data to determine these coefficients. Indeed, some data has been assembled for tankers by the Oil Company International Marine Forum, [OCIMF, 1977]. However, this data is for a limited class of hull forms. Changes in many hull form parameters such as length to draft ration and fore and aft body fineness, as well as the distribution and size of appendages, can change these coefficients.
  The foregoing is no less true for column stabilized floating platforms. Physical model tests are the best tool today for quantifying these important inputs to the simulator. Nonetheless, the scale of the model must be chosen carefully. It has been shown by [Edwards, 1985] that Reynolds number (based upon beam) of approximately 500,000 are required to produce reliable results for the current force and moment coefficients. This implied model scales on the order of 1:20 to 1:30.

- Wave Induced Forces and Moments
  The forces exerted on a floating body by waves at wave-frequency are ignored in current DP system designs, because it is recognized that response times for the systems cannot approach that necessary to effectively control position at wave-frequency and because wave-frequency oscillations in the horizontal plane are not usually large enough to limit operations. On the other hand, the steady component of wave inducted longitudinal and lateral force and yaw moment must be reacted out by a the

positioning system. The slowly varying component of these forces and moments must be at least be attenuated.
Numerical models have been developed which provide estimates of the steady and slowly varying components of the wave drift forces and moments. Nonetheless, to confirm these estimates for new designs, it is advisable to obtain a semi-empirical relationship between the steady force and moment coefficients and wave period in regular waves. Estimates of the slowly varying drift force and moment coefficients can also be derived from experiments in regular wave 'beats' and from irregular wave tests using cross bi-spectral analysis techniques to derive quadratic transfer functions for second order wave forces. These model tests can be conducted using relative small and inexpensive models, on the order of 1:50, because viscous effects are relatively unimportant in physical simulation of wave drift.

- Thruster Effectiveness
  The effectiveness of thrusters in producing forces and moments to react out the environmental forces and moments is necessary information for the simulator. It is not adequate to consider the thruster in isolation, as done in a foregoing section, because depending upon the proximity of thrusters, their inflow and outflow fields can interact, producing deviations in effectiveness from that which would be expected if the thrusters' force and moment applied to the vessel were calculated taking inflow velocity (free stream current), propeller angular speed and pitch into account and using performance curves for the isolated thruster. For vessels where it is impossible to avoid placing the thrusters where the inflow and outflow fields may interfere, physical model tests are the only reliable way to define the effects.
  These experiments are carried out best with a large captive model. The model is restrained in surge, sway and yaw. The model is towed at various speeds and headings and various thruster operating conditions are prescribed. The resulting residual forces and moments are measured. This data base is used in conjunction with a similar data base obtained from towed tests without the thrusters and propulsors operating to derive the effectiveness and interaction polar plots for the thrusters and propulsors.

.

Chapter 11

OPERABILITY

Ship motions and sea loads can influence the behavior and operability of the ship significantly. The ship's speed will be reduced due to an involuntary speed reduction and it can be reduced voluntarily as well. Involuntary speed reduction is the result of added resistance of the ship due to wind and waves and changes in the propeller efficiency due to the waves and the loading of the propeller. Voluntary speed reduction means that the ship's master reduces the speed due to (green) water on deck or heavy slamming or to reduce large accelerations. Environmental conditions can even lead to an involuntary change of the ship's course.
This chapter discusses ship operability in a variety of contexts, but first some necessary theory on statistics is reviewed.

11.1 Statistics

11.1.1 Short Term Predictions

The basis for calculating a response - such as for instance the pressure at a specified point - is the transfer function of that response. As has been shown in chapter 6, the response spectrum is calculated by multiplying transfer function, $|H_{R\zeta}(\omega)| = R_a/\zeta_a(\omega)$, squared by the incident wave spectrum, $S_\zeta(\omega)$:

$$S_{R\zeta} = |H_{R\zeta}(\omega)|^2 \cdot S_\zeta(\omega) \tag{11.1}$$

Assuming stationary Gaussian incoming waves and a narrow banded response spectrum, the response amplitudes are Rayleigh distributed.
Then the Rayleigh short term probability density function of the response is given as:

$$\boxed{f_{ST}(R_a) = \frac{R_a}{m_{0R}} \cdot \exp\left\{-\frac{R_a^2}{2m_{0R}}\right\}} \tag{11.2}$$

in which m_{0R} is defined as the area under the response spectrum.

[0] J.M.J. Journée and W.W. Massie, *"OFFSHORE HYDROMECHANICS"*, First Edition, January 2001, Delft University of Technology. For updates see web site: http://www.shipmotions.nl.

11.1.2 Long Term Predictions

This short term probability density function, $f_{ST}(R_a)$, has to be calculated for all wave direction intervals, μ_i, and sea state intervals, defined by (H_j, T_k), in order to determine the long term probability density function, $f_{LT}(R_a)$, which can be calculated as the weighted sum of all short term results:

$$\boxed{f_{LT}(R_a) = \sum_{i=1}^{N_\mu} \sum_{j=1}^{N_H} \sum_{k=1}^{N_T} f_{ST}(R_a)_{i,j,k} \cdot f_i \cdot f_{j,k}} \tag{11.3}$$

in which:

N_μ	=	number of wave direction intervals, μ_i
N_H	=	number of wave height intervals, H_j
N_T	=	number of wave period intervals, T_k
f_i	=	long term probability of wave direction interval μ_i
$f_{j,k}$	=	long term probability of wave height and period interval (H_j, T_k) within the wave direction interval μ_i

The long term sea state probabilities f_i and $f_{j,k}$ can be obtained from wave scatter diagrams. Diagrams for $f_{j,k}$ have been given in chapter 5 for the North Atlantic Ocean and the northern North Sea for all wave directions together; then: $N_\mu = 1$ and $f_i = f_{N_\mu} = 1$.
The long term probability density function, $f_{LT}(x)$, can be integrated to obtain the long term cumulative distribution function, $F_{LT}(R_a)$:

$$F_{LT}(R_a) = \int_0^{R_a} f_{LT}(x) \cdot dx \tag{11.4}$$

When carrying this out numerically, it is advised to integrate in an opposite direction: from the upper tail (high response amplitudes) to zero. This actually computes $\{1 - F_{LT}(R_a)\}$, which can represent the upper tail part more accurately by minimizing numerical errors.
The zero-crossing period of the response in a certain sea state is given by the spectral moments as $T_{2R} = 2\pi\sqrt{m_{0R}/m_{2R}}$ and the mean period over a number of years can be determined by weighting these periods - using the wave scatter diagram - over the wave directions and sea states.
Then the number of observations or cycles, n, during Y years is thus calculated as:

$$n_{Y \text{ years}} = \frac{Y \cdot 365 \cdot 24 \cdot 60 \cdot 60}{\sum_{i=1}^{N_\mu} \sum_{j=1}^{N_H} \sum_{k=1}^{N_T} f_i \cdot f_{j,k} \cdot T_{2R}(i,j,k)} \tag{11.5}$$

This analysis assumes that the observer is continuously exposed to this one wave climate at that particular location.

11.1.3 Extreme Values

There is a relation between the distribution of the maxima or peaks in one sea state (short term) and the distribution of the extremes in a number of equal sea states (long term).

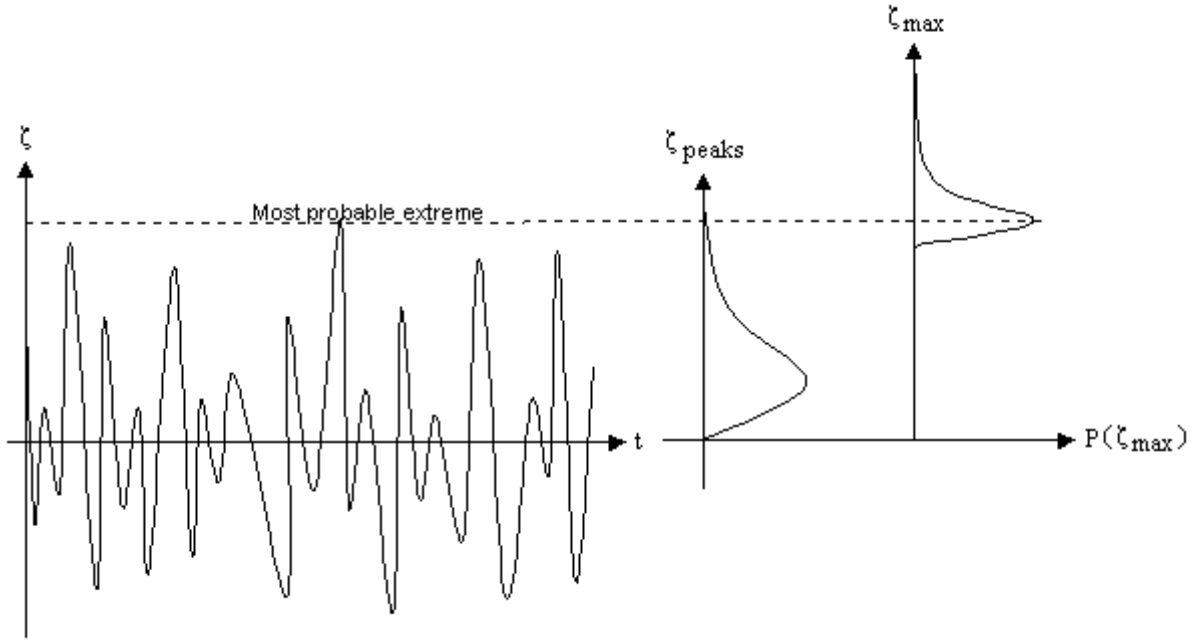

Figure 11.1: Probability Distributions of Maxima and Extremes in an Irregular Sea

Figure 11.1 shows this relation. The short term distribution of the maxima or peaks is the left distribution in this figure and the distribution of the extremes during a long period is the right distribution. This will be discussed in more detail now.

In general the response of a ship to irregular waves is a random variable with an initial probability density function, $f(x)$, and an initial cumulative distribution function, $F(x)$. The extreme value of this irregular response is defined as the largest value expected to occur in a certain number of observations or during a certain period of time.
Let a set of observed (absolute) crest and trough values (x_1, x_2, x_3, ..., x_n) of an irregular response be a random sample of n observations. The elements of this random sample are arranged in an ascending order of magnitude such that $x_1 < x_2 < x_3 < ..... < x_n$; thus the largest value - expected to occur in n observations - is named x_n. This x_n is a random variable as well with its own extreme value probability density function, $g(x_n)$, and extreme value cumulative distribution function, $G(x_n)$.
It is subject of considerable interest in statistics to find the asymptotic behavior of the extreme value cumulative distribution function, $G(x_n)$, for a large sample size n. In other words the question arises: "Do these functions give us the opportunity to determine important phenomena such as the expected maximum response amplitude of a ship during for instance its lifetime or the expected maximum wave height being encountered in for instance a 50-years period, the so-called 50-years wave?" The answer is yes; the probability functions $f(x)$, $F(x)$, $g(x_n)$ and $G(x_n)$ have mathematical relationships which enable us to solve these problems, as will be shown here. The extreme values can be evaluated precisely from the knowledge of the initial probability density function.
From the definition of the cumulative distribution function follows:

$$f(x) = \frac{dF(x)}{dx} \qquad \text{and} \qquad g(x_n) = \frac{dG(x_n)}{dx_n} \tag{11.6}$$

As has been shown in chapter 5 for irregular waves, the probability that an arbitrary response amplitude in irregular waves, R_a, does not exceed a value A is given by:

$$P\{R_a < A\} = \int_0^A f(x) \cdot dx = F(A) \tag{11.7}$$

Thus, the probability that *one* response amplitude in irregular waves does not exceed a value x_n is given by:

$$P\{x < x_n\} \quad \text{in 1 observation} = F(x_n) \tag{11.8}$$

The probability that n response amplitudes in irregular waves does not exceed a value x_n follows from a multiplication of the individual probabilities - assuming independence of the individual response amplitudes - by:

$$\begin{aligned} P\{x < x_n\} \quad \text{in } n \text{ observations} &= (P\{x < x_n\})^n \\ &= \{F(x_n)\}^n \end{aligned} \tag{11.9}$$

Thus, the extreme value cumulative distribution function, $G(x_n)$, in n observations can be formulated as:

$$G(x_n) = \{F(x_n)\}^n \tag{11.10}$$

The extreme value probability density function, $g(x_n)$, in n observations is the derivative of the function $G(x_n)$:

$$\begin{aligned} g(x_n) &= \frac{dG(x_n)}{dx_n} \\ &= n \cdot \{F(x_n)\}^{n-1} \cdot \frac{dF(x_n)}{dx_n} \\ &= n \cdot \{F(x_n)\}^{n-1} \cdot f(x_n) \end{aligned} \tag{11.11}$$

The probability density functions $g(x_n)$ for various n values are shown in figure 11.2.
An explanatory sketch - illustrating the relationship between the probability density functions $f(x)$ and $g(x_n)$ - is shown in figure 11.3.
Figure 11.3 also shows that - following the so-called modal value approach - the extreme value is defined as the value having the highest probability of occurrence. At that point:

$$\frac{dg(x_n)}{dx_n} = 0 \tag{11.12}$$

so that:

$$\frac{df(x_n)}{dx_n} \cdot F(x_n) + (n-1) \cdot \{f(x_n)\}^2 = 0 \tag{11.13}$$

Rewriting this equation and dividing it by $1 - F(x_n)$ results in:

$$\frac{1}{1-F(x_n)} = -\frac{n-1}{F(x_n)} \cdot \frac{f(x_n)}{1-F(x_n)} \cdot \frac{f(x_n)}{\frac{df(x_n)}{dx_n}} \tag{11.14}$$

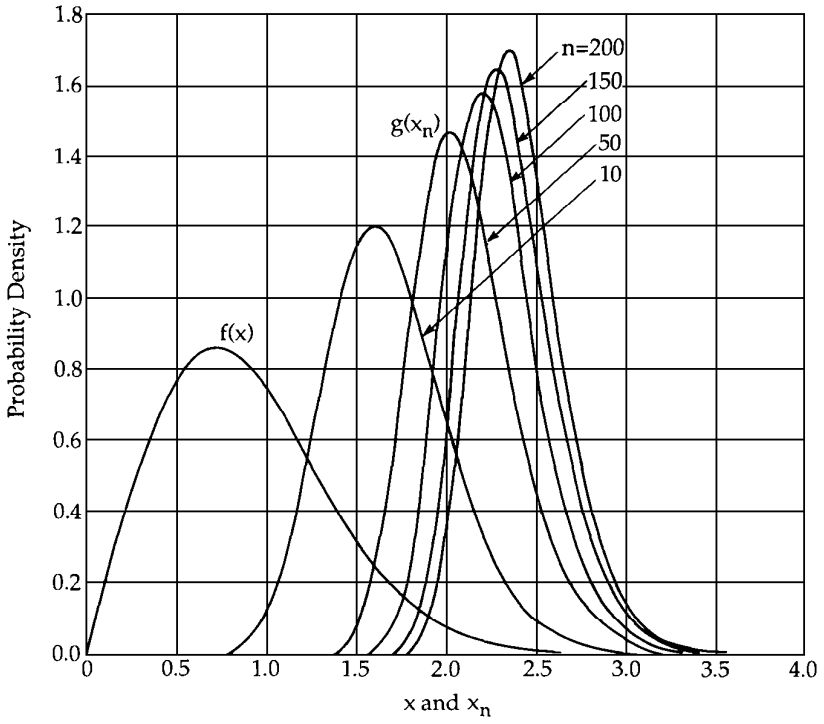

Figure 11.2: Extreme Value Function $g(x_n)$ from Rayleigh Distribution for Various n-Values

Applying the L'Hopital rule:

$$\frac{f\left(x_n\right)}{1-F\left(x_n\right)} = -\frac{\frac{df(x_n)}{dx_n}}{f\left(x_n\right)} \qquad \text{for large } x_n \tag{11.15}$$

results in:

$$\frac{1}{1-F\left(x_n\right)} = \frac{n-1}{F\left(x_n\right)} \approx n \qquad \text{for large } n \text{ and } x_n \tag{11.16}$$

or:

$$\frac{df\left(x_n\right)}{dx_n} \approx \frac{-1}{n} \quad \text{and} \quad F\left(x_n\right) \approx 1-\frac{1}{n} \qquad \text{for large } n \text{ and } x_n \tag{11.17}$$

This last formula 11.17 states that the most probable extreme value expected to occur in n observations, x_n, can be evaluated from the initial cumulative distribution function, $F\left(x_n\right)$, as the value for which the **return period** is equal to n or the probability of exceeding this value is $1/n$. The return period, here, is nothing more than reciprocal frequency. It should not be interpreted directly in terms of an actual time interval between occurrences

Now the extreme wave or response amplitude with an expected average return period of - for instance - 50 years can be determined. Also extreme significant amplitudes - and the most probable extreme amplitude within this response spectrum - can be determined.
For the sake of clearness and simplicity, the examples given here are for the waves only. By using transfer functions, R_a/ζ_a, with an amplitude of 1.0 all previous equations reduce to equations for the probabilities of the irregular waves themselves. This is picked up again later.

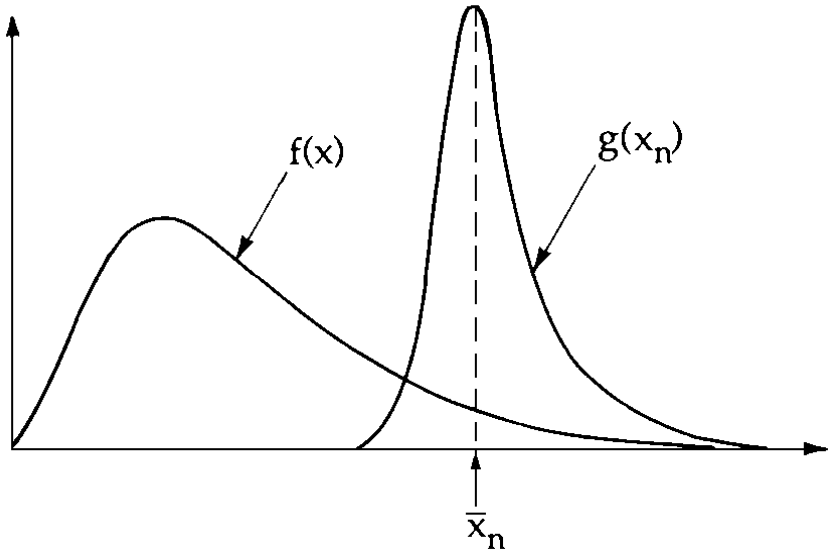

Figure 11.3: Functions $f(x)$ and $g(x_n)$ and Most Probable Extreme Value $\overline{x}_n$

Extreme Wave Amplitude

The wave scatter diagram for the Forties Field - an oil field in the Central North Sea - has been used in this example. This diagram with 126,007 observations of the significant wave height and the mean zero-crossing period during 21.5 years - so one observation every $1\frac{1}{2}$ hours - is given below.

Wave Scatter Diagram of Forties Field

$H_{1/3}$ (m) \ T_2 (s)	2.5	3.5	4.5	5.5	6.5	7.5	8.5	9.5	10.5	11.5	12.5	13.5	Total
12.75													
12.25									1				1
11.75													
11.25									2	1			3
10.75								2	5	2			9
10.25							1	3	7	5			16
9.75							1	9	11	6			27
9.25							4	30	16	6			56
8.75							16	40	16				72
8.25						2	29	61	8	1			101
7.75						2	104	84	2				192
7.25						8	175	72	3				258
6.75					1	71	313	74	4				463
6.25					3	222	401	47	2	1			676
5.75				1	7	621	431	42	2				1104
5.25				2	114	1228	321	29	5				1699
4.75				3	681	1885	243	19					2831
4.25			3	26	2530	1885	237	35	3				4719
3.75			2	407	4892	1371	221	35	9				6937
3.25			14	2827	5604	1019	205	41	8				9718
2.75		3	233	7972	4588	901	184	33	1				13915
2.25		7	2771	11367	3336	766	129	28	9				18143
1.75		315	9872	8688	2133	446	80	21	6		1		21562
1.25	14	3522	12850	5628	1626	351	79	38	7	2	1		24118
0.75	376	6785	6765	2299	732	277	95	29	10	1	1		17370
0.25	159	652	483	240	106	54	24	17	12				1747
Total	549	11284	32993	39460	26353	11109	3293	789	149	25	3		126007

The resulting cumulative probability distribution functions can be plotted on Weibull paper; see figure 11.4.

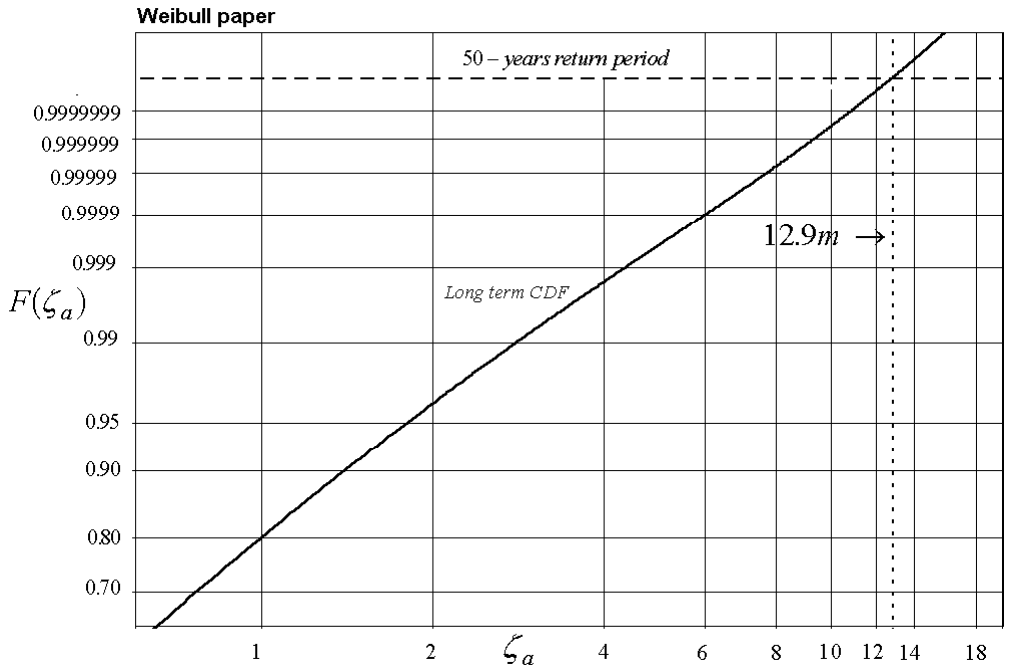

Figure 11.4: Weibull Distribution of Extreme Wave Amplitudes

Long term probability density functions, $f_{LT}(\zeta_a)$, as given in equation 11.3, can be obtained by using the wave scatter diagram of the considered sea area. These functions are integrated, using equation 11.4, to obtain the long term cumulative distribution function, $F_{LT}(\zeta_a)$, - marked by CDF in figure 11.4. So this long term CDF-curve is fully calculated here.
The number of wave cycles during 50 years, $n_{50\text{ years}}$, can be obtained by putting $Y = 50$ in equation 11.5 and using the wave scatter diagram. Equation 11.17 provides the value of the cumulative probability distribution function: $F(\zeta_a) = 1 - 1/n_{50\text{ years}}$. This $F(\zeta_a)$ and the CDF-curve in figure 11.4 provide the **extreme wave amplitude with an expected return period of 50 years**; in this example: $\zeta_a = 12.90$ meter or wave height is 25.80 meter.

Significant Wave Height of an Extreme Sea State

From the wave scatter diagram the probabilities for the significant wave height are known, $F\left(H_{1/3}\right)$; these can be obtained from the most right column. By plotting these probabilities for the significant wave height on Weibull paper - see the Weibull distribution in chapter 5 - the extreme sea state once every 50 years can be determined. Since the total number of observations is 126,007 over 21.5 years the total number of observations in 50 years is $N = 126007 \cdot 50 \,/\, 12.5$. Thus $F\left(H_{1/3}\right)_{50\text{ years}} = 1 - 1/N$. Because the plotted data of the scatter diagram is often not accurate for the higher sea states - the connecting (dotted) line is curved and twisted - a fit has to be carried out. In figure 11.5, the 3-parameter Weibull plot is fitted on all data (dotted line = data).

$$F\left(H_{1/3}\right) = 1 - \exp\left\{-\left(\frac{H_{1/3} - a}{c}\right)^{b}\right\} \qquad \text{(Weibull)} \tag{11.18}$$

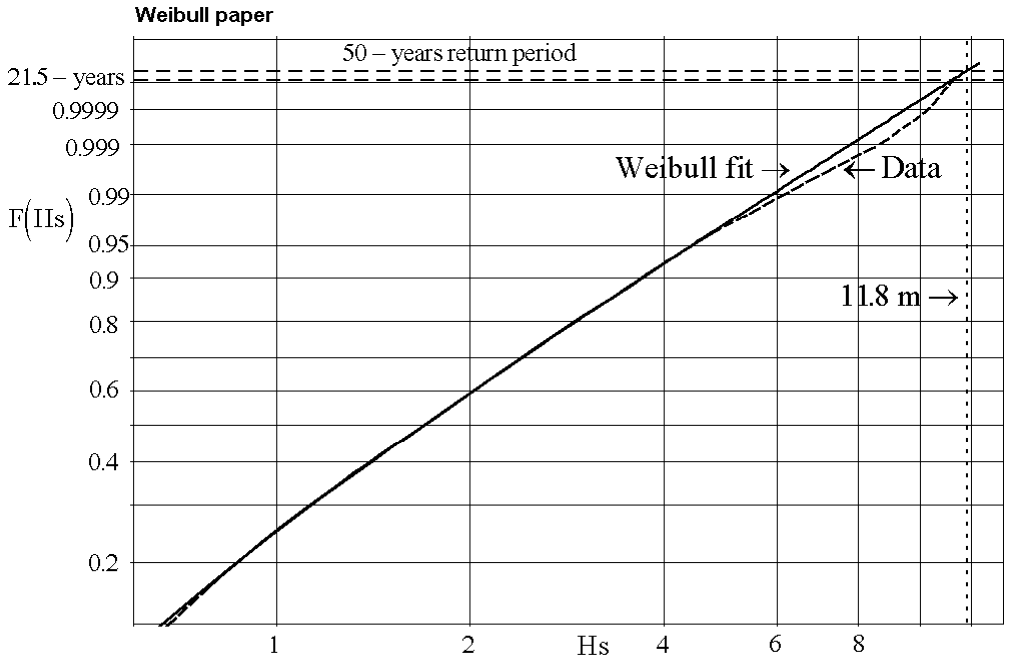

Figure 11.5: Probability Distribution of Significant Wave Heights

This plot gives a straight curve for higher sea states and is then used to determine the extreme significant wave height. From the figure follows that the **extreme significant wave height with a return period of 50 years** is 11.80 meter.
Obviously, the type of fitting is important. How to weigh the importance of the tail? In this case, paying more attention to the upper tail would lead to a fit with a higher extreme significant wave height than a simple extrapolation of the data curve.

Extreme Wave Amplitude in an Extreme Sea State

Consider now this extreme sea state with a return period of 50 years - lasting 3 hours, as generally done in offshore calculations. Using the formulation for the most probable maximum, $F\left(\zeta_a\right) = 1 - 1/N$, the extreme wave amplitude in this sea state can be calculated from the Rayleigh distribution:

$$P\left\{\zeta_a > \zeta_{a\ \max\ (50\ \text{years storm})}\right\} = \exp\left\{-\frac{\zeta^2_{a\ \max\ (50\ \text{years storm})}}{2 \cdot m_{0\zeta}}\right\} = \frac{1}{N} \tag{11.19}$$

or:

$$\zeta_{a\ \max\ (50\ \text{years storm})} = \sqrt{2 \cdot m_{0\zeta} \cdot \ln\left(N\right)} \tag{11.20}$$

The number of cycles, N, can be determined by using a wave period $T_2 = 12.0$ seconds. This is the average (central) period belonging to the extreme significant wave height of 11.80 meter, as obtained from the wave scatter diagram.

The spectral area, $m_{0\zeta}$, is determined by:

$$H_{1/3} = 4 \cdot \sqrt{m_{0\zeta}} \qquad \text{or} \qquad m_{0\zeta} = \frac{1}{4} \cdot H_{1/3}^2 \tag{11.21}$$

in which $H_{1/3}$ is the significant wave height of the extreme sea state with an expected return period of 50 years (11.80 meter in this example).
The resulting **extreme wave amplitude in the extreme sea state** is then 10.90 meter, which is about 1.85 times the significant wave amplitude.
This extreme amplitude is lower than the extreme wave amplitude with an expected return period of 50 years (12.90 meter in this example). It is left to the reader to explain why.

11.2 Operating Limits of Ships

For various types of vessels, some typical phenomena and general operability limiting criteria are given in this section.

11.2.1 Personnel Safety

Some general operability limiting criteria for ships, partially taken from [Faltinsen, 1990], are given below.

General Operability Limiting Criteria for Ships

(NORDFORSK, 1987)

Description	Merchant ships	Naval vessels	Fast small craft
RMS of vertical acceleration at F.P.P.	0.275 g ($L \leq 100$ m) 0.050 g ($L \geq 330$ m)	0.275 g	0.65 g
RMS of vertical acceleration at bridge	0.15 g	0.20 g	0.275 g
RMS of lateral acceleration at bridge	0.12 g	0.10 g	0.10 g
RMS of roll	6.0 deg	4.0 deg	4.0 deg
Probability on slamming	0.03 ($L \leq 100$ m) 0.01 ($L \geq 300$ m)	0.03	0.03
Probability on deck wetness	0.05	0.05	0.05

For intermediate lengths in the criteria for the vertical acceleration forward and the criteria for slamming, a linear interpolation can be used.
The limiting criteria for fast small craft are only indicative of trends. A fast craft is defined as a vessel under about 35 meters in length with a speed in excess of 30 knots. A reason why the vertical acceleration level for fast small craft is set higher than for merchant ships and

naval vessels, is that personnel can tolerate higher vertical acceleration when the frequency of oscillation is high.

Criteria for accelerations and roll for various types of work and for passenger comfort are given in the following table.

Criteria for Accelerations and Roll

(NORDFORSK, 1987)

Description	RMS vertical acceleration	RMS lateral acceleration	RMS roll
Light manual work	0.20 g	0.10 g	6.0 deg
Heavy manual work	0.15 g	0.07 g	4.0 deg
Intellectual work	0.10 g	0.05 g	3.0 deg
Transit passengers	0.05 g	0.04 g	2.5 deg
Cruise liner	0.02 g	0.03 g	2.0 deg

11.2.2 Shipping Water

The relative motions between the ship and the water surface are generally largest at the ends of the ship. In high waves the motions may be so large that the forefoot and propeller are exposed and the deck submerged. This occurs most frequently at high speed in head waves, although it is not unknown in other conditions. The effective dynamic freeboard will differ from the results obtained from the geometric freeboard at zero forward speed in still water and the calculated vertical relative motions of a sailing ship in waves.
When sailing in still water, sinkage, trim and the ship's wave system will effect the local geometric freeboard. A static swell up should be taken into account.
An empirical formula - based on model experiments - for the static swell up at the forward perpendicular is given by [Tasaki, 1963]:

$$f_e = f - \zeta_B \qquad \text{with:} \qquad \zeta_B = 0.75B \cdot \frac{L}{L_E} \cdot F_n^2 \tag{11.22}$$

with:

f_e = effective freeboard at the forward perpendicular
f = geometric freeboard at the forward perpendicular
ζ_B = bow wave
L = length of the ship
B = breadth of the ship
L_E = length of entrance of the waterline
F_n = Froude number

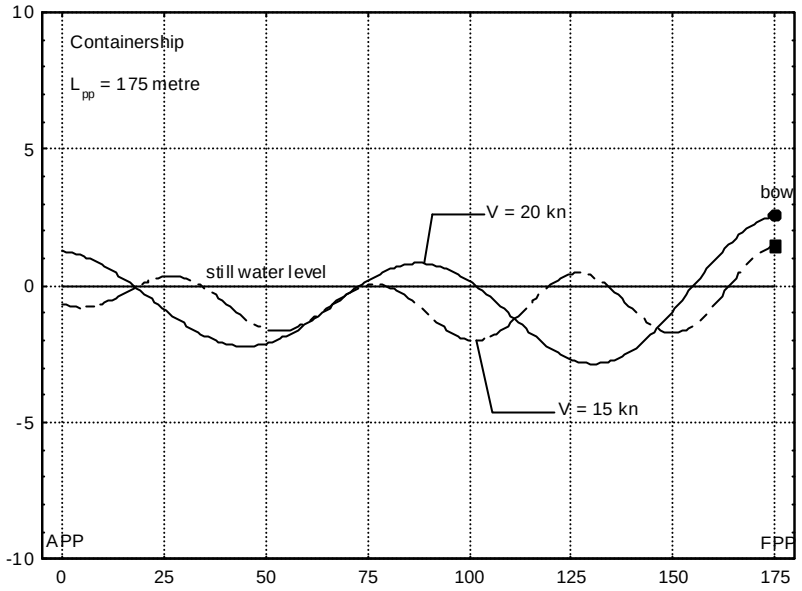

Figure 11.6: Distribution of Static Swell-Up

A very moderate approximation of the disturbance of the still water surface by the bow wave over the ship length can be obtained with:

$$\begin{aligned} \zeta_x &= \zeta_B \cdot \cos\left(2\pi \cdot \frac{\xi - 1}{0.78 - 7.2F_n}\right) \cdot e^{0.35(\xi-1)} \\ &\quad -(0.0050 + 0.0025F_n) \cdot L_{pp} \cos\left(\pi\frac{\xi}{2}\right) \end{aligned} \tag{11.23}$$

with Fn is the Froude number, L_{pp} is the length between perpendiculars and $\xi = 2x/L_{pp}$, where $x = -L_{pp}/2$ is the aft perpendicular and $x = +L_{pp}/2$ is the forward perpendicular, so: $-1.0 \leq \xi \leq +1.0$.
An example of the results of the use of formulas 11.22 and 11.23 for a containervessel is given in figure 11.6.

The amplitude of the vertical relative motion, s_a, of an oscillating ship in undisturbed waves can be calculated from the heave, pitch and wave motions. However, an oscillating ship will produce waves itself and this influences the amplitude of the relative motion.
A dynamic swell up, $\Delta\zeta_a$, should be taken into account so that the actual amplitude of the relative motions becomes:

$$s_a^* = s_a + \Delta\zeta_a \tag{11.24}$$

Then, shipping green water is defined by:

$$s_a^* > f_e \qquad \text{at the bow} \tag{11.25}$$

The spectral density of the vertical relative motion at the forward perpendicular is given by:

$$S_{s^*}(\omega) = \left(\frac{s_a^*}{\zeta_a}\right)^2 \cdot S_\zeta(\omega) \tag{11.26}$$

and the moments are given by:

$$m_{ns^*} = \int_0^\infty S_{s^*}(\omega) \cdot \omega_e^n \cdot d\omega \qquad \text{with: } n = 0, 1, 2, ... \tag{11.27}$$

Using the Rayleigh distribution, the short term probability of shipping green water in a given storm condition is:

$$\boxed{P\{s_a^* > f_e\} = \exp\left(\frac{-f_e^2}{2m_{0s^*}}\right)} \tag{11.28}$$

The number of times per hour that green water will be shipped in a certain sea state follows from the short term probability on shipping green water and the number of oscillations per hour:

$$\boxed{N_{\text{shipping/hour}} = \frac{3600}{T_{2s^*}} \cdot P\{s_a^* > f_e\}} \tag{11.29}$$

in which $T_{2s^*} = 2\pi\sqrt{m_{0s^*}/m_{2s^*}}$ is the average zero-crossing period.

11.2.3 Slamming

Slamming is a two-node vibration of the ship caused by suddenly pushing the ship by the waves. This occurs when the bow of the ship comes completely out of the water and then "crashes down" with an impact against the next wave. Slamming influences the local pressures on the hull plating and a local damage can be the result. The impulse nature of the impact also causes internal vibrations which can contribute to structural fatigue in the ship. Slamming does not necessarily influence the overall vertical displacements of the ship significantly. Slamming forces can be very large, but they act on the ship during a very short time.
A complete prediction of slamming phenomena is a very complex task, which is beyond the scope of any existing theory. Slamming impact pressures are affected by the local hull section shape, the relative velocity between ship and wave at impact, the relative angle between the keel and the water surface, the local flexibility of the ship's bottom plating and the overall flexibility of the ship's structure.

Ochi Criterium

[Ochi, 1964] has translated slamming phenomena into requirements for the vertical relative motions of the ship; he defined slamming by:
- an emergence of the bow of the ship at 10 per cent of the length aft of the forward perpendiculars and
- at the instant of impact the exceedance of a certain critical vertical relative velocity, without forward speed effect, between the wave surface and the bow of the ship.

Ochi defines the vertical relative displacement and velocity of the water particles with respect to the keel point of the ship by:

$$\begin{aligned} s &= \zeta_{x_b} - z + x_b \cdot \theta \\ \dot{s} &= \dot{\zeta}_{x_b} - \dot{z} + x_b \cdot \dot{\theta} \end{aligned} \tag{11.30}$$

with:

$$\begin{aligned} \zeta_{x_b} &= \zeta_a \cdot \cos(\omega_e t - k x_b \cos\mu) \\ \dot{\zeta}_{x_b} &= -\omega_e \zeta_a \cdot \sin(\omega_e t - k x_b \cos\mu) \end{aligned} \tag{11.31}$$

which means that a forward speed effect is not included in his definition of the vertical relative velocity.
The spectral moments of the vertical relative displacements and velocities are defined by m_{0s} and $m_{0\dot{s}}$. Emergence of the bow of the ship happens when the vertical relative displacement amplitude, s_a, at $0.90 \cdot L$ is larger than the ship's draft, d, at this location.
The probability of emergence of the bow follows from:

$$P\{s_a > d\} = \exp\left(\frac{-d^2}{2m_{0s}}\right) \tag{11.32}$$

Ochi's second requirement states that the vertical relative velocity exceeds a threshold value. He used - based on model and full scale experiments with frigates - 12 feet per second as a threshold value for a ship with a length of 520 feet.
Froude scaling of this threshold value results in:

$$\dot{s}_{cr} = 0.093 \cdot \sqrt{g \cdot L} \tag{11.33}$$

The probability of exceeding this threshold value is:

$$P\{\dot{s}_a > \dot{s}_{cr}\} = \exp\left(\frac{-\dot{s}_{cr}^2}{2m_{0\dot{s}}}\right) \tag{11.34}$$

Both occurrences - emergence of the bow and exceeding the threshold velocity - are statistically independent. In case of slamming both occurrences have to appear at the same time.
Thus the probability on a slam is the product of the two independent probabilities:

$$\boxed{P\{\text{slamming}\} = P\{s_a > d\} \cdot P\{\dot{s}_a > \dot{s}_{cr}\}} \tag{11.35}$$

or, using the Rayleigh distribution for each of these:

$$\boxed{P\{\text{slamming}\} = \exp\left(\frac{-d^2}{2m_{0s}} + \frac{-\dot{s}_{cr}^2}{2m_{0\dot{s}}}\right)} \tag{11.36}$$

Conolly Criterium

[Conolly, 1974] has translated slamming phenomena into requirements for the peak impact pressure of the ship; he defined slamming by:
- an emergence of the bow of the ship and
- an exceedance of a certain critical value, p_{cr}, by the peak impact pressure, p, at this location.

The peak impact pressure, p, is defined by:

$$p = C_p \cdot \frac{1}{2}\rho \dot{s}^2 \tag{11.37}$$

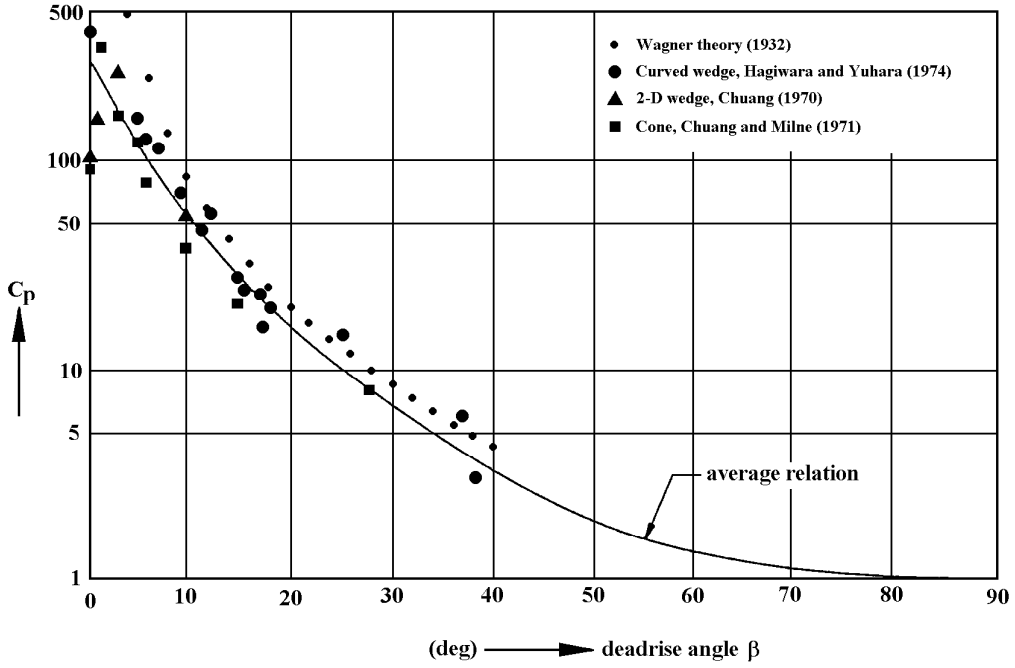

Figure 11.7: Peak Impact Pressure Coefficients

in which $\dot{s}$ is the vertical relative velocity between the ship and the wave.
The pressure coefficient C_p has been taken from experimental slamming drop tests data with wedges and cones, as given in the literature. Some of these data, as presented by [Lloyd, 1989] as a function of the deadrise β, are illustrated in figure 11.7.
The deadrise is the angle of the inclination at the keel of the contour of a cross section. This angle does not remain constant outside the center line. An equivalent deadrise β is defined here by an engineers solution: the deadrise of an equivalent wedge. The contour of the cross section inside 10 percentile of the half breadth $B/2$ of the ship has been used to define an equivalent wedge with a half breadth: $b = 0.10 \cdot B/2$. The accessory draft t of the wedge follows from the section contour. This draft can be larger than 10 percentile of the amidships draft d in the fore body of the ship. If so, the section contour below $0.10 \cdot d$ has to be used to define an equivalent wedge: $t = 0.10 \cdot d$. When this draft, t, is larger than the local draft, d, then the local draft has to be used. The accessory half breadth, b, of the wedge follows from the section contour.
Then the sectional area, A_s, below local draft, t, has to be calculated and the equivalent deadrise angle β (see figure 11.8) follows from:

$$\begin{aligned} \beta &= \arctan\left(\frac{a}{b}\right) \qquad 0 \leq \beta \leq \frac{1}{2}\pi \\ a &= \frac{2(b \cdot t - A_s)}{b} \end{aligned} \tag{11.38}$$

Critical peak impact pressures, p_{cr}, can be taken from [Conolly, 1974]. He gives measured impact pressures over 30 per cent of the ship length from forward for a ship with a length of 112 meters. From this, a boundary of p_{cr} between slamming and no slamming can be assumed. This boundary is presented in figure 11.9.

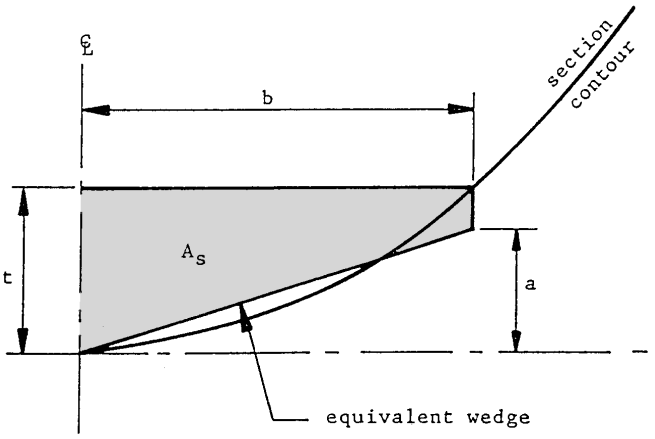

Figure 11.8: Deadrise of an Equivalent Wedge

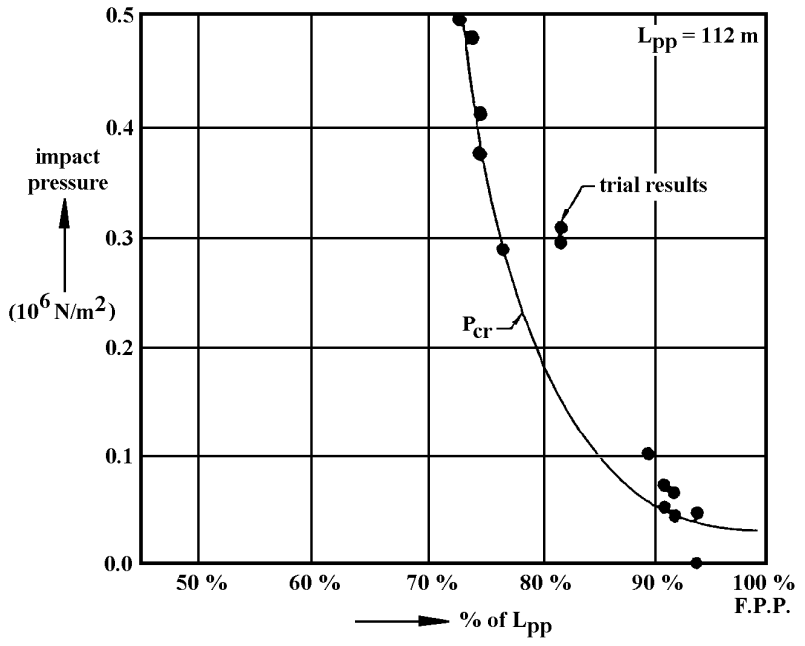

Figure 11.9: Measured Impact Pressures and Lower Limits

These values have to be scaled by Froude's law to the actual ship size. Bow emergence and exceedance of this limit is supposed to cause slamming. This approach can be translated into local hull-shape-dependent threshold values, $\dot{s}_{cr}$, of the vertical relative velocity as well:

$$\dot{s}_{cr} = \sqrt{\frac{2p_{cr}}{\rho C_p}} \tag{11.39}$$

The vertical relative velocity - including a forward speed effect - of the water particles with respect to the keel point of the ship is defined by:

$$\begin{aligned} \dot{s} &= \frac{D}{Dt}\left(\zeta_{x_b} - \dot{z} + x_b \cdot \theta\right) \\ &= \dot{\zeta}_{x_b} - \dot{z} + x_b \cdot \theta - V \cdot \theta \end{aligned} \tag{11.40}$$

with:

$$\begin{aligned} \zeta_{x_b} &= \zeta_a \cos(\omega_e t - k x_b \cos\mu) \\ \dot{\zeta}_{x_b} &= -\omega \zeta_a \sin(\omega_e t - k x_b \cos\mu) \end{aligned} \tag{11.41}$$

Then:

$$P\left\{\text{slamming}\right\} = \exp\left(\frac{-D_s^2}{2m_{0s}} + \frac{-\dot{s}_{cr}^2}{2m_{0\dot{s}}}\right) \tag{11.42}$$

Note that - because the forward speed effect is included here - the spectral moment of the velocities does not follow directly from the spectral density of the relative displacement as used by Ochi.
The average period of the relative displacement is found by:

$$T_{2s} = 2\pi\sqrt{\frac{m_{0s}}{m_{2s}}} = 2\pi\sqrt{\frac{m_{0s}}{m_{0\dot{s}}}} \tag{11.43}$$

Then the number of times per hour that a slam will occur follows from:

$$N_{\text{slams/hour}} = \frac{3600}{T_{2s}} \cdot P\left\{\text{slamming}\right\} \tag{11.44}$$

11.2.4 Sustained Sea Speed

In the last half century ship's officers can obtain routing advice from weather routing offices on shore, often connected with meteorological institutes. With a known or expected rough weather pattern on the ocean, an optimum ship's route with respect to minimum travelling time, minimum fuel consumption or minimum risk of damage can be found.
Wind and wave forecasting is a meteorological problem.
The prediction of the ship's reaction to wind and waves - in particular the ship's speed - is based on predictions and/or routing experience with the ship under consideration or with similar ships. The so-called sustained sea speed depends on the ship's resistance, the characteristics of propeller and engine and the behavior of the ship in waves. In determining the sustained sea speed two factors are considered: the **natural speed reduction** due to added resistance - mainly caused by wind and waves - and the **voluntary speed reduction** by the ships captain, in order to avoid severe motions or their consequences such as damage to ship and cargo or crew and passenger seasickness.

Ship's Resistance

The total resistance of a ship in a seaway can divided in several parts and contributions; the most important of which follow below:

- Still Water Resistance
  Until now it is not possible to make pure theoretical calculations of the ship's resistance in still water. To estimate the required power in a design stage, use must be made of model experiments carried out in a towing tank. These experimental results are extrapolated to full scale by techniques based on physical laws and experience, as has been treated in chapter 4. Numerous empirical methods can be found to estimate the still water resistance, based on model experiments and trial data. Best known is the method of [Holtrop, 1984], which has the advantage that the results are presented in empirical formulas suitable for computer use.

- Wind Resistance
  The wind resistance for ships with high superstructures or with a lot of cargo on deck - such as container ships - can be considerable. A reliable method for estimating the wind resistance of ships was published by [Isherwood, 1973]; see chapter 4.
  The following relation between the absolute wind speed V_w and the significant wave height $H_{1/3}$ - obtained from ITTC recommendations - can be used for a quick analysis:

$$V_w = 10 \cdot {H_{1/3}}^{2/3} \tag{11.45}$$

  in which the wind velocity, V_w, is in knots and the significant wave height, $H_{1/3}$, is in meters.

- Added Resistance due to Waves
  The relative motions of a ship with respect to the water surface cause an added resistance. This has been shown in chapter 8, where two methods are given:
  - the radiated energy method of [Gerritsma and Beukelman, 1972], suitable for head to beam waves and
  - the integrated pressure method of [Boese, 1970], suitable for all wave directions.
  These methods are based on the assumption of the linearity of the ship's response; thus the added resistance varies with the wave amplitude squared.

- Added Resistance due to Steering
  In a seaway, the ship's heading will be disturbed by wind and waves. The beam waves cause sway and yaw motions. To maintain a heading in a sea with a beam wind, rudder angles are necessary to counteract the wind and wave moment at any instant. For instance, a Beaufort 9 sea caused by beam wind can require oscillating rudder angles with an amplitude of 15 degrees or more. All of this results in an increase of the ship's resistance.
  In these beam waves, the ship will sail with yaw motions caused by the sea and by the correcting autopilot. These yaw motions cause centrifugal forces, of which the longitudinal components introduce a resistance; see figure 11.10. Assuming a fixed position of the pivot point (fictive rotation point of the ship) at 10 % from the forward perpendicular and an additional hydrodynamic mass for sway of 80 % of the ship's

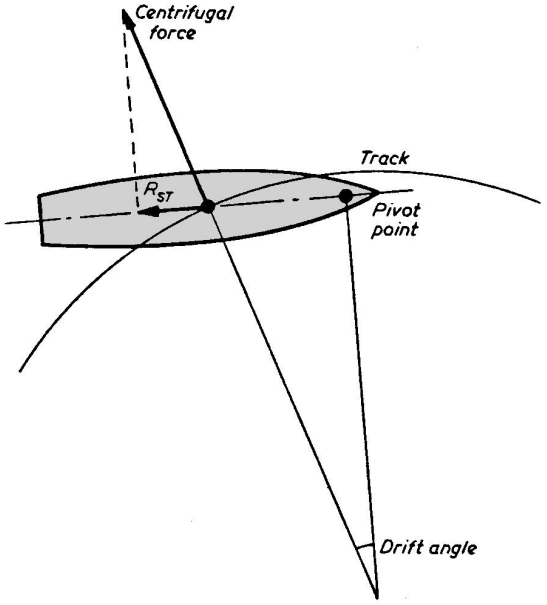

Figure 11.10: Resistance due to Steering

solid mass, the mean added resistance during a harmonic yaw motion will be in the order of:

$$R_{ST} = 0.030 \cdot \nabla L \dot{\psi}_a^{\,2} \tag{11.46}$$

with:

R_{ST}	=	steering resistance in kN
∇	=	volume of displacement in m^3
L	=	length of the ship in m
$\dot{\psi}_a$	=	rate of turn amplitude in deg/min

This means for a 200 meter container vessel - with rate of turn amplitudes of 30 degrees per minute at the service speed in following waves - a resistance increase of 20 % of the still water value. The course deviations in this example are only about 2 degrees. This shows that the setting of the autopilot is important.
Sway motions also increase the total sailed distance and - as a result - a reduced average speed along the given track.

- Added Resistance due to Fouling
  Fouling of the ship's hull can cause a considerable increase in the ship's resistance. The extent of fouling depends on the sailing routes and the time during which the ship will sail in areas with large fouling effects. As fouling is a biological process - depending on the paint used - it is not easy to give accurate mean values for all ships, seasons and areas. Moreover, the effect of fouling depends on the docking period and the time since the last docking of the ship.
  Fouling will only affect the friction part, R_f, of the ship's resistance. Aertssen carried out full scale experiments to investigate the problem of fouling. From his extensive results of full scale measurements it appeared that - for a ship sailing on the Atlantic

route - the effect of fouling on the frictional resistance will be in the order of:

$$\frac{\Delta R_f}{R_f} \cdot 100\% \;=\; 3.6 \cdot y_a + \frac{40 \cdot y_d}{1 + 2 \cdot y_d} \tag{11.47}$$

in which y_a is the age of the ship in years and y_d is the year since the last docking. This means for instance, an increase of the frictional resistance by about 30 % for a ship with an age of five years and a last docking one year previously.
However, the overall effect on the total resistance is smaller and depends on speed and ship type. With low speeds and full ship forms - e.g. tankers - the frictional resistance is the major part of the total resistance, whereas the wave-making resistance dominates in the case of high speed container ships. This means that the effect of fouling is much larger for tankers than for container ships.
An investigation by [Journée, 1976b] of log data of a 200,000 tdw tanker, sailing from Europe to the Persian Gulf, showed an increase of the still water resistance for full load and ballast condition as 26 to 29 % one year after the last docking and 47 to 52 % two years after the last docking. After the oil crisis in the early seventies these ships reduced power by 50 %, resulting in a speed reduction for the clean hull from 16 to 13 knots. To maintain this speed two years after the last docking the power of a fully loaded ship had to be increased from 50 to over 80 %. This behavior is visualized in figure 11.11 as an example to show that fouling is a factor which should not be neglected in sustained sea speed calculations.

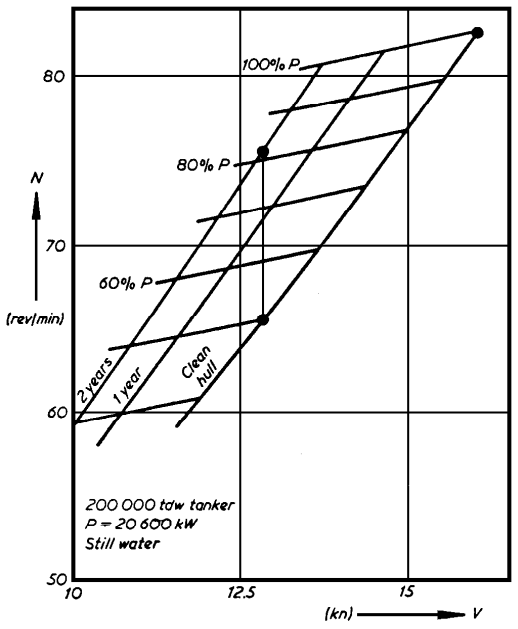

Figure 11.11: Increase of Required Propulsion Power due to Fouling

The sum of these contributions provides the total resistance of the ship under operational conditions.

Propulsion

The propeller behind a ship can be considered as an energy transformer: torque with engine speed will be transformed into thrust with a speed of advance of the propeller, relative to the mean velocity of the incoming water. At a constant engine setting there should be an equilibrium between the engine speed and the ship's speed in such a way that two conditions are fulfilled: the torque required by the propeller must be in equilibrium with the torque delivered by the engine and the thrust delivered by the propeller must be in equilibrium with the total resistance of the ship in the self-propelled condition. This has been treated in chapter 4.

- Propeller
  The characteristics of an open water propeller in its normal operating range are usually expressed in its thrust coefficient, K_T, and torque coefficient, K_Q, as a function of the speed (or advance) ratio, J:

$$K_T = \frac{T}{\rho D^4 n^2} \qquad K_Q = \frac{Q}{\rho D^5 n^2} \qquad J = \frac{V_e}{nD} \tag{11.48}$$

  with T is thrust, Q is torque, ρ is density of water, D is propeller diameter, n is number of propeller revolutions per second and V_e is relative speed of advance.
  These characteristics depend on the number of propeller blades, the pitch ratio and the expanded blade area ratio and can be obtained by means of open water model experiments. Results of such experiments with systematically varied propeller series can be found in various publications.
  One of the best known is the Wageningen B-propeller series of MARIN. Over 120 systematically varied propeller models have been tested and the results are given in polynomials, together with a correction for scale effect. These results are valid for the open water condition.
  For the "behind the ship condition" the open water torque must be multiplied by the relative rotative efficiency η_R:

$$\eta_R = \frac{Q_{\text{open water}}}{Q_{\text{behind ship}}} \tag{11.49}$$

  which varies from about $\eta_R = 1.04$ for single screw ships to about $\eta_R = 0.97$ for twin screw ships. This efficiency reflects the difference in torque in the wake and in open water at the same thrust.
  The relative speed of the water, V_e, into the propeller disc is not equal to the forward ship speed, V. A wake fraction, w, should be taken into account:

$$V_e = V \cdot (1 - w) \tag{11.50}$$

  This wake fraction varies from 0.2 to 0.4 and can be obtained directly from model experiments - taking into account the scale effect - or from empirical formulas given in the literature.
  From model experiments it appears that the wake fraction is hardly affected by an increase of the propeller loading due to a resistance increase, caused by - for instance - towing a barge, motions in waves, etc.
  As discussed in chapter 4, the thrust of the propeller, T, is not equal to the ship's

resistance, R, found from resistance tests. A thrust deduction fraction, t, should be taken into account:

$$R = T \cdot (1 - t) \tag{11.51}$$

The thrust deduction fraction in still water is usually about 60 to 80 % of the wake fraction and can be obtained from model experiments or by empirical formulae.
This fraction however, will decrease with an increased loading of the propeller; in the bollard condition - at zero forward ship speed - this fraction will be about 0.03 to 0.05. From model experiments it appears that, at a constant propeller rotation rate, the thrust deduction fraction decreases - at an increasing loading of the propeller - quadratically with the forward ship speed. It can drop down to a value of about 0.03 to 0.05 in the bollard condition (zero speed).
The influence on the efficiency of oscillations of the propeller behind a ship in waves can be neglected for practical purposes.

- Engine
  The relation between the delivered torque of an engine and the engine speed at a constant setting and an increased loading in a seaway is also important. In this connection two different types of engines are distinguished: a turbine and a diesel engine.

  – Turbine
    As a first approximation, it is often accepted that - for an increasing loading of the engine at a constant engine setting - the delivered power remains constant; this means a hyperbolic relation between the torque at the propeller and the engine speed:

$$Q = c \cdot \eta_m \cdot \frac{Q_0 \cdot n_0}{n} \qquad \text{for a turbine} \tag{11.52}$$

    in which c is the engine setting, η_m is the mechanical efficiency of the shaft bearings and $2\pi Q_0 n_0$ is the maximum continuous rating power with n_0 in rev/sec.
    More precisely however, there is a linear relation between torque and engine speed:

$$Q = c \cdot \eta_m \cdot Q_0 \cdot \left(a - (a-1) \cdot \frac{n}{n_0} \right) \qquad \text{for a turbine} \tag{11.53}$$

    in which the coefficient a depends on the type of the turbine ($2 \leq a \leq 3$).
    If one takes into account that - at a constant setting - the turbine speed will not be reduced by more than 15 %; the assumption of constant power is sufficiently accurate for practical purposes such as the calculation of the ship's speed.

  – Diesel Engine
    For a diesel engine it is usually accepted that the torque remains constant for an increasing loading of the engine at a constant engine setting:

$$Q = c \cdot \eta_m \cdot Q_0 \qquad \text{for a diesel engine} \tag{11.54}$$

    This yields that the coefficient a in equation 11.53 is equal to1.0.
    In practice, there are some deviations from this assumption. At a constant engine setting and an increasing loading of the engine the torque will first increase

to a maximum value and will then decrease again. This can be approximated by a linear relation between torque and engine speed, provided that the number of revolutions per minute does not reduce more than about 15 %. Then the linear relation in equation 11.53 can be used for a diesel engine, too, with for instance $a = 1.0 - 1.5$.
Often the engine speed will be kept constant. This means that the coefficient a goes to infinity and the engine setting c has no meaning anymore; n will be equal to n_0.

Speed Calculation

[Journée, 1976b] describes a method to calculate the ship's speed in seaway at a given engine setting. Comparisons with published full scale data have shown a reasonable agreement between 'theory' and results of full scale experiments.
The principle of the calculation method is shown in figure 11.12. For a number of ship speeds, the relation between the torque required by the propeller and the number of revolutions per minute are calculated from the torque characteristics of the assumed B-series propeller behind the ship and a wake fraction. The relation between the torque delivered by the engine to the propeller and the number of revolutions per minute is known from engine characteristics and shaft losses. These relations give an equilibrium relation for speed and number of revolutions per minute, which - together with the thrust deduction faction - results in a resistance that can be overcome by propeller and engine as a function of the speed. This is the right hand part of figure 11.12. The actual total resistance of the ship in a seaway as a function of the speed is known by adding up its components; the required equilibrium yields the ship's speed.
If greater speed-accuracy is required, speed, propeller rate and power data, for instance derived at the ship's trial, can be used to adjust the resistance curve and the propeller characteristics.
Figure 11.13 shows the sustained sea speed (or speed loss) of a ship in relation to its course with respect to the waves in various sea states. The circular curves in this figure are curves of constant ship speeds in knots; the non-circular curves are the sustained sea speeds of the ship, each at a constant sea state defined by a significant wave height - ranging from 2 until 8 meters - only. Note that head waves are indicated here by 0^0; a convention often used in ship navigation.
Often, a fixed relation between the significant wave height and the mean wave period will be used in these speed graphs. Figure 11.14-a gives the results of speed loss calculations in head waves of a 200,000 tdw tanker at a range of wave heights and wave periods. It shows a striking influence of the wave period on the ship's speed.

Voluntary Speed Reduction

When a ship enters a severe storm the ship's captain can reduce speed or change course in order to reduce motions. Phenomena that are important for the decision to reduce speed are shipping of green water and slamming as discussed before, but also heavy vertical accelerations forward and sometimes propeller racing (if it comes partially out of the water). Accelerations forward - exceeding certain limits - can damage ship or cargo and are therefore often a reason for voluntary speed reduction. This can be too simple; figure 11.14-b shows

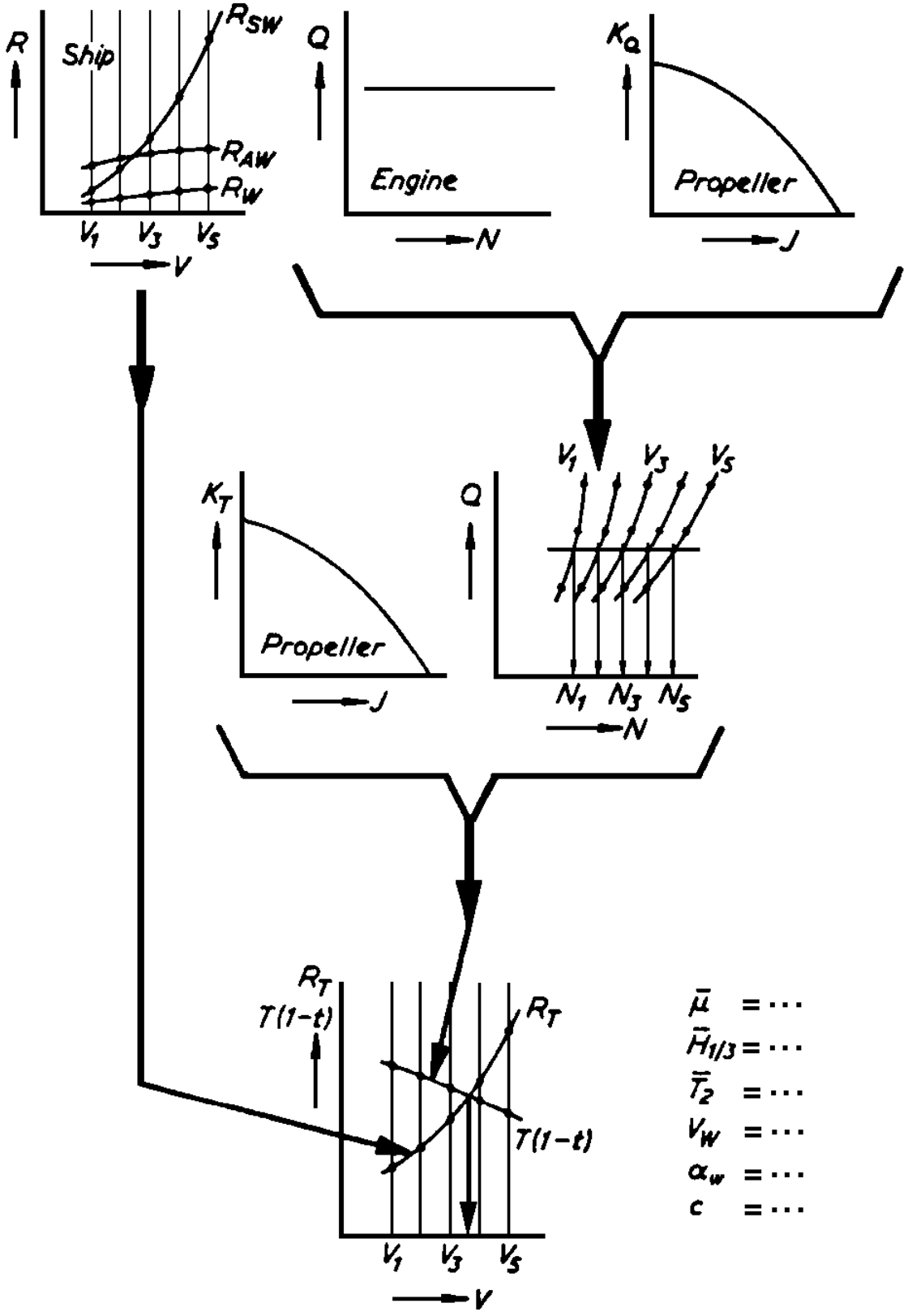

Figure 11.12: Scheme of Forward Speed Calculation

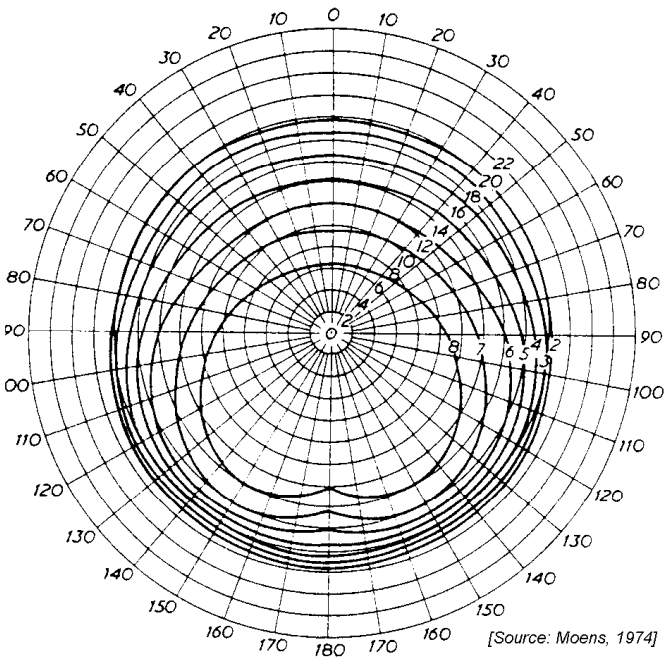

Figure 11.13: Speed Loss Graph with Sustained Sea Speeds

the considerable influence of the forward ship speed on the vertical accelerations forward for a container vessel.
Propeller racing is the rapid increase of the rate of turn due to a lack of loading, because of propeller emergence; it is largely prevented nowadays by rpm-governors on the engine. However, large thrust and torque fluctuations occur in waves, even at a constant number of revolutions per minute. This is reason why propeller racing is sometimes defined as an emergence of the propeller which causes a decrease of torque in excess of 25 %. However, often a more simple definition is used which defines propeller racing as an emergence of the propeller by more than one third of the propeller diameter.

Criteria for reducing speed can be found in various publications. They are commonly expressed as probability limits for the accelerations forward and probability limits for the occurrence of shipping water at the bow and slamming. In some cases, probability limits for propeller racing are included too.
Well-known voluntary speed reduction criteria are those of [Ochi and Motter, 1974]. They give probability limits below which no voluntary speed reduction should be expected. These criteria distinguish between two typical loading conditions of the ship:

- **Fully laden condition:**

$$P\left\{\text{bowdeck wetness} \quad \text{and/or} \quad \ddot{z}_{a_{1/3}}(\text{bow}) \geq 0.4 \text{ g}\right\} \leq 0.07 \tag{11.55}$$

This probability criterium of Ochi and Motter can be rewritten as:

$$P\left\{\text{bowdeck wetness} \quad \text{and/or} \quad \ddot{z}_a(\text{bow}) \geq 0.46 \text{ g}\right\} \leq 0.07 \tag{11.56}$$

or:

$$\begin{aligned} &P\left\{\text{bowdeck wetness}\right\} + P\left\{\ddot{z}_a(\text{bow}) \geq 0.46 \text{ g}\right\} \\ &-P\left\{\text{bowdeck wetness}\right\} \cdot P\left\{\ddot{z}_a(\text{bow}) \geq 0.46 \text{ g}\right\} \quad \leq \quad 0.07 \end{aligned} \tag{11.57}$$

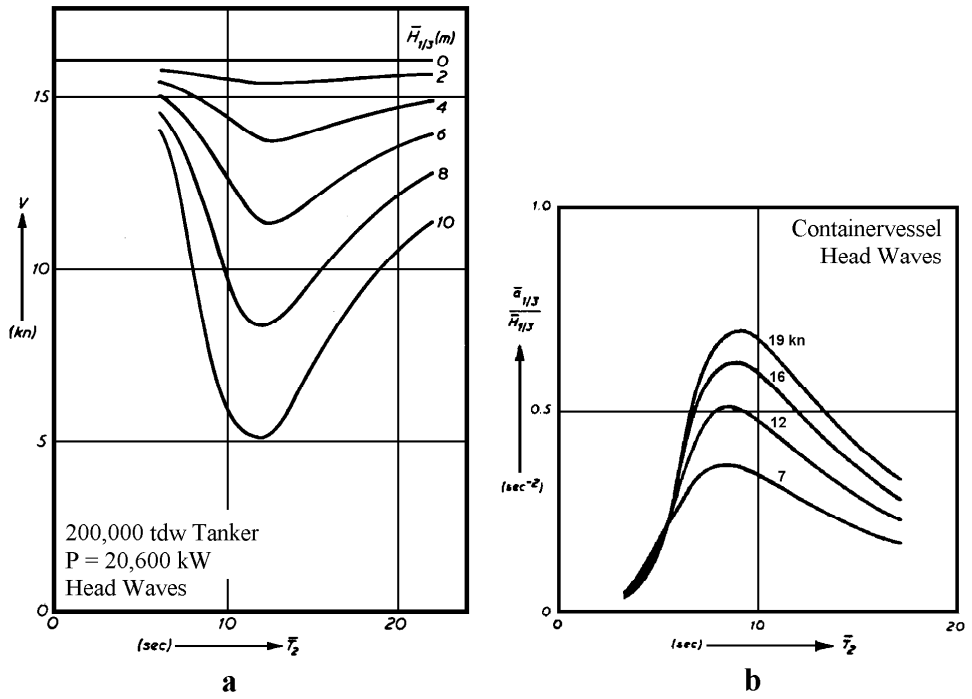

Figure 11.14: Effect of Wave Period on Sustained Sea Speed and on Accelerations Forward

- **Light laden condition:**

$$P\left\{\text{slamming} \quad \text{and/or} \quad \ddot{z}_{a_{1/3}}(\text{bow}) \geq 0.4 \text{ g}\right\} \leq 0.03 \tag{11.58}$$

This probability criterium of Ochi and Motter can be rewritten as:

$$P\left\{\text{slamming} \quad \text{and/or} \quad \ddot{z}_a(\text{bow}) \geq 0.53 \text{ g}\right\} \leq 0.03 \tag{11.59}$$

or:

$$\begin{aligned} &P\left\{\text{slamming}\right\} + P\left\{\ddot{z}_a(\text{bow}) \geq 0.53 \text{ g}\right\} \\ &-P\left\{\text{slamming}\right\} \cdot P\left\{\ddot{z}_a(\text{bow}) \geq 0.53 \text{ g}\right\} \quad \leq \quad 0.03 \end{aligned} \tag{11.60}$$

Use has been made here of the following probability relation, valid for two **statistically independent events** A and B:

$$\begin{aligned} P\left\{A \text{ and/or } B\right\} &= P\left\{A\right\} + P\left\{B\right\} - P\left\{A \text{ and } B\right\} \\ &= P\left\{A\right\} + P\left\{B\right\} - P\left\{A\right\} \cdot P\left\{B\right\} \end{aligned} \tag{11.61}$$

In these criteria, bowdeck wetness has to be determined at FPP (forward perpendicular), slamming at $0.90 \cdot L_{pp}$ and the vertical accelerations of the bow at FPP.
Note that these criteria are rather moderate; in fact they should also depend on the type of the ship and its cargo.

Figure 11.15 shows an example of the sustained sea speed as a function of the Beaufort scale for Victory Class ships. In order to avoid severe motions, these ships have to reduce power already in rough weather conditions defined by Beaufort 6, approximately.

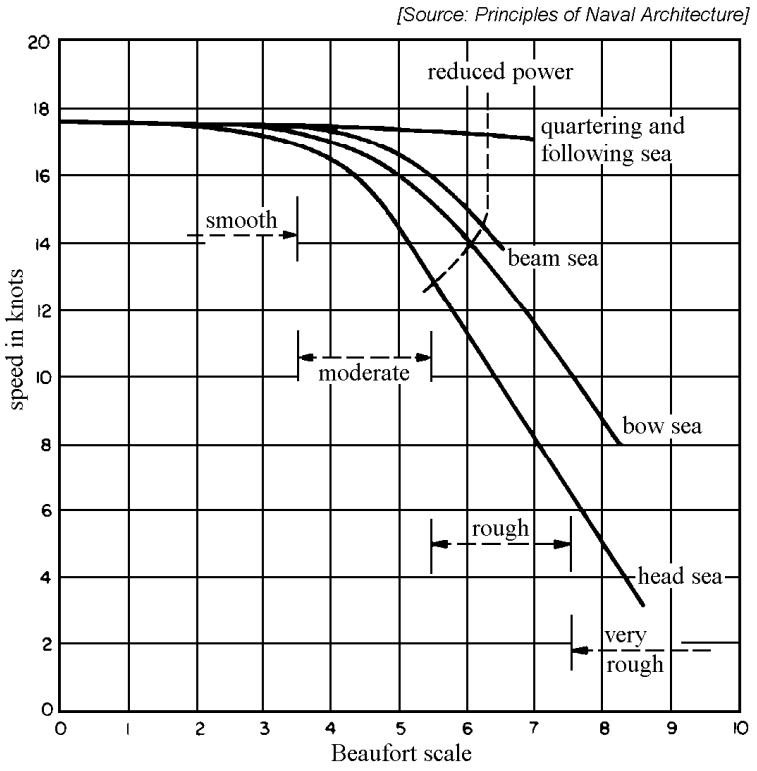

Figure 11.15: Speed Loss of Victory Class Ships

Applications

When designing a ship, much attention is paid to the still water resistance with respect to hull form, expensive bulbous bows and propeller design. On the North Atlantic Ocean however, a sea state of Beaufort 6 is exceeded 70 % of the time during the winter season and 45 % during the summer season. Depending on the ship's size, the added resistance - caused by vertical ship motions - can be considerable. In head waves in this sea state, a ship with a length of about 135 meters and a service speed of 16 knots in still water will have an added resistance equal to its still water resistance at about 12 knots. Thus, it is worthwhile to pay attention to this added resistance, caused by vertical ship motions in a seaway.

Speed and power calculations of a ship in a seaway can be used to support the work of routing officers. Together with the meteorological information, accurate speed loss graphs will help them to give well-founded routing advice to the ship's captain. This is of importance from an economic point of view as well as from the ship's safety point of view. Ship motions can be calculated with a fair accuracy but the limits with respect to the voluntary speed reduction are less certain. Computations use moderate limits, derived from the available literature. However, these limits can be adjusted at sea to correspond to those permitted by the ship's captain.

This kind of calculation can also be used in developing operational performance systems on board of ships. The calculated speed, power, fuel consumption and motion data can be used in these systems with respect to decisions for course deviations or speed reductions. Another application of these calculations can be found in economical studies of the

operation of these ships with respect to travelling time, fuel consumption, etc. This brings one to a very interesting economic calculation which should include such factors as safety limits in relation to insurance costs, the total transit time for both the ship and its cargo (think of the lost production from a jack-up drilling rig being moved on a heavy-transport ship), fuel consumption and its costs and personnel costs.

11.3 Dredger Limitations

Dredging masters tend to be experienced-based rather than theoretical. Since they often spend a significant part of their career on one ship, they can circumvent the response computations and thus express operational limits directly in terms of the conditions (wind, waves and currents) which cause the limit conditions. Note that this experienced-based direct approach can have significant errors from an economic point of view (stopping operations too soon or continuing too long). It is also difficult to use for special dredgers of an extreme size or with a non-standard form.

11.3.1 Dredger Wave Limitations

With these limitations, the following are considered to be general operating limits - in terms of significant wave height - in short waves (sea) or longer waves (swell) for each of the given dredging operations.

Floating Object	Maximum $H_{1/3}$ (m) in short waves	Maximum $H_{1/3}$ (m) in long waves
Small equipment discharging into barges	0.30 - 0.50	0.20 - 0.40
Large equipment discharging into barges	0.50 - 1.00	0.40 - 0.80
Small equipment with floating pipeline	0.20 - 0.50	0.20 - 0.50
Large equipment with floating pipeline	0.50 - 1.00	0.30 - 0.60
Self-propelled barges with suction pipe	0.60 - 1.00	0.40 - 0.80
Trailer with swell compensator	2.00 - 4.00	2.00 - 4.00

This is not the whole story however. Consider the case when a trailing suction dredge (with swell compensator) is being used to pick up sand, bring it near shore, and discharge it into a pipeline (at an exposed location), for instance to restore a beach. Even though the ship may be able to dredge (pick up sand) in 2 to 4 meter waves, it will likely not be appropriate to come into shallow water (where the discharge pipeline starts) or even to use a small boat to assist in connecting to this line. The proper analysis of such a dredging cycle must account for these differences as well as the sequence and duration of each component step. This can be a very interesting topic, but one which is beyond the scope of this text.

11.3.2 Dredger Current Limitations

If the anchors hold sufficiently, it makes a considerable difference as to whether the ship can work with the current or whether it has to work at an angle to the current, as for instance a cutter suction dredger. For a cutter suction dredger the situation is particularly dangerous when the current is directed against the ladder side. The current direction in this figure approaches from the ladder side, which is convenient in that it helps supply material to the suction mouth in the cutter. On the other hand, when the current is too strong or the deviation angle gets too large the anchoring system on the ladder can fail. When this happens, the dredge will swing around her spud pile which can result in a broken discharge pipe, a broken (or bent) spud pile, a broken ladder when it hits the channel side or even a capsized dredger, if the spud pile and/or the ladder do not fail.
Here, again, dredging masters are experience-based. For most of the larger cutter suction dredgers the safe limit can be estimated at about 2 knots velocity of the current. For bucket dredgers and stationary dredgers the limit is about 3 knots provided the anchorage and freeboard of the ship are sufficient. Self-propelled barges are preferable when working in strong currents; this avoids the need for moorings between the dredge and transportation barge.